Studies of Heterogeneous Ice Chemistry Relevant to the Atmosphere

by

Vivian Faye McNeill

B.S. Chemical Engineering
California Institute of Technology, 1999

M.S. Chemical Engineering Practice
Massachusetts Institute of Technology, 2001

SUBMITTED TO THE DEPARTMENT OF CHEMICAL ENGINEERING
IN PARTIAL FULFILLMENT OF THE REQUIREMENTS FOR THE DEGREE OF

DOCTOR OF PHILOSOPHY IN CHEMICAL ENGINEERING
AT THE
MASSACHUSETTS INSTITUTE OF TECHNOLOGY

February, 2005

Signature of Author.....
Department of Chemical Engineering
20 December 2004

Certified by .....
Mario J. Molina
Institute Professor
Thesis Supervisor

Certified by .....
Bernhardt L. Trout
Associate Professor of Chemical Engineering
Thesis Supervisor

Accepted by .....

Daniel Blankschtein
Professor of Chemical Engineering
Chairman, Committee for Graduate Students

Studies of Heterogeneous Ice Chemistry Relevant to the Atmosphere

by

Vivian Faye McNeill

Submitted to the Department of Chemical Engineering
on 20 December 2004, in partial fulfillment of the
requirements for the degree of
Doctor of Philosophy in Chemical Engineering

Abstract

Characterization of the interaction of hydrogen chloride (HCl) with polar stratospheric cloud (PSC) ice particles is essential to understanding the processes responsible for ozone depletion. The interaction of HCl with ice was studied between -87 °C and -30 °C using the complementary approach of a) ellipsometry to monitor the ice surface with chemical ionization mass spectrometry (CIMS) detection of the gas phase, and b) flow tube experiments with CIMS detection. The flow tube-CIMS technique was also used to study the chlorine activation reaction of chlorine nitrate ($ClONO_2$) and HCl on ice, the co-adsorption of acetic acid (CH_3COOH) and HCl on ice, and the adsorption of CFC-12 (CCl_2F_2) on ice. CH_3COOH and CCl_2F_2 were employed as nonreactive probe molecules to provide information about the state of the ice surface in the HCl-ice system. The ellipsometer-CIMS studies were performed on single-crystalline ice samples, and the flow tube-CIMS studies were performed on smooth and vapor-deposited polycrystalline ice films and on zone-refined ice cylinders. A numerical modeling framework is presented for the interpretation of the flow tube-CIMS studies.

A disordered surface region, or quasi-liquid layer (QLL), was detected on bare ice using ellipsometry down to -30 °C. We also found using ellipsometry that trace amounts of HCl induce QLL formation on the ice surface in the vicinity of the solid-liquid equilibrium line on the HCl-ice phase diagram, including conditions encountered in the polar stratosphere during PSC events. These results are supported by the results of the flow tube-CIMS studies of the reaction of $ClONO_2$ and HCl on ice, CH_3COOH/HCl co-adsorption on ice, and HCl adsorption on ice. This is the first report of direct experimental evidence of HCl-induced QLL formation at stratospheric conditions.

It appears that the real part of the refractive index of the QLL formed via exposure to gas-phase HCl is closer to that of liquid water or aqueous HCl solution than to that of ice. We estimate the thickness of the QLL in our experiments to be on the order of 100 nm.

We found using the flow tube-CIMS technique that the presence of the QLL enhances the chlorine-activation reaction of HCl with $ClONO_2$. The presence of the QLL also enhances CH_3COOH adsorption. We find that the solubilities of HCl and CH_3COOH in the QLL are intermediate between the solubilities of each species in liquid H_2O and those in ice.

In a flow-tube CIMS study of HCl adsorption on different types of ice surface, we found that HCl adsorption on polycrystalline ice films typically used in laboratory studies consists of two modes: one relatively strong mode leading to irreversible adsorption, and one relatively weak binding mode leading to reversible adsorption. We have indirect experimental evidence that these two modes of adsorption correspond to adsorption to sites at crystal faces and those at grain boundaries, but there is not enough information to enable us to conclusively assign each adsorption mode to a type of site. We also found indirect evidence that HCl hexahydrate formation on ice at conditions relevant to the polar stratosphere is a process involving hydrate nucleation and propagation on the crystal surface, rather than one originating in grain boundaries, as has been suggested for ice formed at lower temperatures.

The ellipsometry measurements in this work were performed with Dr. Thomas Loerting. The study of HCl hexahydrate formation on smooth ice was performed with Prof. Franz Geiger.

Thesis Supervisor: Mario J. Molina
Title: Institute Professor

Thesis Supervisor: Bernhardt L. Trout
Title: Associate Professor

This work is dedicated to
the memory of my grandfather,
Paul R. Heller, Jr.

Contents

List of Figures

List of Tables

List of Symbols and Acronyms used in this thesis:

A	cross-sectional area of the flow tube
b	surface adsorption equilibrium constant, Langmuir constant
C	gas-phase solute concentration
$\overline{C}$	radially averaged gas-phase solute concentration
C_i	solid-phase (ice) solute concentration
C_o	inlet gas-phase solute concentration
c_s	surface concentration (area basis)
C_s	near-surface concentration (volume basis)
D	solute-He binary diffusion constant
D_i	diffusion constant of solute in ice
D_s	surface diffusion constant
H	Henry's law constant
J	surface flux
k	imaginary part of the refractive index
k_{ads}	adsorption rate constant
k_{des}	desorption rate constant
l_i	ice film thickness
l	QLL or near-surface region thickness
L	length of ice film
L	length of flow tube
n	real part of the refractive index
P_{HCl}	partial pressure of HCl
R_{loss}	rate of solute loss
R	radial coordinate
Re	Reynolds' number
R	ice sample radius
S	total surface sites for adsorption
t	time
U	radially averaged average gas velocity
V	volume
$\underline{v}$	gas phase velocity vector
x	coordinate pointing into ice slab
z	axial coordinate

Greek Letters

χ_A	shape factor (area-volume)
χ_V	shape factor (volume-volume)
Δt	timestep for numerical simulation
Δz	step size in axial direction for numerical simulation
η	similarity variable
μ	gas viscosity
ρ	gas density

τ_{diff}	characteristic time for diffusion
τ_{diff}	characteristic time for convection
θ	fractional surface coverage.

Acronyms

CFC: Chorofluorocarbon

HCFC: Hydrochlorofluorocarbon

CIMS: Chemical Ionization Mass Spectrometry

EIMS: Electron Impact Mass Spectrometry

NAT: Nitric Acid Trihydrate

PSC: Polar Stratospheric Cloud

QLL: Quasi-liquid Layer

RGA: Residual Gas Analyzer

TPD: Temperature Programmed Desorption

UHV: ultra-high vacuum

Acknowledgements

Many people have contributed to my graduate career and made this thesis possible. My appreciation goes beyond what I can express, but I would like to extend my thanks to the following people:

To Mario and Luisa Molina and Bernhardt Trout, for being mentors and role models. For directing my energy and challenging me, being patient with me, and ultimately leading me to produce something beyond anything I could have envisioned on my own.

To my thesis committee, Prof. Greg McRae and Prof. Jeff Steinfeld, for being generous with their time and for bringing their expertise and fresh perspectives to this thesis.

To my undergraduate research advisor, Prof. Rick Flagan, for having faith in a struggling student, giving me a push in the right direction, and instilling in me a love of atmospheric science.

To the Molina and Trout Groups, past and present, particularly Keith, Lenny, Thomas, Franz, Bilal, Andrey, Kirsten, Rainer, Carmen, Phil, Ico, Juan, Ed, Ingrid, Yael, Matt, Allan, Geoff, Yves, Kent, Cynthia, Ravi, Brian, and Xi. Thank you for being my technical and emotional support systems during these five and a half long years, and teaching me about science, life, and the world.

To Prof. Clark Colton, Prof. Ken Smith, and Bill Dalzell, for teaching me about applying modern tools to classical chemical engineering education, and for inspiring me in my thesis research, thanks to the parallels between heat and mass transfer.

To my parents, Mark and Lynne Smith. None of this would be possible without your constant love, support and encouragement. Thank you for giving me strength, and for always having faith in me.

To my father, Michael McNeill, for being a true friend, and for rescuing me from the grey concrete of MIT once a year to go sailing in the breathtaking blue waters of the Caribbean.

To my grandparents, Vivian and Robert McNeill, and Paul R. Heller, who have inspired me in every area of my life. Thank you for being my biggest fan club, and I'll

continue to do my best to make you proud.

To my friends, particularly Mary, Natalia, Caroline, Julia, Elina, Mike, Daniel, Zari, and all members of the MIT Casino Rueda Group, past and present, for being there for me through everything. You have made my life at MIT rich and varied, and I will miss you all very much when I leave Boston.

And to Sid, for being an inspiration, and for challenging me while at the same time loving the person I am. Thank you for enriching my life with your sweetness, warmth, and laughter. And special thanks for all of your long-distance moral, emotional, and technical support during the writing process. Ami aschi, bor.

Chapter 1

Introduction

1.1 Motivation for research

Heterogeneous reactions that occur on the surfaces of polar stratospheric cloud (PSC) ice particles play a key role in the annual decrease of stratospheric ozone that has been observed at polar latitudes[1-3]. This effect is commonly termed the "Ozone Hole."

A steady-state concentration of ozone (O_3) in the stratosphere is created by the following set reactions, which are collectively called the Chapman mechanism[4,5]:

$$O_2 + h\nu \rightarrow O + O \qquad (1.1)$$

$$O + O_2 + M \rightarrow O_3 + M \qquad (1.2)$$

$$O_3 + h\nu \rightarrow O_2 + O \qquad (1.3)$$

$$O_3 + O \rightarrow O_2 + O_2 \qquad (1.4)$$

Chlorofluorocarbons (CFCs), due to the chemical inertness that makes them ideal for many commercial and industrial applications, have sufficiently long tropospheric lifetimes (20-300 years)[5] that they may diffuse into the stratosphere, where they can then be photolyzed to create chlorine radicals. Atomic chlorine is highly reactive towards ozone and catalyzes its destruction via the following cycle[4,5]:

$$Cl + O_3 \rightarrow ClO + O_2 \qquad (1.6)$$

$$ClO + O \rightarrow Cl + O_2 \qquad (1.7)$$

Net: $O_3 + O \rightarrow O_2 + O_2$.

Up to 99% of the active chlorine in the stratosphere is sequestered in relatively inert forms, chlorine nitrate ($ClONO_2$) and hydrogen chloride (HCl)[4]. The net effect of the following set of reactions, referred to as chlorine activation processes, is the conversion of the chlorine reservoir species $ClONO_2$ and HCl into chlorine gas, Cl_2:

$$ClONO_2 + HCl \rightarrow Cl_2 + HNO_3 \qquad (1.8)$$

$$ClONO_2 + H_2O \rightarrow HOCl + HNO_3 \qquad (1.9)$$

$$HOCl + HCl \rightarrow Cl_2 + H_2O. \qquad (1.10)$$

Reactions (1.8)-(1.10) are prohibitively slow in the gas phase[6], but they proceed efficiently in the presence of PSC surfaces[2,7-15]. The Cl_2 produced by these processes is readily photolyzed to form free radicals capable of catalyzing ozone destruction via reactions (1.6) and (1.7).

PSCs form only during the polar night, when temperatures are sufficiently low that the very little water that exists in the stratosphere can condense into particle form[4]. PSC particles have been classified into three types: nitric acid trihydrate (type Ia PSC), a supercooled ternary solution of $HNO_3/H_2SO_4/H_2O$ (type Ib PSC), and water-ice (type II PSC). However, the exact compositions and formation mechanisms of the particles are unknown[16,17]. The type II water-ice PSCs are thought to be composed of single crystalline hexagonal ice, since they form very slowly and at low temperatures. The size of a type II PSC particle is on the order of 1-10 μm[18].

Characterization of the interaction of HCl with ice is the first step towards understanding chlorine activation. HCl has been found to be the most abundant chlorine reservoir during PSC

events, and its reaction with $ClONO_2$ on ice, reaction (1.8), is thought to be the most important of the chlorine activation processes[3]. The reaction probability, γ of reaction (1.8) on ice has been found in several laboratory studies to be high ($\gamma > 0.1$)[2,7-13] and independent of HCl partial pressure, even at very high HCl partial pressures which are known to induce melting of the ice sample[9].

The HCl-ice system has been investigated using a variety of experimental[2,7-9,19-58] and theoretical[59-74] approaches. While much uncertainty remains about the fate of HCl upon adsorption to ice, these studies have lead to a consensus that HCl has a high affinity for ice surfaces, with near monolayer coverage at conditions relevant to PSC events ($3 \cdot 10^{-8}$ Torr < P_{HCl} < $2 \cdot 10^{-7}$ Torr, -85 °C < T < -70°C). Assuming that HCl makes at most a very strong hydrogen bond with a refractory ice surface, calculations predict at least two orders of magnitude less surface coverage than what has been reported[3].

To explain the catalytic role PSC particle surfaces play during chlorine activation, we have hypothesized that HCl might induce the formation of a disordered region on the ice surface, or 'quasi-liquid layer' (QLL), at stratospheric conditions[3]. The QLL is known to exist on the surface of ice at temperatures near the melting point, but the existence of a disordered region on the surface of ice has not been confirmed at stratospheric temperatures.

The goals of this research have been to test this hypothesis, clarify the catalytic role that the ice surface plays in chlorine activation, and further elucidate the fate of HCl upon adsorption to ice. We have studied the interaction of HCl with ice under a wide range of conditions including those encountered in the stratosphere during PSC events using the complementary approach of a) ellipsometry to monitor the ice surface with chemical ionization mass spectrometry (CIMS) detection of the gas phase, and b) flow tube experiments with CIMS

detection to further study the kinetics of HCl adsorption on various ice surfaces.

We have also studied the $ClONO_2$+HCl reaction on ice and the co-adsorption of acetic acid, CH_3COOH, and HCl on ice using the flow-tube CIMS technique, to obtain further information about the state of the ice surface and the fate of the HCl molecules upon adsorption to ice. Characterizing the interaction of CH_3COOH with ice surfaces is also relevant to understanding the scavenging potential of cirrus cloud ice particles in the upper troposphere.

These studies are part of a multipart approach which also included molecular-level modeling work performed by Yves Mantz of the Molina group in collaboration with Prof. Bernhardt Trout's group in the MIT Department of Chemical Engineering[59,60,75].

1.2 The HCl-ice system: Literature review

The HCl-ice system has been studied intensely over the past two decades, with hundreds of publications available in the literature on the subject. In this section we provide an overview, focusing on the state of the ice surface and the fate of HCl upon adsorption on ice.

1.2.1 The ice surface

At stratospheric temperatures and pressures, the stable phase of ice is the crystalline hexagonal form, ice I_h[76]. The structure of ice I_h is shown in Figure 1-1.

Ice is a high vapor pressure substrate, with a vapor pressure of approximately 10^{-4} Torr at -73 °C. Haynes et al.[77] studied the dynamic nature of ice surface via a classical molecular dynamics simulation and found that at stratospheric conditions, the equilibrium evaporation and recondensation rate of water at the surface of an ice particle is 10-1000 monolayers per second, implying a turnover period for the ice surface of 0.1-0.001 s.

A disordered region, or 'quasi-liquid layer' (QLL), is known to exist on the ice surface at

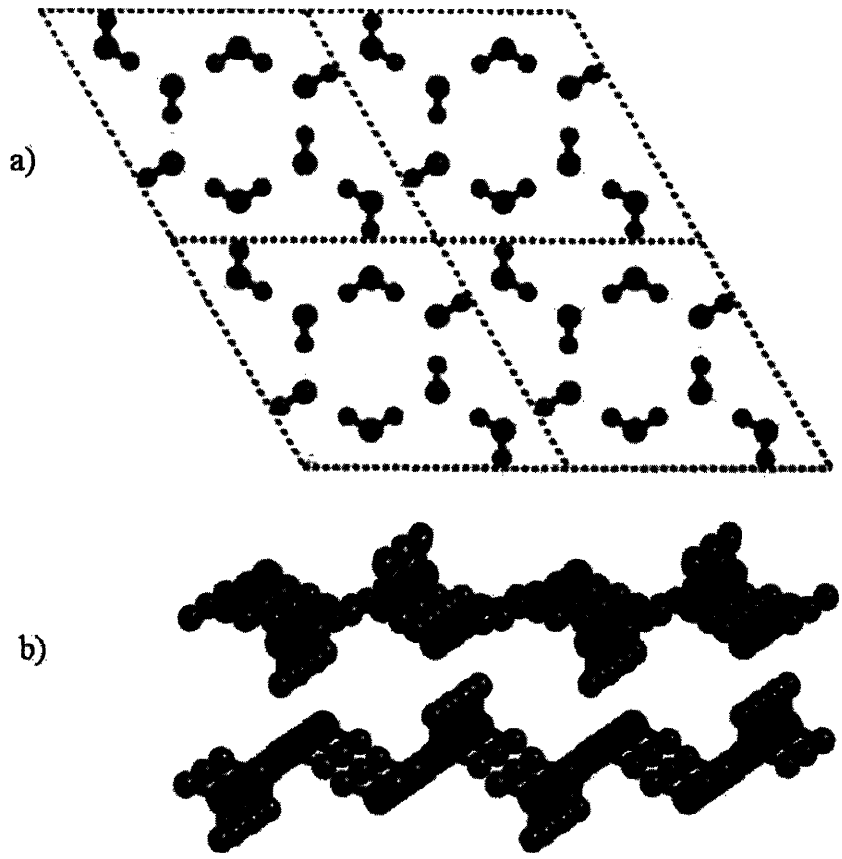

Figure 1-1. Ice I_h: a) top view of the 001 surface, along the c axis b) side view of the top two bilayers. Large spheres represent oxygen molecules, small spheres represent hydrogen. The hydrogen molecules coming out of the plane of the surface are referred to as 'dangling –OH groups.' Images courtesy of Yves Mantz.

temperatures near the melting point. Thermodynamic theories based on Gibbs surface free energies disallow the possibility of a QLL at temperatures below approximately -30°C [78], and no experimental observation of the QLL has been reported thus far for conditions relevant to the polar stratosphere.

A variety of experimental[26,79-96] and theoretical[59,60,75,78,97-101] techniques have been used to study surface disorder on ice. Reported values of the temperature below which the QLL cannot be detected experimentally, T_{QLL}, vary depending on the ice samples studied (e.g., thin films,

single crystals, polycrystalline samples, or amorphous forms). Furthermore, the experimental techniques used vary in their sensitivity to surface properties, and each implicitly employs its own definition of the QLL. Figure 1-2 shows a summary of QLL thickness v. temperature data available in the literature.

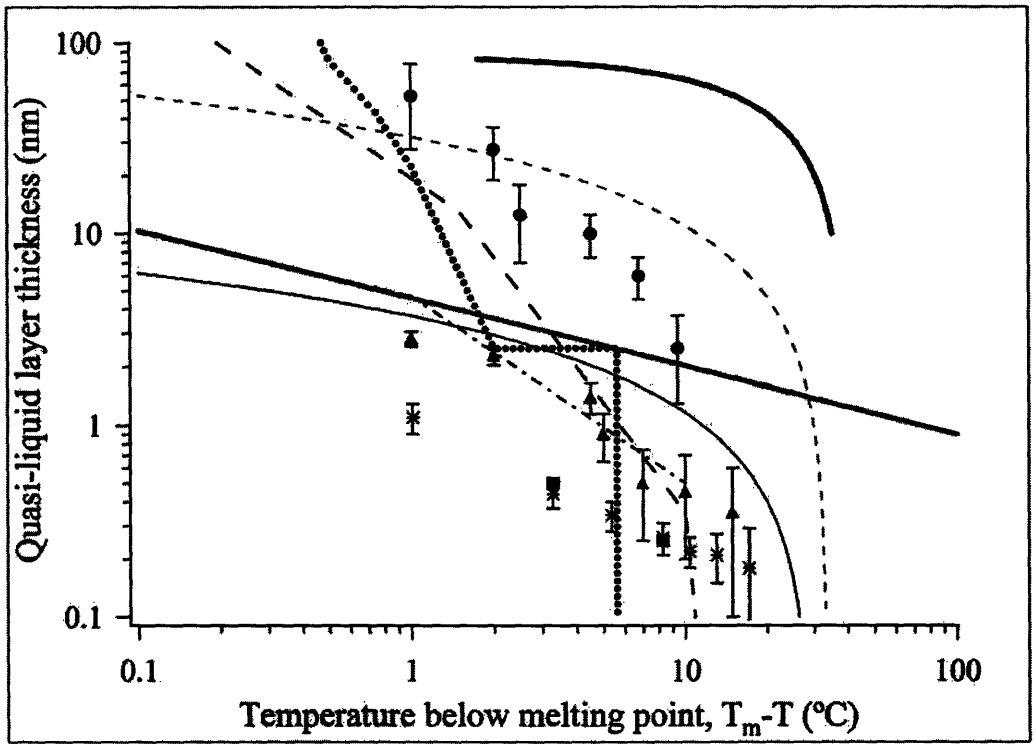

Figure 1-2. Literature summary of experimental QLL thickness v. temperature data for the basal face of ice. See the text for more details. The thick black line denotes the proton channeling data of Golecki and Jaccard[88]. The dashed grey line and the stars represent the AFM data of Doeppenschmidt et al.[84] and Pittenger et al. [85], respectively. Circles are data obtained using glancing angle X-ray scattering[87]. The dashed and dotted black lines represent data from the ellipsometer studies of Beaglehole and Nason[91] and Furukawa et al. [92], respectively. The solid grey line represents wire regelation data[94]. The thin black line represents data from a study of the Volta potential difference between single crystals of ice and different metals[95]. The dot-dashed black line represents IR data[82]. Triangles are data obtained using photoelectron spectroscopy[83]. Squares are data obtained using neutron scattering for ultrathin films [96].

Investigators using pulsed spin-lattice relaxation NMR to study small ice particles (less than 150 μm in diameter) observed surface water molecules rotating at higher frequencies than bulk water molecules at temperatures as low as -100°C [79]. It should be noted that at -100°C ice I_h may no longer be the stable phase. Sum frequency generation (SFG) spectroscopy shows disorder in the dangling –OH groups on the basal face of single crystals of ice I_h at temperatures above -73 °C [80,81]. Studies performed on vapor-deposited thin ice films using infrared extinction[82] and photoelectron spectroscopy[83] indicate that the free hydrogen peak disappears below approximately -20 °C.

Several studies of surface disordering on ice have been performed using experimental techniques that define T_{QLL} as the onset temperature for increased translational mobility of the water molecules in the upper layers of the ice surface, including atomic force microscopy (AFM)[84,85], scanning force microscopy (SFM)[86], glancing angle X-ray scattering[87], and proton channeling[88]. Doeppenschmidt and Butt used AFM to study premelting on the surfaces of ~1mm thick polycrystalline ice samples formed by freezing from the melt, and found that T_{QLL} = -34 °C [84]. Pittenger et al. also used AFM and reported that T_{QLL} = -10 °C for 0.5 mm thick vapor-deposited ice samples[85]. Petrenko used scanning force microscopy[86] to study the surface of single crystals of ice and found that capillary forces between the probe and the surface disappeared at -20°C. Dosch et al. used glancing angle X-ray scattering to study disordering on the basal face of ice I_h single crystals and reported T_{QLL} = -13.5 °C [87]. Golecki and Jaccard found using proton channeling that the basal plane face of ice I_h single crystals is highly disordered above -40 °C [88]. Wilson et al. used differential scanning calorimetry to study polycrystalline ice samples formed by freezing from the melt, and found that T_{QLL} = -15 °C [89]. Orem and Adamson studied the adsorption of *n*-alkanes to powdery ice samples between -53°C

and -30°C and observed a transition in the adsorbate-surface interaction at -35 °C [90]. Above that temperature *n*-alkane adsorption to the ice surface resembled adsorption to the surface of liquid water. The temperature at which the transition between ice-like and liquid-like adsorption behavior was observed by Orem and Adamson, -35 °C, lies towards the low end of the range of reported values that can be found in the literature for T_{QLL}. This may imply that the presence of the *n*-alkane molecules suppressed T_{QLL} in Orem and Adamson's experiments.

Finally, the results of three studies of the structure of the basal and prismatic faces of hexagonal ice using low-sensitivity ellipsometry[91,92] and optical reflectometry[93], both of which measure the optical properties of the surface, showed no sign of surface disorder at temperatures below approximately -5°C.

In summary, all of the experimental studies discussed here indicate that surface disorder does exist on ice near the melting point, and that the thickness of the disordered layer increases with increasing temperature. However, reported values of T_{QLL} and the temperature dependence of the QLL thickness vary widely with definition of the QLL inherent to the experimental technique, the ice samples analyzed, and the sensitivity of the technique.

Theoretical models of the surface of ice include those based on the minimization of surface free energy[78], mean field theory[97], the theory of dispersion forces[98], the transition of ice at the surface into the Bernal-Fowler state[99], and molecular dynamics studies[59,60,75]. All support the same general picture presented by the experimental studies of a disordered layer on ice near the melting point, with thickness increasing with increasing temperature. However, like the experimental studies, the theoretical predictions for T_{QLL} and layer thickness vary depending on the approach.

Wettlaufer[101] predicted theoretically that T_{QLL} could be suppressed by the presence of an

ionic impurity on the ice surface, and that the dependence of layer thickness on temperature could be altered by the presence of the impurity as well. Support for these results for T > -30 °C and HCl partial pressures close to the solid-liquid equilibrium line on the HCl-ice phase diagram can be found in the experimental work of Diehl et al[26].

The issue of HCl-induced surface disordering at stratospherically relevant temperatures has not been studied as extensively as the QLL near the melting point. Dermidjian et al.[19] used neutron diffraction and quasielastic neutron scattering to study HCl-induced surface disordering on ultrathin ice films (5 H_2O bilayers on an MgO substrate). They found that the presence of HCl does induce surface translational mobility on the films, but only for temperatures greater than -23°C. However, they also observed a phase transition at -23°C from crystalline to amorphous structure for the ultrathin ice films used in the study, indicating that those films are poor proxy surfaces for PSC particles. Geiger et al.[102] used the spectroscopic technique Second Harmonic Generation (SHG) to study the interactions of $ClONO_2$, HOCl, and HNO_3 with single crystals of ice at stratospherically relevant conditions. They found that the adsorption of HNO_3 and HOCl to the ice surface did not induce any change in the symmetry of the surface at -88 °C, and suggested that this rules out the possibility of surface melting under those conditions. Livingston et al.[21], using laser-induced thermal desorption (LITD), observed that the presence of HCl enhances D_2O desorption from ice surfaces by a factor of ~2 at temperatures from -123 °C to -102 °C. They inferred from this that HCl enhances overall mobility of H_2O in ice, perhaps via substitutional incorporation of HCl into ice lattice or HCl-induced ice 'softening.' Fluckiger et al.[23,24] studied $ClONO_2$ titration of HCl- dosed ice with a Knudsen cell apparatus and estimated the thickness of an HCl-rich near-surface region to be on the order of 100 nm for single-crystalline ice, and larger for polycrystalline ice samples.

HCl-induced disorder at stratospheric temperatures was predicted theoretically by Mantz et al[59]. They modeled HCl interacting with a periodic ice slab using density functional theory. Using their model, they predicted that HCl adsorbed to surface sites with a high local density of dangling –OH bonds would form a contact ion pair and induce surface disorder down to the second bilayer at approximately -83 °C.

1.2.2 HCl-ice phase diagram

Several investigators have studied the HCl-ice system at a wide range of conditions to determine the thermodynamically stable phases of the system as a function of the temperature and HCl partial pressure. Wofsy et al.[27] were the first to construct an HCl-ice phase diagram using extrapolations of solubility and vapor pressure data that were available in the literature at that time. Hanson and Mauersberger[28] performed vapor pressure measurements over solid and liquid HCl-water systems at low temperatures. They used this information to expand the HCl-ice phase diagram, and their contributions include introducing the metastable phase HCl hexahydrate ($HCl{\cdot}6H_2O$) to the phase diagram. There is a nucleation barrier to HCl hexahydrate formation[29]. It was reported by several groups that it is difficult to generate HCl hexahydrate by exposing ice to HCl vapor or freezing from the liquid but it can be formed readily by rewarming a solution that has been supercooled to -150 °C [9,28,30,31].

Abbatt et al.[9] used a variety of experimental techniques, and, in addition to investigating the hydrate stability regimes of the phase diagram, verified that high concentrations of HCl melt the ice crystal upon adsorption to form a liquid HCl-water solution. Wooldridge et al.[30] used thermodynamic calculations to predict stability regions for the HCl hydrate phases and coupled these calculations with vapor pressure measurements to provide a more detailed phase diagram.

The phase diagram presented in Molina et al.[3], reproduced in Figure 1-3, is a digest of these early studies. As shown in Figure 1-3, 'Ice' is the stable phase under polar stratospheric conditions.

In a recent FTIR study, Xueref and Dominé[32] studied co-condensed HCl/ice mixtures at -83 °C, with HCl:H_2O ratios of 5:1, 1:10, 1:50, and 1:200. They found that in all cases the HCl was in ionic form once it had been incorporated into the bulk, and that the lattice did not take the form of the any of the known crystalline HCl hydrate phases but rather was disorganized. They suggested that such co-condensed materials might be more relevant to stratospheric chemistry than the more typical laboratory system of HCl gas adsorbing to a pure ice surface.

1.2.3 HCl in bulk ice: Diffusion and solubility

HCl has been reported to have low solubility and low diffusivity in bulk ice. Hanson and Mauersberger[28] used vapor pressure data and applied Raoult's law to determine that the solubility of HCl in ice is less than 0.01 mol% under stratospheric conditions. Wolff and Mulvaney[33], using X-ray analysis, reported strong partitioning of HCl towards the grain boundaries of polycrystalline ice, and they showed that HCl is not easily incorporated into ice crystals. They reported the diffusion coefficient for HCl diffusion into bulk ice to be between 10^{-13} and 10^{-10} cm^2s^{-1} at an ice temperature of 185 K. In 1997, Thibert and Dominé[34] reported a diffusion coefficient of HCl in large single crystals of ice at -15°C of 10^{-12} cm^2s^{-1}. They also found a correlation for solubility that can be used to extract a value of $3.5 \cdot 10^{-7}$ moles $HCl \cdot cm^{-3}$ for adsorption at -73 °C with 10^{-6} Torr HCl.

Based on a kinetic analysis of their $ClONO_2$ titration Knudsen cell experiments, Fluckiger et al. inferred the diffusion coefficient $D_{HCl\text{-}ice}$ to be between $1.2(5) \cdot 10^{-13}$ $cm^2 \cdot s^{-1}$ for bulk ice and $1.2(5) \cdot 10^{-13}$ cm^2s^{-1} for single-crystalline ice at stratospherically relevant temperatures[24].

Krieger et al.[35] used Rutherford backscattering to obtain near-surface elemental depth profiles of frozen HCl solutions at two concentrations. For low concentrations (0.022 mol %), they observed that the HCl concentrated at the sample surface, and they attributed this to the low

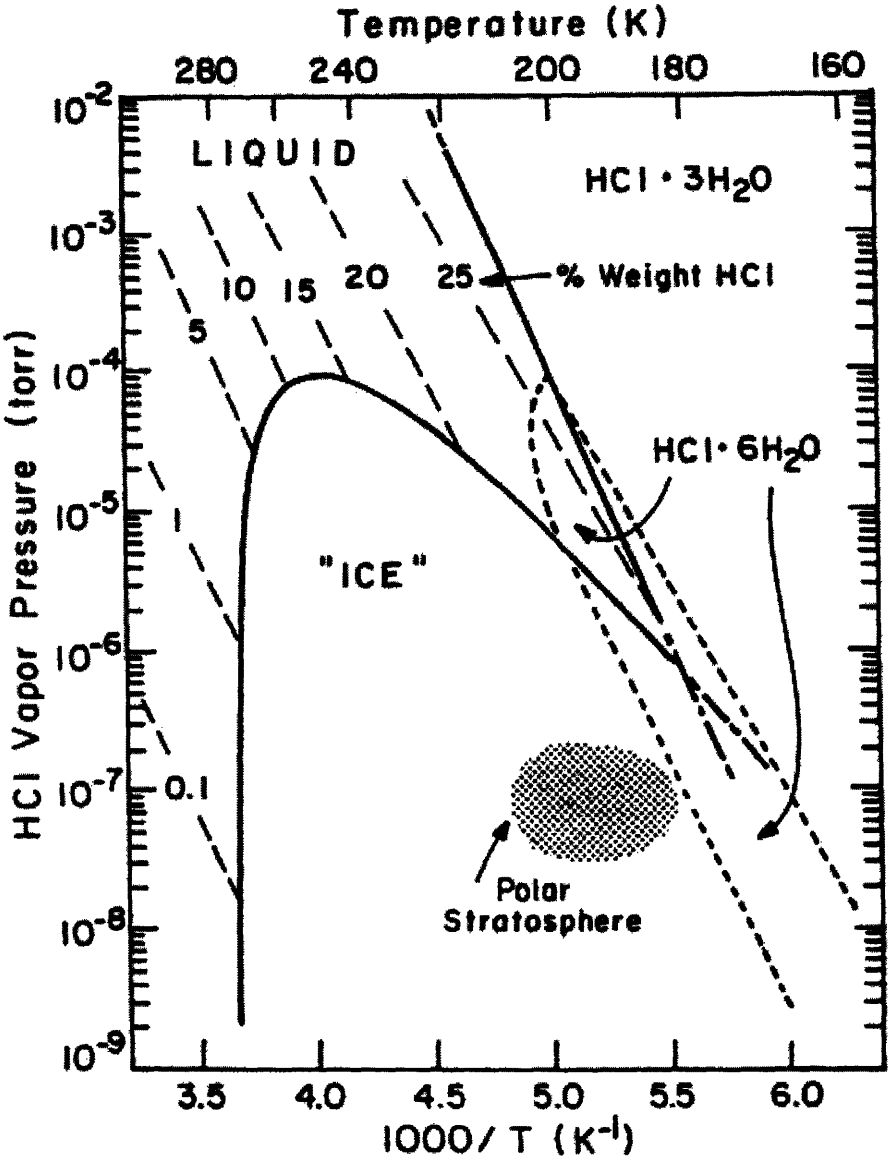

Figure 1-3. The HCl-ice phase diagram, reproduced from Molina[3]. Thermodynamically stable phases are shown as a function of temperature and HCl partial pressure[3,28]. "Ice" is the stable phase under polar stratospheric conditions (circled area). "Liquid" refers to a liquid solution, and "Trihydrate" and "Hexahydrate" refer to the crystalline hydrate states.

diffusivity and solubility of HCl in ice. From their measurements they estimated that $5 \cdot 10^{-12}$ cm^{2}s^{-1}< $D_{HCl\text{-}ice}$ < $3 \cdot 10^{-11}$ cm^{2}s^{-1} for the low-concentration samples. For higher concentrations (5.4 mol %), they observed a more linear depth profile for HCl concentration and estimated that $4 \cdot 10^{-9}$ cm^{2}s^{-1}< $D_{HCl\text{-}ice}$ < $1.6 \cdot 10^{-8}$ cm^{2}s^{-1}. They concluded from their observations that with increased doping in polycrystalline ice, grain boundaries or triple junctions containing concentrated HCl solution become the dominant sink for HCl uptake.

1.2.4 HCl adsorption on ice surfaces

We begin this subsection by discussing several studies of the interaction of gas phase HCl with ice surfaces using techniques that allow experimentation at stratospherically relevant temperatures, including flow tube and Knudsen cell studies. We then address studies that were conducted at lower temperatures.

1.2.4.1 Stratospherically relevant conditions

One of the most widely used experimental techniques for studying the adsorption of HCl onto ice surfaces is the coupling of a coated-wall fast flow tube reactor with mass spectrometer detection. This technique is simple but powerful in that it allows study of the HCl-ice system under stratospherically relevant conditions and with the ice sample at equilibrium conditions. One drawback of this technique is that it does not offer direct information about the physical state of the surface or the state of molecules adsorbed on the surface, but offers analysis only of the gas phase. With careful experimental design, however, the gas phase analysis can be used to infer information about surface processes. An additional drawback of this technique is that the laminar flow profile in the flow tube causes reactions on the surface to be diffusion-limited, limiting the range of accuracy of kinetic studies of heterogeneous reactions on the ice surface[7].

Abbatt et al.[9], in addition to other techniques, used a flow tube coupled to an electron impact mass spectrometer (EIMS) to study HCl uptake onto vapor-deposited ice films at stratospherically relevant temperatures. They observed that HCl was taken up in near-monolayer amounts on the ice surface in the 'ice' region of the HCl-ice phase diagram. They also reported some apparently irreversible loss of HCl to the bulk, which they attributed to diffusion into the ice matrix.

Hanson and Ravishankara[8] used a flow tube with high-sensitivity chemical ionization mass spectrometry (CIMS) detection to study HCl adsorption on vapor-deposited ice films under polar stratospheric conditions. They observed a memory effect in that an average uptake of $5(1)\cdot10^{14}$ molecules$\cdot$cm^{-2} was observed upon the first exposure of an ice film to HCl, but in subsequent exposures uptake was approximately $2\cdot10^{14}$ molecules$\cdot$cm^{-2} (surface coverages were reported assuming the surface area of the vapor-deposited ice film to be equal to the geometric area). Additionally, upon the first exposure of a fresh ice surface to HCl, only a fraction of HCl was recovered upon desorption, indicating both reversible and irreversible adsorption processes. The irreversibly adsorbed HCl was observed to be unrecoverable up to 30 min after exposure. The authors made the argument that since the penetration depth, which they estimated as being equal to $(Dt)^{1/2}$, is less than 1μm on the time scale of the experiment (~1000 s), diffusion should play a minor role in the observed HCl uptake, and diffusion into the bulk would be so slow that almost all HCl should be concentrated at the surface.

Chu et al.[36] performed similar flow tube-CIMS studies of HCl adsorption on vapor-deposited ice samples, also at stratospherically relevant conditions. They paid special attention to the preparation method of the ice samples, and reported that HCl uptake on vapor deposited ice films is sensitive to the thickness of the film. They reported a linear dependence of uptake on

HCl pressure. They analyzed this pressure dependence with a Langmuir-type model, and reported that HCl surface coverage goes like the square root of the partial pressure of HCl, implying a dissociative adsorption scenario where the adsorbate occupies two identical surface sites. Finally, they made a similar argument to that presented by Hanson and Ravishankara against significant diffusion into the bulk.

More recently, Hynes et al.[37] used the flow tube-EIMS technique to study the interaction of HCl with smooth ice samples formed from the melt at tropospherically relevant conditions (between -68 °C and -43 °C). Like Hanson and Ravishankara, they observed a memory effect, and reported that up to 70% of incident HCl molecules were irreversibly adsorbed in their experiments at -68 °C. At $1.1 \cdot 10^{-6}$ Torr HCl, they observed that the uptake coefficient, γ, of HCl on ice decreased smoothly from $\gamma > 0.1$ at -73 °C (referring to the data of Fluckiger et al.[22], which was measured at much higher P_{HCl}) to $\gamma < 0.01$ for temperatures of approximately -50 °C and higher.

Another powerful experimental technique that allows study of the HCl-ice system under stratospherically relevant conditions is the Knudsen cell. This technique does not have the diffusion limitations of the flow tube technique and can thus provide real-time kinetic information, although like the flow tube, it can only provide indirect information about surface processes via gas-phase analysis. An additional drawback to the Knudsen cell technique is that the partial pressure of HCl for each experiment cannot be known *a priori* and must be inferred from the experimental data[22]. Finally, when studying ice, a Knudsen cell apparatus must be modified to maintain the sample in equilibrium with water vapor and prevent net evaporation during the experiment[38].

The Rossi group has used the Knudsen cell technique extensively to study the interaction

of HCl with various types of ice between -83 °C and -63 °C [22-25]. Their early studies were performed at such high partial pressures of HCl as to be on or near the solid-liquid equilibrium line on the HCl-ice phase diagram, which may have complicated the interpretation of their results[22]. Subsequent studies were performed at or above $3.6 \cdot 10^{-6}$ Torr HCl, conditions where we observed HCl-induced surface disordering using ellipsometry[23]. They reported a memory effect and also irreversible surface-to-bulk loss of HCl[22,23,25]. To further investigate the fate of the irreversibly adsorbed HCl, they used the reaction with $ClONO_2$ to probe the availability of HCl in the surface region, for ice samples that had been exposed to gas phase HCl and for co-condensed ice samples. In exposing the surface to $ClONO_2$, they titrated away the available HCl, but also consumed the ice sample via the hydrolysis reaction of $ClONO_2$ and H_2O, forming a HNO_3 hydrate layer. Based on a kinetic analysis of these experiments, they concluded that, under these conditions, HCl diffuses from the surface to a near-surface region where it is still readily available for reaction. By applying a model which assumes a saturated near-surface region with diffusion from that relatively concentrated region into the bulk, they inferred the HCl-ice diffusion coefficient, $D_{HCl\text{-}ice}$, and the thickness, h, of the near-surface region. They reported $D_{HCl\text{-}ice} = 8.0(5) \cdot 10^{-15}$ $cm^2 \cdot s^{-1}$ and $h = 60$ +/- 10 nm for single-crystalline ice and $D_{HCl\text{-}ice} = 1.2(5) \cdot 10^{-13}$ $cm^2 \cdot s^{-1}$ and $h = 130$ +/- 20 nm for bulk (polycrystalline) ice[24].

Huthwelker et al.[38] also used a Knudsen cell to study ice films at -83 °C and -70 °C. The ice sample was kept in equilibrium with water vapor. They report two adsorption modes, an initial fast adsorption mode and at longer times a 'diffusion-like' uptake mode where the uptake coefficient exhibits a $t^{-1/2}$ time dependence. They observed memory effect in that a larger initial uptake was observed upon the first exposure of an ice crystal to HCl than in subsequent exposures. In subsequent exposures, the diffusion-like adsorption mode was dominant. They

inferred dissociative adsorption from the pressure dependence of their data using a Langmuir model with an additional diffusive component. They also offered as an alternative interpretation of the observed diffusion-like loss that it could be attributed to ongoing surface restructuring.

1.2.4.2 Low temperature studies

Many surface science techniques requiring ultra-high vacuum (UHV) conditions provide additional insight that is not available from the flow tube and Knudsen cell techniques into the state of the ice surface and the state of adsorbed molecules. However, since ice is a high vapor-pressure substrate (the water vapor pressure over ice is approximately 10^{-4} Torr at -73 °C), for any experimental technique requiring UHV conditions, studies of ice surfaces must be conducted at temperatures lower than those relevant to the polar stratosphere. As a result, many such studies have been conducted in the region of the HCl-ice phase diagram where HCl trihydrate or HCl hexahydrate is the stable phase. Many studies are conducted on samples of ice which are in a different phase from the hexagonal crystalline structure I_h, which is dominant at stratospherically relevant conditions, such as amorphous ice. Given the different physical and chemical state of the HCl-ice system under these conditions, it is difficult to draw conclusions about PSCs based on the results of low temperature studies.

Temperature programmed desorption (TPD) coupled with gas phase detection has been used by a number of groups to study the HCl-ice system at lower temperatures[39-43]. In TPD studies, the ice sample is dosed with HCl and then warmed. The evolution of HCl from the dosed sample as a function of temperature is then observed, and information about the state of adsorbed species can be inferred. More strongly bound species, or those confined to the bulk, desorb at higher temperatures, while species held to the surface via weaker bonds desorb at lower temperatures.

Graham and Roberts[39-42] used TPD/FTIR to study HCl adsorbed on amorphous and low-temperature crystalline ices. They observed two adsorbed HCl states, HCl hexahydrate and HCl molecularly adsorbed onto the hexahydrate surface. They found that hexahydrate formation was faster and surface adsorption more likely on amorphous ice than crystalline ice, and concluded that this is due to a lower concentration of dangling –OH groups and defects on the crystalline ice surface. Sadtchenko et al.[43] studied HCl interacting with amorphous ice, annealed amorphous (crystalline) ice, and crystalline vapor-deposited ice using TPDMS. Like Graham and Roberts, they observed molecular surface-adsorbed HCl. They observed two hexahydrate modes, corresponding to bulk hexahydrate and surface hexahydrate. Sadtchenko et al. suggested that HCl hexahydrate formation originates in the grain boundaries for lower temperature ices.

Molecular beam mass spectrometric techniques have also been used to study the sticking of HCl on low-temperature ices. In a pulsed molecular beam study employing HCl doses corresponding to coverages of 0.01 ML per pulse and ice temperatures between -173 °C and -103 °C , Isakson and Sitz[44] reported both first-order adsorption and an irreversible surface loss of HCl, which they attributed to HCl ionization or hydration, but not diffusion into the bulk of the ice substrate. Andersson et al.[45], using molecular beam techniques at 127-180 K, determined that the residence time for HCl on bare ice is greater than 0.001 s at those temperatures, even for a slowly evaporating surface.

The high efficiency of reaction (1.8) suggests a reaction mechanism in which HCl is in ionic form. There is overwhelming experimental evidence that HCl ionizes upon adsorption to ice films at very low temperatures[46-57], but only indirect evidence of ionization at polar stratospheric conditions exists[36-38,103]. Barone et al.[58] performed FTIR studies which were designed to test the possibility of HCl ionization at stratospheric temperatures, and found

ionization in the "liquid" area in the phase-diagram, but could not unambiguously identify H_3O^+ for the 'ice' regime.

1.2.4.3 Theoretical studies

For a review of the many theoretical studies of HCl interacting with model ice surfaces or small water clusters in the literature, see Girardet and Toubin[104]. In general, HCl is found to act as a hydrogen donor, and HCl-water binding energies have been reported to be between 19 and 31 kJ/mol[59-72]. As mentioned in Section 1.2.1, Mantz et al[59] modeled HCl interacting with a periodic ice slab using density functional theory and predicted that HCl adsorbed to surface sites with two or more local dangling –OH bonds would form a contact ion pair and induce surface disorder down to the second bilayer at approximately -83 °C. They found that the contact ion pair formed in a stepwise mechanism, and that the ionized form was 21 kJ/mol more stable than molecularly adsorbed HCl under the same conditions. Similarly, Svanberg et al., using a coupled quantum mechanics/molecular mechanics (QM/MM) technique, reported that dissociation on the ice surface was not observed unless HCl was surrounded by four water molecules or more[68]. Calatayud et al., using density functional theory and a periodic model of the ice surface, showed barrierless ionization of HCl in cubic ice if HCl is placed within the ice lattice rather than on the surface[73]. Similar conclusions were drawn from an *ab initio* study of HCl embedded in an orthorhombic ice cluster model[74].

1.3 Experimental techniques

1.3.1 Ellipsometer-CIMS experiments

A schematic of the experimental setup used in the ellipsometer-CIMS experiments is

shown in Figure 1-4.

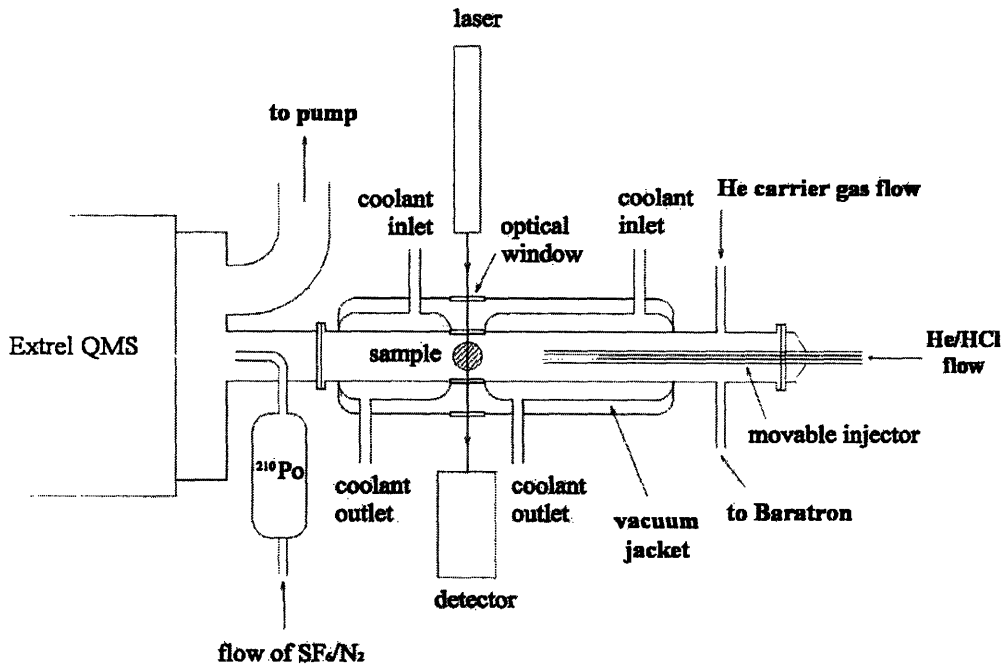

Figure 1-4. Experimental apparatus for the ellipsometer-CIMS experiments.

The ellipsometer used in this study (Beaglehole Instruments) employs a photoelastic birefringence modulator, allowing high sensitivity measurements. The light source is a 50 mW He/Ne laser, focused to a diameter of approximately 1 mm. We observed true melting at 0 °C, and did not observe surface disorder far from the solid-liquid equilibrium line in the HCl-ice phase diagram. Therefore, we infer that the laser does not melt the ice surface due to local heating. The ice sample was placed in an aluminum sample holder and housed in a vacuum-jacketed flow tube. The flow tube was fitted with quartz windows to allow the laser beam to pass through the cooling jacket and flow tube walls, and was operated in the laminar flow regime ($Re < 100$) with helium, He, as a carrier gas. Ice was placed upstream of the main ice sample to

ensure that the sample was in equilibrium with water vapor, i.e., no net evaporation or condensation took place. The flow tube was interfaced with a CIMS system (Extrel C50) to monitor the gas phase composition via chemical ionization by SF_6^- reagent ions. SF_6^- ions were generated in a sidearm attached at a right angle to the flow tube using α-particle bombardment from a ^{210}Po source operating at -4 kV. HCl was monitored as SF_5Cl^- (162 amu). In the HCl uptake experiments, the ice sample was exposed to a dilute mixture of HCl in He that was introduced to the main He flow through a moveable injector positioned near the centerline of the flow tube. The injector was heated to prevent experimental artifacts due to adsorption of HCl to the injector walls, creating a temperature gradient of less than 1°C in the flow tube.

1.3.2 Flow tube-CIMS experiments

A schematic diagram of a typical experimental setup for the flow tube-CIMS experiments is shown in Figure 1-5. All flow tube-CIMS experiments employed a 2.5 cm i.d. flow tube operating in the laminar flow regime (Re < 100) that was interfaced with a CIMS system (Extrel C50). Detection occurred via chemical ionization using SF_6^- as a reagent ion. SF_6^- ions were generated in a sidearm attached at a right angle to the flow tube using a discharge needle operating at -4 kV. HCl and CCl_2F_2 were monitored as SF_5Cl^- (162 amu), $ClONO_2$ was monitored as $ClONO_2F^-$ (116 amu), Cl_2 was monitored as Cl_2^- (70 amu), and CH_3COOH was monitored as $CH_3CO_2HF^-$ (79 amu).

All flows were monitored with calibrated flow meters (Tylan General). He (BOC gases) was used as a carrier gas. A 1600 L/min rotary pump (Edwards EM280) established flow velocities of 1000-2000 cm/sec, with the corresponding Reynolds numbers well below the turbulence limit. The pressure inside the flow tube, measured with a 0-10 Torr MKS Baratron, was maintained constant at 1.5-2 Torr. A circulating cooler (Neslab ULT-95) was used to

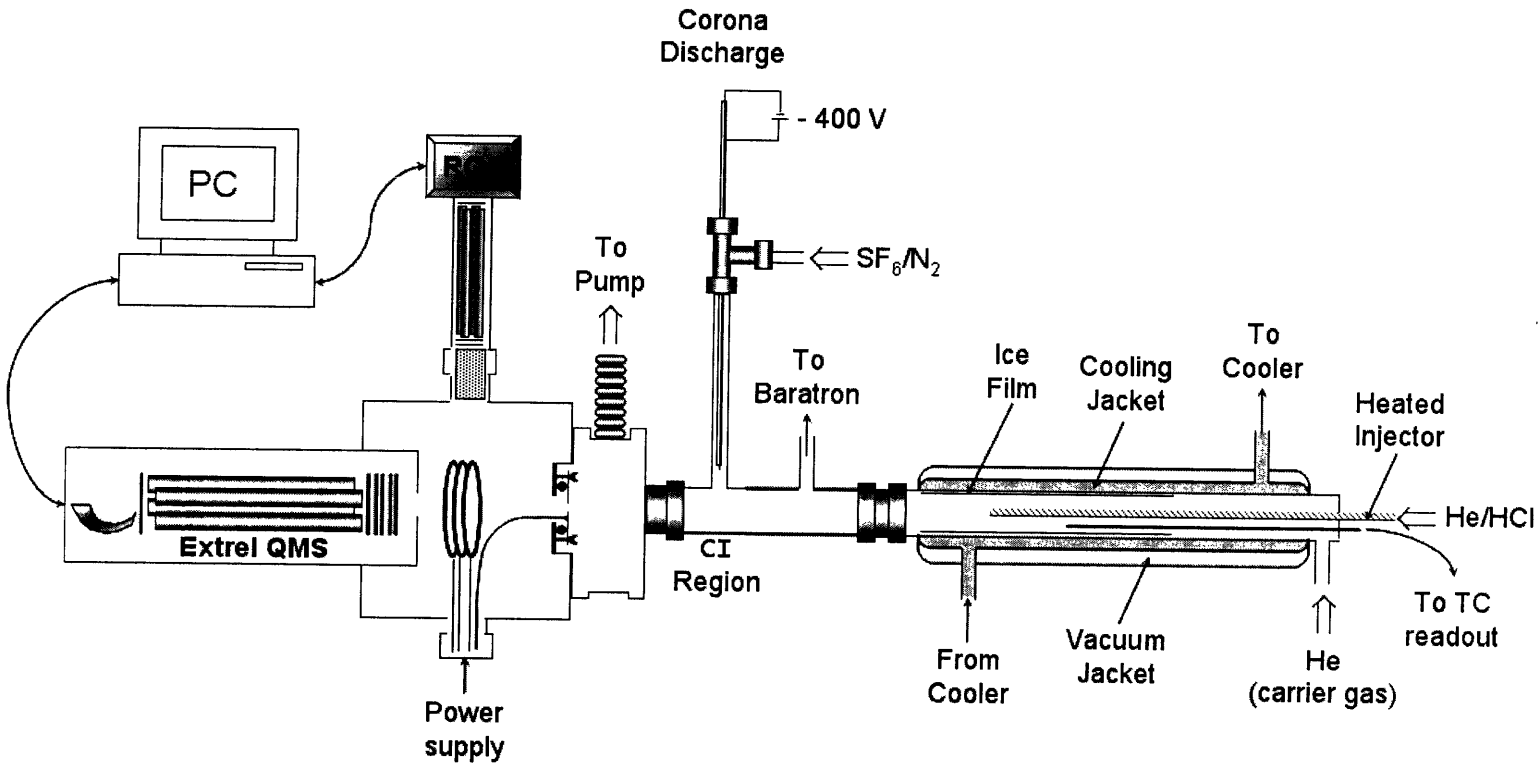

Figure 1-5. Experimental setup for flow tube-CIMS HCl adsorption experiments.

establish constant flow tube temperatures between -40 °C and -90 °C. Cooling fluid flowed through the cooling jacket of the flow tube countercurrent to the gas flow. In all uptake experiments a dilute mixture of each probe molecule of interest in He was introduced to the main He flow through a moveable injector positioned near the centerline of the flow tube. Two injectors were employed in the $ClONO_2$ + HCl experiments and the acetic acid/HCl coadsorption experiments, one for each molecule of interest.

The injectors were heated to prevent experimental artifacts due to adsorption of HCl to the injector walls. The temperature inside the flow tube was monitored using a copper/Constantan® thermocouple (Omega). The thermocouple was housed in a 1/8" glass tube, which was inserted into the cooled region of the flow tube parallel to the injector. The axial location of the thermocouple was arbitrary since there were no temperature gradients greater than 1 °C in the cooled region of the flow tube.

1.3.3 Water vapor pressure measurements

In additional experiments, an electron impact residual gas analyzer (Ametek Dycor MA200 RGA) was used to measure the water vapor pressures of ice films between -85 °C and -78 °C that were exposed to various pressures of HCl. The RGA was attached to a side port on the MS prechamber. Water vapor was monitored via the oxygen ion signal at 16 amu. We tested that the 16 amu oxygen ion signal was proportional to the absolute water vapor pressure in the flow tube by monitoring the signal as a function of time while heating the ice film. The resulting shape of the water vapor pressure curve agreed well with the shape of the vapor pressure curve reported by Marti and Mauersberger[105].

1.3.4 Ice sample preparation

Ice samples for the ellipsometry study were prepared from single crystals of ice grown using an adaptation of the Bridgeman technique[106]. These ice samples were observed using crossed polaroids to have grain sizes on the order of a few centimeters.

For the zone-refined ice experiments, hollow cylindrical ice samples were prepared using a modification of the Bridgeman technique[106] as follows: A 20 cm section of plexiglass tubing was plugged and filled with HPLC-grade water, with a cylindrical mask to form the central flow channel. The filled tube assembly was placed inside a freezer, and the water was allowed to solidify. The ice sample was then zone-refined using a heated ring which advanced slowly ($1 \mu m \cdot s^{-1}$) to the top of the cylinder, locally melting and refreezing the sample. For an adsorption experiment, the flow tube was first pre-cooled to -40 °C. The finished cylinder was inserted into the flow tube, and then the system was slowly cooled to the operating temperature to minimize cracking. He flow was maintained during insertion to create an overpressure in the flow tube and the injector in order to prevent condensation of water vapor from the ambient air inside the cold flow tube or the injector. The valve to the Edwards pump was throttled until the temperature reached at least -60 °C to prevent pumping away the sample. The sample thickness (~ 2 mm) could be measured directly outside the flow tube using calipers.

Ice samples prepared in this manner were observed using crossed polaroids to have grain sizes on the order of several millimeters. Figure 1-6 is a photograph of ice cylinder fragments before and after zone-refining, lit from behind and viewed through crossed polaroids. The zone-refined ice fragment consists of a few large crystals of ice, and therefore acts as a prism, visibly separating the white light into its constituent colors. The unrefined fragment, having smaller crystal domains, does not.

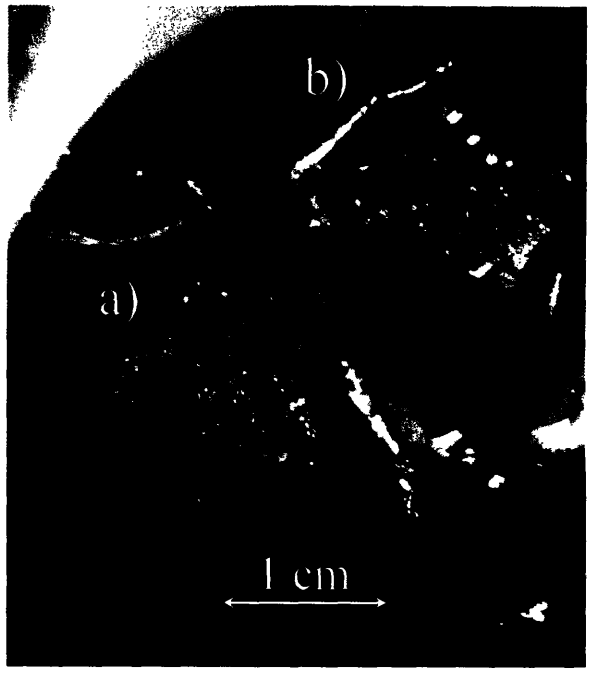

Figure 1-6. Ice cylinder fragments (a) before and (b) after zone-refining. The fragments are lit from behind and viewed through crossed polaroids.

Smooth ice films formed by freezing from liquid H_2O were prepared following the method of Abbatt[107]. The inside of a 35 cm long glass tube (2.5 cm i.d.) was washed with a 5% solution of HF in deionized water, thereby creating a wettable glass substrate. After thorough rinsing with HPLC grade water, the inside of the glass insert was wetted with a film of HPLC grade water. The insert was then placed inside the flow tube, which had been pre-cooled to operating temperature, while He was flowing to maintain an overpressure in the flow tube. Freezing occurred quickly due to the low temperature in the flow tube, yielding a polycrystalline ice film. The ice films formed this way were transparent and did not appear frost-like. Since approximately 5mL of water was used to prepare each ice film, and each film was approximately 10 cm long, we estimate the thickness of these films to be several hundreds of microns.

We also prepared vapor deposited ice films on the inside of the glass insert described in

the previous section. The procedure for vapor deposition of ice films has been described in the literature[9,108]. Dry He was passed through a water bubbler, and then the saturated stream was introduced to the flow tube via a wide-bore (0.25") injector, resulting in a water vapor deposition rate of 3-5 $mg \cdot min^{-1}$. The injector was heated to prevent water vapor from freezing inside and clogging the injector. The resulting deposition temperature was approximately -40 °C. 10 cm-long films were prepared by withdrawing the deposition injector 1 cm every 15-20 min, resulting in films of a calculated thickness of a few hundred microns. Extra ice was deposited upstream of the ice sample to ensure that the sample was in equilibrium with water vapor, i.e., no net evaporation or condensation took place.

1.4 Modeling the flow tube experiments: General framework

Here we present the tools that will be used to analyze the results of the flow tube-CIMS experiments presented in Chapters 4 and 5. We discuss models of solute interaction with the ice film and present a numerical framework which can be used directly to analyze the experimental results of the flow-tube CIMS studies. This work is similar in approach to that of Behr, et al.[109].

1.4.1 Ice surface analysis

If adsorption is assumed to be barrierless, the adsorption rate constant, k_{ads}, is given by gas kinetic theory as[110]

$$k_{ads} = \frac{\gamma \omega A}{4V} = \frac{\gamma \omega}{2R} \qquad 1\text{-}1.$$

where γ is the sticking coefficient, and R is the flow tube radius. The molecular velocity, ω, is

$$\omega = \left(\frac{8 k_B T}{\pi M} \right)^{1/2} \qquad 1\text{-}2.$$

where M is the weight of one adsorbed molecule, k_B is the Boltzmann constant, and T is the temperature in Kelvin.

The rate constant for desorption is as follows:

$$k_{des} = A\exp\left(-\frac{E_{ac}^{d}}{\mathbf{R}T}\right) \qquad 1\text{-}3.$$

where E_{ac}^{d} is the activation energy of desorption, and **R** is the gas constant. In this study, k_{des} will be treated as a parameter to be determined.

For absorption of a solute into a film in which the solubility of the solute, C_{sat}, is known, at equilibrium

$$k_{ads}C = k_{des}C_{sat}\frac{V_{film}}{V_{gas}} \qquad 1\text{-}4.$$

where C is the gas phase solute concentration, and V_{film} and V_{gas} are the film and gas volumes, respectively.

One model for surface adsorption is the Langmuir model, based on the concept of a set number of adsorption sites on the surface. The fraction of occupied surface sites, θ, is dimensionless and is related to the surface coverage, c_s, as follows:

$$\theta = \frac{c_s}{S} \qquad 1\text{-}5.$$

where S is the surface site density. 10^{15} molecules·cm^{-2} is the value of S widely quoted for ice, although for a polar molecule such as HCl, and a real ice surface with defects, grain boundaries, variable density of dangling –OH groups, and surface disorder, the definition of an adsorption site becomes less certain. For one adsorbing species, the surface coverage is governed by the following rate equation which describes the balance of molecules adsorbing and desorbing from the surface:

$$\frac{d\theta}{dt} = k_{ads} C(1-\theta) - k_{des}\theta . \qquad 1\text{-}6.$$

Here, C is the gas phase solute concentration. Inherent in this formulation is the assumption that each adsorbing molecule occupies one site, and that neighboring molecules do not interact with one another. In the Langmuir model, k_{ads} is[111]

$$k_{ads} = \frac{\gamma}{S(2\pi M k_B T)^{1/2}} \qquad 1\text{-}7.$$

and the rate constant for desorption is approximated as

$$k_{des} = \frac{1}{S\tau}\exp\left(-\frac{\Delta G_{des} + E_{ac}^{d}}{\mathbf{R}T}\right) \qquad 1\text{-}8.$$

where τ is the residence time of a molecule on the surface and ΔG_{des} is the free energy of desorption. At equilibrium eq. 1-6 yields the Langmuir isotherm,

$$\theta = \frac{bP_{HCl}}{1 + bP_{HCl}} \qquad 1\text{-}9.$$

where b is the surface equilibrium constant,

$$b = \frac{k_{ads}}{k_{des}} . \qquad 1\text{-}10.$$

For an experimental system that is well-described by the Langmuir model, $b(T)$ can be determined from measured adsorption isotherm data using eq. 1-9. The plot of $\ln(b)$ vs $1/T$ will be linear and the slope of the line will yield energetic information as follows:

$$\ln b = a_1 + \frac{1}{T}\left(\frac{\Delta G_{des} + E_{ac}^{d}}{\mathbf{R}}\right) . \qquad 1\text{-}11.$$

For $bP_{HCl} << 1$, the Langmuir isotherm can be approximated as linear:

$$c_s \sim bSP_{HCl} . \qquad 1\text{-}12.$$

Additional effects may be incorporated into the surface balance in eq. 1-6 such as nearest-neighbor interaction, adsorbate disassociation (i.e. occupation of two adsorption sites by each adsorbate molecule), diffusion of the adsorbate on the surface, or incorporation of surface adsorbed solute molecules into the bulk.

First-order incorporation of surface adsorbed solute molecules into the bulk may be accounted for as follows:

$$\frac{d\theta}{dt} = k_{ads}C(1-\theta) - k_{des}\theta - k_{inc}\theta \qquad 1\text{-}13.$$

where k_{inc} is a rate constant for the incorporation process. The near-surface concentration would then be governed by

$$\frac{dC_s}{dt} = \frac{k_{inc}\theta}{l} \qquad 1\text{-}14.$$

where l is the thickness of the region of interest.

1.4.2. Diffusion through an ice slab

A schematic diagram of a solute diffusing from the surface into the interior of an ice slab is shown in Figure 1-7.

The concentration profile of the solute within the slab is governed by the mass transfer analog to the heat equation,

$$\frac{\partial C_i}{\partial t} = D_i \nabla^2 C_i \qquad 1\text{-}15.$$

where C_i is the solute concentration within the slab, and D_i is the diffusion coefficient of the solute in ice at the conditions of interest.

D_i has been reported to be 10^{-12} cm^2sec^{-1} for HCl in large single crystals of ice at -15°C by Thibert and Dominé[34]. We have estimated our thinnest ice samples, the smooth ice films, to

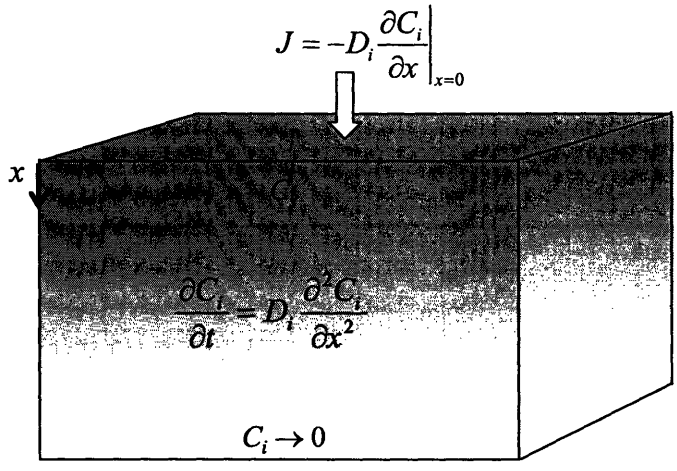

Figure 1-7. Schematic diagram of solute diffusion from the surface into the interior of an ice slab.

be approximately 700 μm thick. By scaling of eq. 1-15, the characteristic time for diffusion through these samples is then

$$\tau_{diff} = \frac{l_i^2}{D_i} = 4.9 \cdot 10^9 \text{s} . \qquad 1\text{-}16.$$

The characteristic time for diffusion through the ice film is substantially longer than the timescale for the experiment (3600 seconds or less). Therefore, we can model diffusion from the ice surface as diffusion into a semi-infinite slab. The boundary conditions are as follows:

$$C_i(t,x) = \begin{cases} C_s & x = 0 \\ 0 & x \to \infty \\ 0 & t = 0 \\ C_s & t \to \infty \end{cases} . \qquad 1\text{-}17.$$

Note that C_s is the 'surface concentration', the concentration on a volume basis in a near-surface region. The saturation HCl concentration in single crystals of ice was measured by Thibert and Dominé to be $3.5 \cdot 10^{-7}$ moles·cm^{-3} for adsorption at 200 K and 10^{-6} Torr HCl[34]. This value can

serve as an upper bound for C_s in the ice crystal for a scenario with surface adsorption but no surface disordering.

These boundary conditions allow us to simplify the analysis by defining the similarity variable, η, as follows[112]:

$$\eta \equiv \frac{x}{\sqrt{4D_i t}}. \qquad 1\text{-}18.$$

Eq. 1-15 is then transformed to

$$-2\eta \frac{dC_i}{d\eta} = \frac{d^2 C_i}{d\eta^2} \qquad 1\text{-}19.$$

subject to the boundary conditions

$$C_i(\eta) = \begin{cases} C_s & \eta = 0 \\ 0 & \eta \to \infty \end{cases}. \qquad 1\text{-}20.$$

The solution is then

$$\frac{C_i}{C_s} = 1 - \mathrm{erf}\left(\frac{x}{\sqrt{4D_i t}}\right) \qquad 1\text{-}21.$$

where erf is the Gaussian error function. Shown in Figure 1-8 is the concentration depth profile at several elapsed times for HCl diffusing through an ice slab, calculated using eq. 1-21. It can be seen that one hour after exposure the HCl is for the most part still confined within the topmost 1 μm of the ice film, and the region within 150 nm of the concentrated surface region has reached within 90% of the surface concentration via diffusion alone.

The flux of solute into the bulk, J, is derived from eq. 1-21 as follows:

$$J = -D_i \frac{\partial C_i}{\partial x} = -C_s \sqrt{\frac{D_i}{\pi t}}. \qquad 1\text{-}22.$$

It is notable that the flux into the bulk is determined by the concentration at the surface. In a

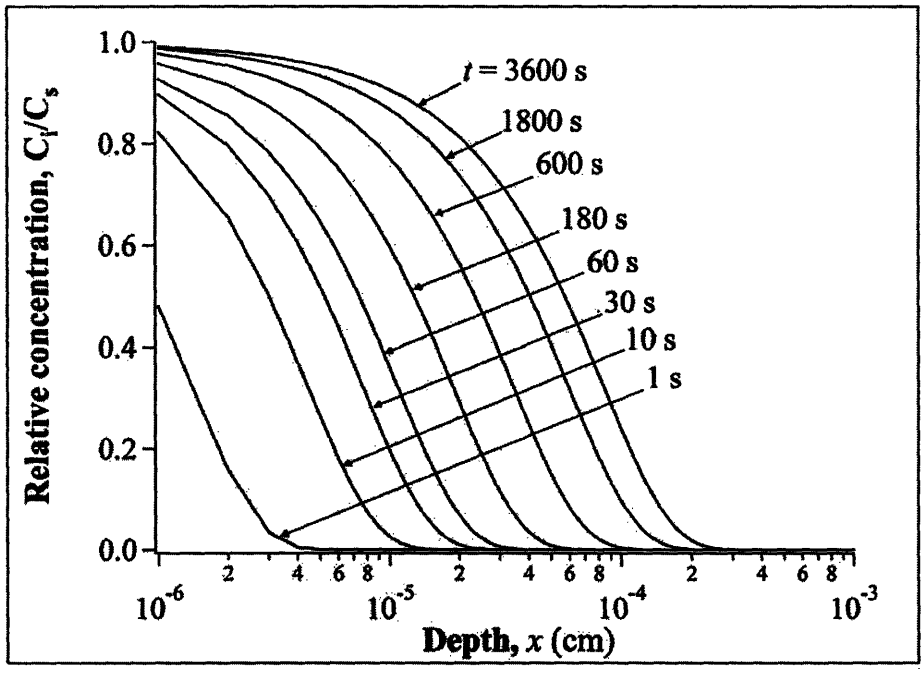

Figure 1-8. The time evolution of the concentration depth profile on a log scale for HCl diffusion through an ice slab with constant surface concentration, C_s, calculated according to eq. 1-21. Here the diffusion coefficient for HCl in ice, D_i, is assumed to be 10^{-12} cm^2s^{-1}.

scenario in which a thin layer on an ice surface contains a relatively high concentration C_s of HCl, diffusive flux from that layer into the bulk could be significant. This is illustrated in Figure 1-9, which shows flux as a function of time for different values of C_s and D_i. In practical application to our experiments, the large flux at time $t = 0$ created by the inverse dependence of eq. 1-22 on time should not be significant because C_s will not be constant throughout the experiment (as in this model), but, rather, initially $C_s = 0$. For a surface layer with $C_s = 3.5 \cdot 10^{-7}$ moles·cm^{-3}, and $D_i = 10^{-12}$ cm^2s^{-1}, there is a long-term surface flux of between $2 \cdot 10^9$ and $6 \cdot 10^9$ molecules·$cm^{-2}s^{-1}$, which is established within 500 seconds of the initial exposure and persists through the duration of the experiment. For a surface layer with $C_s = 10^{-4}$ moles·cm^{-3}, this long-term surface flux could be as high as $5 \cdot 10^{11}$ molecules·$cm^{-2}s^{-1}$.

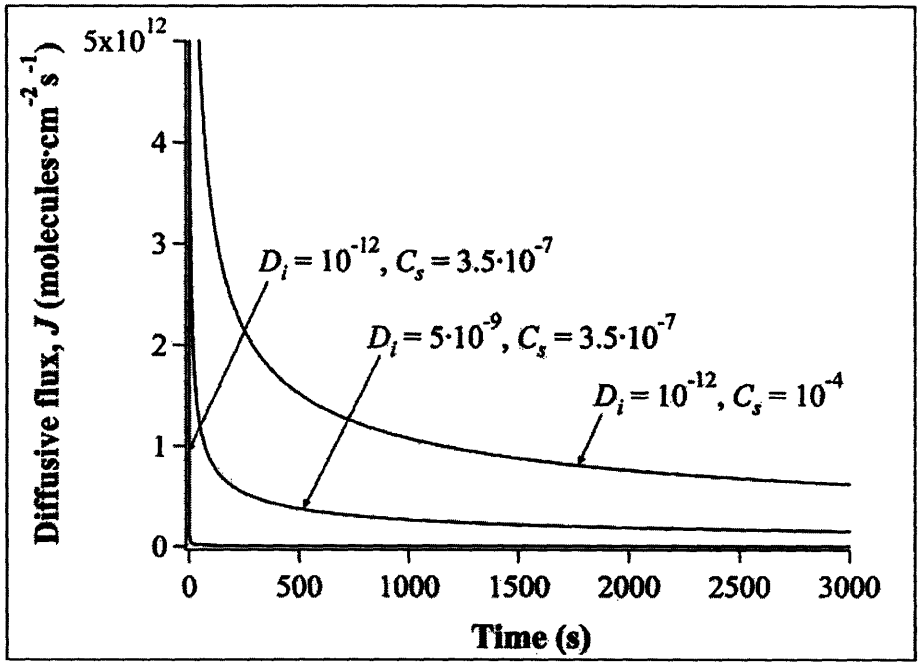

Figure 1-9. Diffusive flux , J, as calculated by eq. 1-22 for different values of the diffusion coefficient of HCl in ice, D_i (cm^2s^{-1}), and the near-surface concentration, C_s ($moles \cdot cm^{-3}$).

1.4.3 Flow tube analysis I. Governing equations

A schematic diagram of the flow tube is shown in Figure 1-10.

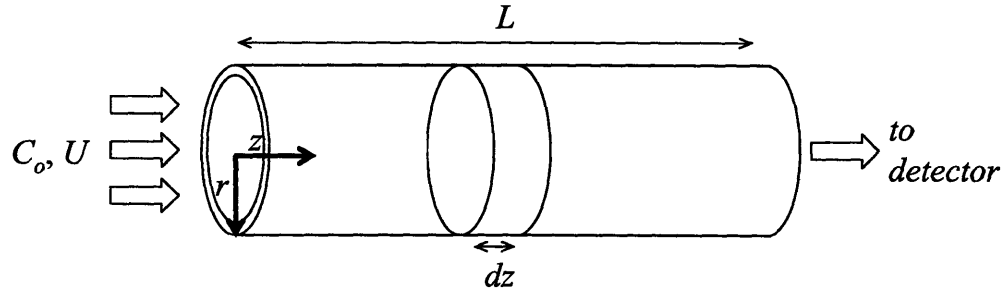

Figure 1-10. Schematic diagram of flow tube.

The gas phase concentration profile of a solute in our flow tube is governed by the general species conservation equation:

$$\frac{\partial C}{\partial t} + \nabla \cdot C\underline{v} = D\nabla^2 C - R_{loss} \qquad 1\text{-}23.$$

where $\underline{v}$ is the velocity vector, C is the concentration of the solute in He, and D is the binary diffusion coefficient for the solute in He at the conditions of the experiment, and R_{loss} is the rate of solute loss to the walls (or gas phase reaction).

The Reynolds number, Re, is

$$\mathrm{Re} = \frac{\rho U \mathbf{L}}{\mu} \qquad 1\text{-}24.$$

where ρ and μ are the density and viscosity of the gas. Re may be interpreted as the ratio of inertial to viscous forces in the flow. The value of Re determines whether a flow is laminar (Re < 2000) or turbulent (Re > 2000). Since we operate at very low pressures (1-2 Torr), the gas density is very low, and therefore even though flow through the tube may be 'fast,' for this system Re < 1, indicating that flow within the tube is in the laminar regime and that the velocity profile is parabolic. Using this information, we can rewrite eq. 1-23 to give the rate equation for a dilute solution in laminar flow through a tube:

$$\frac{\partial C}{\partial t} + 2U\left(1 - \left(\frac{r}{R}\right)^2\right)\frac{\partial C}{\partial z} = D\left(\frac{1}{r}\frac{\partial}{\partial r}\left(r\frac{\partial C}{\partial r}\right) + \frac{\partial^2 C}{\partial z^2}\right) - R_{loss} \; . \qquad 1\text{-}25.$$

By assuming that the characteristic time for diffusion of the solute to the wall is much less than the residence time of a solute molecule within the flow tube, we may take a cross-sectional average of the concentration, thus simplifying eq. 1-25, without losing much information. We then express eq. 1-25 as

$$\frac{\partial \overline{C}}{\partial t} + U\frac{\partial \overline{C}}{\partial z} = D\frac{\partial^2 \overline{C}}{\partial z^2} - R_{loss} \qquad 1\text{-}26.$$

where

$$\overline{C} = \frac{1}{A}\int C dA \ . \qquad 1\text{-}27.$$

The loss term, R_{loss}, may include solute loss to the ice film (surface or bulk) or to gas phase reaction. For surface adsorption, R_{loss} may be expressed as follows:

$$R_{loss} = \chi_A \frac{dc_s}{dt} \qquad 1\text{-}28.$$

where

$$\chi_A = \frac{A_{film}}{V_{gas}} = \frac{2}{R} \ . \qquad 1\text{-}29.$$

For absorption into a near-surface region of thickness l where $l << R$,

$$R_{loss} = \chi_V \frac{\partial C_s}{\partial t} \qquad 1\text{-}30.$$

where

$$\chi_V = \frac{V_{film}}{V_{gas}} = \frac{(\pi R^2 - \pi(R+l)^2)dz}{\pi R^2 dz} \cong \frac{2l}{R} \ . \qquad 1\text{-}31.$$

C_s and c_s may be described using the models for solute-ice interaction discussed in section A.

Now, let us check the assumption that radial diffusion may be neglected. From scaling arguments, the characteristic time for diffusion to the wall is

$$\tau_{diff} = \frac{R^2}{D} \qquad 1\text{-}32.$$

and the characteristic time for convection through the tube is

$$\tau_{conv} = \frac{\mathbf{L}}{U} \qquad 1\text{-}33.$$

Listed in Table1-1 are the characteristic times for radial diffusion and axial convection for smooth ice experiments and those using zone-refined ice films, which have smaller internal radii.

Ice sample	τ_{diff}	τ_{conv}
Smooth ice films	0.01	0.04
Zone-refined ice cylinders	0.004	0.02

Table 1-1. Characteristic times for radial diffusion and axial convection in experiments using smooth ice films (R = 1.25 cm) and zone-refined ice cylinders (R = 0.74 cm).

It can be seen from Table 1-1 that $\tau_{diff} << \tau_{conv}$ for the zone-refined ice cylinders, and therefore radial diffusion may be neglected and the above analysis holds. It is also true that $\tau_{diff} < \tau_{conv}$ for the smooth ice films, but the convective forces are less dominant here than in the zone-refined ice cylinder system. Therefore, although the analysis described in this section may yield less accurate results when modeling experiments performed with the smooth ice films, the assumption that radial diffusion may be neglected is not unreasonable. Accounting for radial diffusion would significantly increase the computational complexity of the program and would require a level of modeling sophistication beyond the scope of this work.

1.4.4 Flow tube analysis II. Numerical solution

By conceptually dividing the flow tube into a series of well-mixed segments of width *dz*, we can achieve a numerical solution of eq. 1-26 and model an adsorption experiment in a variety of cases. All simulations described were programmed and executed using MATLAB 6.0.

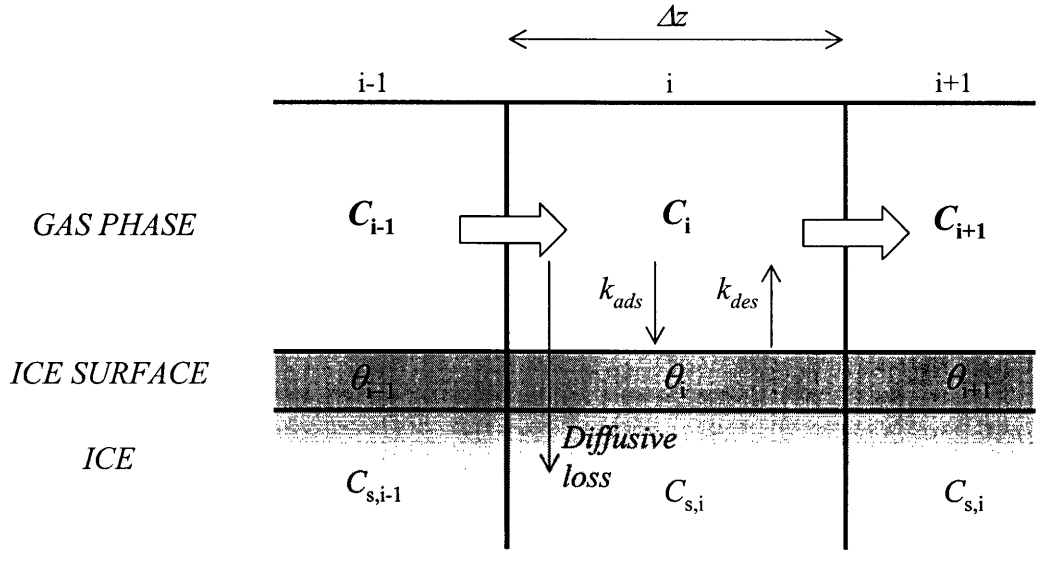

Figure 1-11. Schematic diagram for numerical modeling of flow tube with solute-wall interaction including diffusive loss.

For surface adsorption on the flow tube walls, eq. 1-26 can be discretized for numerical solution by an explicit finite difference scheme as follows[112,113]:

$$\Delta\overline{C}_z(t) = \overline{C}_{t,z} - \overline{C}_{t-1,z} = \frac{\Delta t}{(\Delta z)^2} D\left(-2\overline{C}_{t-1,z} + \overline{C}_{t-1,z-1} + \overline{C}_{t-1,z+1}\right) - \frac{\Delta t}{\Delta z} U\left(\overline{C}_{t-1,z} - \overline{C}_{t-1,z-1}\right) - \Delta t \chi \Delta c_{s_z}(t) \quad . \qquad 1\text{-}34.$$

The limiting condition for Eulerian stability is[113]

$$\frac{\Delta t}{\Delta z}U \leq 1 \ . \qquad \text{1-35.}$$

The boundary and initial conditions for an adsorption experiment are

$$C(t,z) = \begin{cases} C_o & for\ z = 0 \\ 0 & for\ t < 0 \end{cases} \qquad \text{1-36.}$$

and

$$c_s(0,z) = C_s(0,z) = 0 \ . \qquad \text{1-37.}$$

For the desorption stage of an adsorption experiment, the boundary and initial conditions are

$$C(t,z) = \begin{cases} 0 & for\ z = 0 \\ C_0 & for\ t < 0 \end{cases} \qquad \text{1-38.}$$

$$c_s(0,z) = c_{s,0} \qquad \text{1-39.}$$

and

$$C_s(0,z) = C_{s,0} \qquad \text{1-40.}$$

where $c_{s,0}$ and $C_{s,0}$ are the equilibrium surface and near-surface concentrations corresponding to a gas-phase concentration of C_o, assuming that the adsorption phase of the experiment proceeded to equilibrium.

For all cases we are interested in solving for $C(t, L)$, the concentration observed by the detector.

For Langmuir adsorption, we must solve for θ and C simultaneously. Eq. 1-6 is discretized as follows:

$$\Delta c_s(t) = S\Delta\theta(t) = S\left(k_{ads}C_{t-1,z}(1-\theta_{t-1,z}) - k_{des}\theta_{t-1,z}\right)\Delta t \ . \qquad \text{1-41.}$$

Eqs. 1-35 and 1-41 are used to calculate θ and C as functions of time and space and ultimately obtain the uptake curve.

Listed in Table 1-2 is a summary of parameters relevant for modeling this system.

Parameter	Symbol	Value
Gas phase HCl density	C	$2\text{-}5 \cdot 10^{10}$ molecules·cm^{-3}
Solubility of HCl in liquid water	C_{sat}	$6.1 \cdot 10^{-3}$ moles HCl·cm^{-3} H_2O at -70.5 °C, $1.1 \cdot 10^{5}$ Torr HCl[3]
Solubility of HCl in ice	C_{sat}	$3.17 \cdot 10^{-11} \exp\left(\frac{2806.5}{T}\right) P_{HCl}^{1/2.73}$ moles HCl·cm^{-3} ice[34] (P_{HCl} in Pa, T in K)
Diffusion coefficient, HCl in ice	D_i	10^{-12} cm^{2}s^{-1} [34]
Diffusion coefficient, HCl in He	D	168.4 cm^{2}s^{-1} (-60 °C) 147.4 cm^{2}s^{-1} (-77 °C)[114]
Diffusion coefficient, CCl_2F_2 in He	D	84.3 cm^{2}s^{-1} (-73 °C)[114, 115]
Diffusion coefficient, CH_3COOH in He	D	102.6 cm^{2}s^{-1} (-60 °C)[114, 116]
Film thickness	l_i	700 μm (smooth ice) 2 mm (zone-refined ice)
Flow tube length	**L**	40 cm
Ice sample length	L	4- 10 cm
QLL thickness	L	10-100 nm
Tube inner radius	R	1.25 cm (smooth ice) 0.74 cm (zone-refined ice)
Theoretical saturation surface coverage	S	10^{15} molecules·cm^{-2}
Gas velocity	U	1400 cm·s^{-1} (smooth ice) 2000 cm·s^{-1} (zone-refined ice)

Table 1-2. Parameters used for modeling flow tube experiments.

1.5 Thesis outline

The main goal of this research has been to test the hypotheses that a) HCl induces the formation of a disordered region on the ice surface, or 'quasi-liquid layer' (QLL), at stratospheric conditions, and b) the existence of the QLL explains the catalytic role PSC particle surfaces play during chlorine activation. Another goal was to gain insight into the fate of HCl upon adsorption to ice.

In Chapter 2, we present our study of the ice surface alone and in the presence of trace amounts of HCl using the direct surface probe ellipsometry. We show that trace amounts of HCl induce a disordered region on the ice surface near the solid-liquid equilibrium line on the HCl-ice phase diagram, including at stratospherically relevant conditions. We estimate the real part of the refractive index of the QLL formed via exposure to gas-phase HCl to be 1.35, closer to that of liquid water or aqueous HCl solution than to that of ice. Based on this estimate of refractive index, we estimate the thickness of the QLL in our experiments to be on the order of 100 nm. The ellipsometer measurements described in Chapter 2 were performed with Dr. Thomas Loerting, currently at the University of Innsbruck, Austria.

Chapter 3 describes flow-tube CIMS studies of the chlorine activation reaction of HCl with $ClONO_2$ (reaction (1.8)) on smooth and zone-refined ice surfaces. We show that the presence of surface disorder enhances reaction (1.8). The results of this study lend support for the trend observed via ellipsometry that surface disorder is induced by the presence of HCl in the vicinity of the solid-liquid equilibrium line on the HCl-ice phase diagram, but that no detectable disorder was observed on the interior of the 'ice' phase envelope.

In Chapter 4 we present a detailed flow tube-CIMS investigation of the interaction of HCl with zone-refined, smooth and vapor-deposited ice films. The results of the HCl uptake

experiments on zone-refined ice lend further support to the trend observed via ellipsometry that HCl-induced surface disordering is confined to the vicinity of the solid-liquid equilibrium line on the HCl-ice phase diagram. The results also indicate that the QLL is not like liquid water in its ability to absorb HCl, but rather has a solubility that is between that of liquid water and that of bulk crystalline ice I_h.

We also show that HCl adsorption onto polycrystalline ice samples consists of two modes of adsorption, one relatively strong mode leading to irreversible adsorption, and one relatively weak binding mode leading to reversible adsorption. We present indirect evidence that these two modes of adsorption correspond to adsorption to sites on crystal faces and those at grain boundaries, but there is not enough experimental evidence to conclusively assign each adsorption mode to a type of site.

Additionally, we show indirect evidence that HCl hexahydrate formation is a surface process rather than one originating in the grain boundaries, as has been suggested for lower temperature ices[43]. The study of HCl hexahydrate formation on smooth ice described in Chapter 4 was conducted in conjunction with Prof. Franz Geiger, currently of Northwestern University.

Chapter 5 describes studies of the interaction of two other probe molecules, CH_3COOH and CCl_2F_2, with ice, with and without HCl present. We show that the presence of the QLL enhances CH_3COOH adsorption, and these findings suggest that the presence of surface disorder on cirrus cloud ice particles enhance their scavenging ability. The results of this study also lend further support for the trend observed via ellipsometry HCl-induced surface disordering is confined to the vicinity of the solid-liquid equilibrium line on the HCl-ice phase diagram, and provide additional evidence that the QLL is not truly liquid-like in its adsorption properties. We also show that the sticking coefficient for adsorption of CCl_2F_2 to ice changes with time during

adsorption.

Finally, in Chapter 6 the main conclusions of the work are reviewed and recommendations are made for future work.

References for Chapter 1

1. Solomon, S., Garcia, R.R., Rowland, F.S. & Wuebbles, D.J. On the Depletion of Antarctic Ozone. *Nature* **321**, 755-758 (1986).

2. Molina, M.J., Tso, T.L., Molina, L.T. & Wang, F.C.Y. Antarctic Stratospheric Chemistry of Chlorine Nitrate, Hydrogen Chloride and Ice - Release of Active Chlorine. *Science* **238**, 1253-1257 (1987).

3. Molina, M.J. The Chemistry of the Atmosphere: The Impact of Global Change. Calvert, J.G. (ed.), pp. 27-38 (Blackwell Scientific Publications, Boston,1994).

4. Seinfeld, J.H. & Pandis, S.N. Atmospheric chemistry and physics: From air pollution to climate change. Wiley, New York (1998).

5. Finlayson-Pitts, B.J. & Pitts, J.N. Chemistry of the Upper and Lower Atmosphere. Academic Press, New York (2000).

6. Molina, L.T., Molina, M.J., Stachnik, R.A. & Tom, R.D. An Upper Limit to the Rate of the Hydrogen Chloride + $ClONO_2$ Reaction. *J. Phys. Chem.* **89**, 3779-81 (1985).

7. Leu, M.T. Laboratory Studies of Sticking Coefficients and Heterogeneous Reactions Important in the Antarctic Stratosphere. *Geophys. Res. Lett.* **15**, 17-20 (1988).

8. Hanson, D.R. & Ravishankara, A.R. Investigation of the Reactive and Nonreactive Processes Involving $ClONO_2$ and HCl on Water and Nitric-Acid Doped Ice. *J. Phys. Chem.* **96**, 2682-2691 (1992).

9. Abbatt, J.P.D. *et al.* Interaction of HCl vapor with water-ice: Implications for the stratosphere. *J. Geophys. Res.* **97**, 15819-15826 (1992).

10. Lee, S.H., Leard, D.C., Zhang, R., Molina, L.T. & Molina, M.J. The HCl+$ClONO_2$ reaction rate on various water ice surfaces. *Chem. Phys. Lett.* **315**, 7-11 (1999).

11. Oppliger, R., Allanic, A. & Rossi, M.J. Real-time kinetics of the uptake of $ClONO_2$ on ice and in the presence of HCl in the temperature range $160K \leq T \leq 200K$. *J. Phys. Chem. A* **101**, 1903-1911 (1997).

12. Abbatt, J.P.D. & Molina, M.J. Heterogeneous Interactions of $ClONO_2$ and HCl on Nitric-Acid Trihydrate at 202 K. *J. Phys. Chem.* **96**, 7674-7679 (1992).

13. Chu, L.T., Leu, M.T. & Keyser, L.F. Heterogeneous Reactions of HOCl+HCl $\rightarrow$ Cl_2+H_2O and $ClONO_2$+HCl $\rightarrow$ Cl_2+HNO_3 on Ice Surfaces at Polar Stratospheric Conditions. *J. Phys. Chem.* **97**, 12798-12804 (1993).

14. Abbatt, J.P.D. & Molina, M.J. The Heterogeneous Reaction of HOCl+HCl $\rightarrow$ Cl_2+H_2O on Ice and Nitric-Acid Trihydrate - Reaction Probabilities and Stratospheric Implications. *Geophys. Res. Lett.* **19**, 461-464 (1992).

15. Hanson, D.R. & Ravishankara, A.R. The Reaction Probabilities of $ClONO_2$ and N_2O_5 on Polar Stratospheric Cloud Materials. *J. Geophys. Res.-Atmos.* **96**, 5081-5090 (1991).

16. Toon, O.B. & Tolbert, M.A. Spectroscopic Evidence Against Nitric-Acid Trihydrate in Polar Stratospheric Clouds. *Nature* **375**, 218-221 (1995).

17. Prenni, A.J. & Tolbert, M.A. Studies of Polar Stratospheric Cloud Formation. *Acc. Chem. Res.* **34**, 545-553 (2001).

18. Toon, O.B., Turco, R.P., Jordan, J., Goodman, J. & Ferry, G. Physical Processes in Polar Stratospheric Ice Clouds. *J. Geophys. Res.-Atmos.* **94**, 11359-11380 (1989).

19. Demirdjian, B. *et al.* Structure and dynamics of ice I_h films upon HCl adsorption between 190 and 270 K. I. Neutron diffraction and quasielastic neutron scattering experiments. *J. Chem. Phys.* **116**, 5143-5149 (2002).

20. Livingston, F.E. & George, S.M. Diffusion kinetics of HCl hydrates in ice measured using infrared laser resonant desorption depth-profiling. *J. Phys. Chem. A* **105**, 5155-5164 (2001).

21. Livingston, F.E. & George, S.M. Effect of HNO_3 and HCl on D_2O desorption kinetics from crystalline D_2O ice. *J. Phys. Chem. A* **102**, 10280-10288 (1998).

22. Fluckiger, B., Thielmann, A., Gutzwiller, L. & Rossi, M.J. Real time kinetics and thermochemistry of the uptake of HCl, HBr and HI on water ice in the temperature range 190 to 210 K. *Ber. Bunsen. Phys. Chem.* **102**, 915-928 (1998).

23. Fluckiger, B., Chaix, L. & Rossi, M.J. Properties of the HCl/ice, HBr/ice, and H_2O/ice interface at stratospheric temperatures (200 K) and its importance for atmospheric heterogeneous reactions. *J. Phys. Chem. A* **104**, 11739-11750 (2000).

24. Fluckiger, B., Chaix, L. & Rossi, M.J. Properties of the HCl/ice, HBr/ice, and H_2O/ice interface at stratospheric temperatures (200 K) and its importance for atmospheric heterogeneous reactions (vol 104, pg 11739, 2002). *J. Phys. Chem. A* **107**, 2768 (2003).

25. Aguzzi, A., Fluckiger, B. & Rossi, M.J. The nature of the interface and the diffusion coefficient of HCl/ice and HBr/ice in the temperature range 190-205 K. *Phys. Chem. Chem. Phys.* **5**, 4157-4169 (2003).

26. Diehl, K., Mitra, S.K. & Pruppacher, H.R. A laboratory study on the uptake of HCl, HNO_3, and SO_2 gas by ice crystals and the effect of these gases on the evaporation rate of the crystals. *Atmos. Res.* **47-48**, 235-244 (1998).

27. Wofsy, S.C., Molina, M.J., Salawitch, R.J., Fox, L.E. & McElroy, M.B. Interactions between HCl, NO_x, and H_2O Ice in the Antarctic Stratosphere - Implications for Ozone. *J. Geophys. Res.-Atmos.* **93**, 2442-2450 (1988).

28. Hanson, D.R. & Mauersberger, K. HCl/H_2O Solid-Phase Vapor Pressures and HCl Solubility in Ice. *J. Phys. Chem.* **94**, 4700-5 (1990).

29. Henson, B.F. *et al.* Experimental isotherms of HCl on H_2O ice under stratospheric conditions: Connections between bulk and interfacial thermodynamics. *J. Chem. Phys.* **121**, 8486-8499 (2004).

30. Wooldridge, P.J., Zhang, R. & Molina, M.J. Phase Equilibria of H_2SO_4, HNO_3, and HCl Hydrates and the Composition of Polar Stratospheric Clouds. *J. Geophys. Res.* **100**, 1389-96 (1995).

31. Foster, K.L., Tolbert, M.A. & George, S.M. Interaction of HCl with Ice: Investigation of the Predicted Trihydrate, Hexahydrate, and Monolayer Regimes. *J. Phys. Chem. A* **101**, 4979-4986 (1997).

32. Xueref, I. & Domine, F. FTIR spectroscopic studies of the simultaneous condensation of HCl and H_2O at 190 K - Atmospheric applications. *Atmos. Chem. Phys.* **3**, 1779-1789 (2003).

33. Wolff, E.W., Mulvaney, R. & Oates, K. Diffusion and Location of Hydrochloric-Acid in Ice - Implications for Polar Stratospheric Clouds and Ozone Depletion. *Geophys. Res. Lett.* **16**, 487-490 (1989).

34. Thibert, E. & Domine, F. Thermodynamics and Kinetics of the Solid Solution of HCl in Ice. *J. Phys. Chem. B* **101**, 3554-3565 (1997).

35. Krieger, U.K. *et al.* Rutherford backscattering to study the near-surface region of volatile liquids and solids. *Science* **295**, 1048-1050 (2002).

36. Chu, L.T., Leu, M.T. & Keyser, L.F. Uptake of HCl in Water Ice and Nitric-Acid Ice Films. *J. Phys. Chem.* **97**, 7779-7785 (1993).

37. Hynes, R.G., Mossinger, J.C. & Cox, R.A. The Interaction of HCl With Water-ice at Tropospheric Temperatures. *Geophys. Res. Lett.* **28**, 2827-2830 (2001).

38. Huthwelker, T., Malmstrom, M.E., Helleis, F., Moortgat, G.K. & Peter, T. Kinetics of HCl uptake on ice at 190 and 203 K: implications for the microphysics of the uptake process. *J. Phys. Chem. A* **108**, 6302-6318 (2004).

39. Graham, J.D. & Roberts, J.T. Interaction of HCl with Crystalline and Amorphous Ice - Implications for the Mechanisms of Ice-Catalyzed Reactions. *Geophys. Res. Lett.* **22**, 251-254 (1995).

40. Graham, J.D. & Roberts, J.T. Interaction of Hydrogen Chloride with an Ultrathin Ice Film: Observation of Adsorbed and Absorbed States. *J. Phys. Chem.* **98**, 5974-83 (1994).

41. Graham, J.D. & Roberts, J.T. Formation of $HCl{\cdot}6H_2O$ from ice and HCl under ultrahigh vacuum. *Chemom. Intell. Lab. Sys.* **37**, 139-148 (1997).

42. Roberts, J.T. Chemistry at the Surfaces of Ice and Sulfuric Acid: Toward an Understanding of Adsorption at Molecular Solids. *Acc. Chem. Res.* **31**, 415-421 (1998).

43. Sadtchenko, V., Giese, C.F. & Gentry, W.R. Interaction of Hydrogen Chloride with Thin Ice Films: The Effect of Ice Morphology and Evidence for Unique Surface Species on Crystalline Vapor-Deposited Ice. *J. Phys. Chem. B* **104**, 9421-9429 (2000).

44. Isakson, M.J. & Sitz, G.O. Adsorption and Desorption of HCl on Ice. *J. Phys. Chem. A* **103**, 2044-2049 (1999).

45. Andersson, P.U., Ngrd, M.B. & Pettersson, J.B.C. Molecular beam studies of HCl interactions with pure and HCl-covered ice surfaces. *J. Phys. Chem. B* **104**, 1596-1601 (2000).

46. Rieley, H. & Aslin, H.D. Sticking of HCl and HBr on a type-II polar stratospheric cloud mimic. *J. Chem. Soc. , Faraday Trans.* **91**, 2349-51 (1995).

47. Koehler, B.G., McNeill, L.S., Middlebrook, A.M. & Tolbert, M.A. Fourier-Transform Infrared Studies of the Interaction of HCl with Model Polar Stratospheric Cloud Films. *J. Geophys. Res.-Atmos.* **98**, 10563-10571 (1993).

48. Kang, H., Shin, T.H., Park, S.C., Kim, I.K. & Han, S.J. Acidity of Hydrogen Chloride on Ice. *J. Am. Chem. Soc.* **122**, 9842-9843 (2000).

49. Kondo, M., Kawanowa, H., Gotoh, Y. & Souda, R. Ionization and solvation of HCl adsorbed on the D_2O-ice surface. *J. Chem. Phys.* **121**, 8589-8593 (2004).

50. Horn, A.B., Sodeau, J.R., Roddis, T.B. & Williams, N.A. Mechanism of the heterogeneous reaction of hydrogen chloride with chlorine nitrate and hypochlorous acid on water ice. *J. Phys. Chem. A* **102**, 6107-6120 (1998).

51. Koch, T.G. *et al.* Mechanisms for the heterogeneous hydrolysis of hydrogen chloride, chlorine nitrate and dinitrogen pentoxide on water- rich atmospheric particle surfaces. *J. Geophys. Res.-Atmos.* **102**, 1513-1522 (1997).

52. Delzeit, L., Devlin, M.S., Rowland, B., Devlin, J.P. & Buch, V. Adsorbate-induced partial ordering of the irregular surface and subsurface of crystalline ice. *J. Phys. Chem.* **100**, 10076-10082 (1996).

53. Devlin, J.P., Uras, N., Sadlej, J. & Buch, V. Discrete stages in the solvation and ionization of hydrogen chloride adsorbed on ice particles. *Nature* **417**, 269-271 (2002).

54. Gilbert, A.S. & Sheppard, N. Infrared-Spectra of Hydrates of Hydrogen-Chloride and Hydrogen Bromide - Absorption-Bands of H_5O^{+2} Species. *J. Chem. Soc.-Faraday Trans. II* **69**, 1628-1642 (1973).

55. Bournel, F., Mangeney, C., Tronc, M., Laffon, C. & Parent, P. Cl2p, O1s PSD-NEXAFS study of the adsorption of HCl on ice: a direct experimental evidence of the HCl ionization. *Surf. Sci.* **528**, 224-229 (2003).

56. Bournel, F., Mangeney, C., Tronc, M., Laffon, C. & Parent, P. Acidity of hydrogen chloride at the surface of low-temperature (40-150 K) water-ice films. *Phys. Rev. B* **65**, 201404 (2002).

57. Banham, S.F., Sodeau, J.R., Horn, A.B., McCoustra, M.R.S. & Chesters, M.A. Adsorption and ionization of HCl on an ice surface. *J. Vac. Sci. Technol. , A* **14**, 1620-1626 (1996).

58. Barone, S.B., Zondlo, M.A. & Tolbert, M.A. Investigation of the Heterogeneous Reactivity of HCl, HBr, and HI on Ice Surfaces. *J. Phys. Chem. A* **103**, 9717-9730 (1999).

59. Mantz, Y.A., Geiger, F.M., Molina, L.T., Molina, M.J. & Trout, B.L. The interaction of HCl with the (0001) face of hexagonal ice studied theoretically via Car-Parrinello molecular dynamics. *Chem. Phys. Lett.* **348**, 285-292 (2001).

60. Mantz, Y.A., Geiger, F.M., Molina, L.T., Molina, M.J. & Trout, B.L. First-Principles Theoretical Study of Molecular HCl Adsorption on a Hexagonal Ice (0001) Surface. *J. Phys. Chem. A* **105**, 7037-7046 (2001).

61. Bussolin, G., Casassa, S., Pisani, C. & Ugliengo, P. *Ab initio* study of HCl and HF interaction with crystalline ice. I. Physical adsorption. *J. Chem. Phys.* **108**, 9516-9528 (1998).

62. Bacelo, D.E., Binning, R.C. & Ishikawa, Y. *Ab initio* Monte Carlo simulated annealing study of $HCl(H_2O)(n)$ (n=3, 4) clusters. *J. Phys. Chem. A* **103**, 4631-4640 (1999).

63. Geiger, F.M., Hicks, J.M. & de Dios, A.C. *Ab initio* Study of HOCl, HCl, H_2O, and Cl_2 Interacting with Four Water Molecules. *J. Phys. Chem. A* **102**, 1514-1522 (1998).

64. Hannachi, Y., Silvi, B. & Bouteiller, Y. Structure and Vibrational Properties of Water Hydrogen Halide- Complexes. *J. Chem. Phys.* **94**, 2915-2922 (1991).

65. Gertner, B.J. & Hynes, J.T. Model molecular dynamics simulation of hydrochloric acid ionization at the surface of stratospheric ice. *Faraday Discuss.* 301-322 (1998).

66. Packer, M.J. & Clary, D.C. Interaction of HCl with Water Clusters - $(H_2O)(N)HCl$, N=1-3. *J. Phys. Chem.* **99**, 14323-14333 (1995).

67. Re, S., Osamura, Y., Suzuki, Y. & Schaefer, H.F. Structures and stability of hydrated clusters of hydrogen chloride, $HCl(H_2O)(n)$, n=1-5. *J. Chem. Phys.* **109**, 973-977 (1998).

68. Svanberg, M., Pettersson, J.B.C. & Bolton, K. Coupled QM/MM Molecular Dynamics Simulations of HCl Interacting with Ice Surfaces and Water Clusters: Evidence of Rapid Ionization. *J. Phys. Chem. A* **104**, 5787-5798 (2000).

69. Robertson, S.H. & Clary, D.C. Solvation of hydrogen halides on the surface of ice. *Faraday Discuss.* **100**, 309-320 (1996).

70. Toubin, C., Hoang, P.N.M., Picaud, S. & Girardet, C. Time Study of Pollutants at the Surface of Ice at 200 K. *Chem. Phys. Lett.* **329**, 331-335 (2000).

71. Wang, T.X. & Margerum, D.W. Kinetics of Reversible Chlorine Hydrolysis - Temperature- Dependence and General Acid Base-Assisted Mechanisms. *Inorg. Chem.* **33**, 1050-1055 (1994).

72. Gertner, B.J. & Hynes, J.T. Molecular dynamics simulation of hydrochloric acid ionization at the surface of stratospheric ice. *Science* **271**, 1563-6 (1996).

73. Calatayud, M., Courmier, D. & Minot, C. Ionization of HCl and HF in ice: a periodic DFT study. *Chem. Phys. Lett.* **369**, 287-292 (2003).

74. Casassa, S. Ab initio study of periodic ice surfaces containing HCl. *Chem. Phys. Lett.* **321**, 1-7 (2000).

75. Mantz, Y.A., Geiger, F.M., Molina, L.T., Molina, M.J. & Trout, B.L. First Principles Molecular Dynamics Study of Surface Disordering of the (0001) Face of Hexagonal Ice. *J. Chem. Phys.* **113**, 10733-10743 (2000).

76. Hobbs, P.V. Ice physics. Clarendon Press, Oxford (1974).

77. Haynes, D.R., Tro, N.J. & George, S.M. Condensation and Evaporation of H_2O on Ice Surfaces. *J. Phys. Chem.* **96**, 8502-8509 (1992).

78. Wettlaufer, J.S., Dash, J.G. & Untersteiner, N. Ice Physics and the Natural Environment. [In: NATO ASI Ser., Ser. I, 1999; 56]. 355 pp. (1999).

79. Mizuno, Y. & Hanafusa, N. Studies of Surface-Properties of Ice Using Nuclear-Magnetic- Resonance. *J. Phys. (Paris)* **48**, 511-517 (1987).

80. Wei, X., Miranda, P.B. & Shen, Y.R. Surface Vibrational Spectroscopic Study of Surface Melting of Ice. *Phys. Rev. Lett.* **86**, 1554-1557 (2001).

81. Wei, X., Miranda, P.B., Zhang, C. & Shen, Y.R. Sum-Frequency Spectroscopic Studies of Ice Interfaces. *Phys. Rev. B* **66**, 085401 (2002).

82. Sadtchenko, V. & Ewing, G.E. Interfacial melting of thin ice films: An infrared study. *J. Chem. Phys.* **116**, 4686-4697 (2002).

83. Bluhm, H., Ogletree, D.F., Fadley, C.S., Hussain, Z. & Salmeron, M. The premelting of ice studied with photoelectron spectroscopy. *J. Phys. : Condens. Matter* **14**, L227-L233 (2002).

84. Doeppenschmidt, A. & Butt, H.-J. Measuring the Thickness of the Liquid-like Layer on Ice Surfaces with Atomic Force Microscopy. *Langmuir* **16**, 6709-6714 (2000).

85. Pittenger, B. *et al.* Premelting at ice-solid interfaces studied via velocity-dependent indentation with force microscope tips. *Phys. Rev. B* **6313**, 134102 (2001).

86. Petrenko, V.F. Study of the surface of ice, ice/solid and ice/liquid interfaces with scanning force microscopy. *J. Phys. Chem. B* **101**, 6276-6281 (1997).

87. Dosch, H., Lied, A. & Bilgram, J.H. Glancing-angle X-ray scattering studies of the premelting of ice surfaces. *Surf. Sci.* **327**, 145-64 (1995).

88. Golecki, I. & Jaccard, C. Intrinsic Surface Disorder in Ice Near Melting Point. *J. Phys. C* **11**, 4229-4237 (1978).

89. Wilson, P.W., Arthur, J.W. & Haymet, A.D.J. Ice premelting during differential scanning calorimetry. *Biophys. J.* **77**, 2850-2855 (1999).

90. Orem, M.W. & Adamson, A.W. Physical adsorption of vapor on ice. II. *n*-Alkanes. *J. Colloid Sci.* **31**, 278-286 (1969).

91. Beaglehole, D. & Nason, D. Transition layer on the surface on ice. *Surf. Sci.* **96**, 357-63 (1980).

92. Furukawa, Y., Yamamoto, M. & Kuroda, T. Ellipsometric study of the ice surface structure just below the melting point. *J. Phys. (Paris)* 1-495 (1987).

93. Elbaum, M., Lipson, S.G. & Dash, J.G. Optical Study of Surface Melting on Ice. *J. Cryst. Growth* **129**, 491-505 (1993).

94. Gilpin, R.R. Wire Regelation at Low-Temperatures. *J. Colloid Sci.* **77**, 435-448 (1980).

95. Mazzega, E., Pennino, U.D., Loria, A. & Mantovani, S. Volta Effect and Liquid-Like Layer at Ice Surface. *J Chem Phys* **64**, 1028-1031 (1976).

96. Toubin, C. *et al.* Dynamics of Ice Layers Deposited on MgO(001): Quasielastic Neutron Scattering Experiments and Molecular Dynamics Simulations. *J. Chem. Phys.* **114**, 6371-6381 (2001).

97. Baker, M. & Baker, M.B. A model for the ice-vapor interface at equilibrium. *J. Cryst. Growth* **169**, 393-404 (1996).

98. Elbaum, M. & Schick, M. Application of the Theory of Dispersion Forces to the Surface Melting of Ice. *Phys. Rev. Lett.* **66**, 1713-1716 (1991).

99. Ryzhkin, I.A. & Petrenko, V.F. Violation of ice rules near the surface: A theory for the quasiliquid layer. *Phys. Rev. B* **65**, 012205 (2002).

100. Makkonen, L. Surface melting of ice. *J. Phys. Chem. B* **101**, 6196-6200 (1997).

101. Wettlaufer, J.S. Impurity Effects in the Premelting of Ice. *Phys. Rev. Lett.* **82**, 2516-2519 (1999).

102. Geiger, F.M., Tridico, A.C. & Hicks, J.M. Second Harmonic Generation Studies of Ozone Depletion Reactions on Ice Surfaces under Stratospheric Conditions. *J. Phys. Chem. B* **103**, 8205-8215 (1999).

103. Baldelli, S., Schnitzer, C. & Shultz, M.J. First spectroscopic evidence for molecular HCl on a liquid surface with sum frequency generation. *J. Chem. Phys.* **108**, 9817-9820 (1998).

104. Girardet, C. & Toubin, C. Molecular atmospheric pollutant adsorption on ice: a theoretical survey. *Surf. Sci. Rep.* **44**, 159-238 (2001).

105. Marti, J. & Mauersberger, K. A Survey and New Measurements of Ice Vapor-Pressure at Temperatures between 170 and 250 K. *Geophys. Res. Lett.* **20**, 363-366 (1993).

106. Ohtomo, M., Ahmad, S. & Whitworth, R.W. A technique for the growth of high quality single crystals of ice. *J. Phys. (Paris)* 595-598 (1987).

107. Abbatt, J.P.D. Interaction of HNO_3 with Water-Ice Surfaces at Temperatures of the Free Troposphere. *Geophys. Res. Lett.* **24**, 1479-1482 (1997).

108. Leu, M.T., Keyser, L.F. & Timonen, R.S. Morphology and surface areas of thin ice films. *J. Phys. Chem. B* **101**, 6259-6262 (1997).

109. Behr, P., Terziyski, A. & Zellner, R. Reversible Gas Adsorption in Coated Wall Flow Tube Reactors. Model Simulations for Langmuir Kinetics. *Z. Phys. Chem.* (2004).

110. Atkins, P.W. Physical Chemistry. W. H. Freeman & Co., New York (1994).

111. Adamson, A.W. Physical chemistry of surfaces. Wiley, New York (1990).

112. Incropera, F.P. & DeWitt, D.P. Fundamentals of heat and mass transfer. Wiley, New York (1996).

113. Heath, M.T. Scientific computing: An introductory survey. McGraw-Hill, New York (1997).

114. Reid, R.C., Prausnitz, J.M. & Poling, B.E. The properties of gases and liquids. McGraw-Hill, New York (1987).

115. No data were available for CCl_2F_2, so averages of the available parameters for CF_4 and CCl_4 were used to estimate the diffusion coefficient.

116. No data were available for CH_3COOH, so the parameters for acetone were used to estimate the diffusion coefficient.

Chapter 2

Ellipsometer-CIMS Studies of Surface Disorder on Ice

2.1 Introduction

Characterization of the interaction of hydrogen chloride (HCl) with polar stratospheric cloud (PSC) ice particles is essential to understanding the processes responsible for ozone depletion[1,2]. To explain the catalytic role PSC particle surfaces play during chlorine activation[2-5], we proposed previously that HCl might induce the formation of a disordered region on the ice surface, or 'quasi-liquid layer' (QLL), at stratospheric conditions[6]. The QLL is known to exist on the surface of ice at temperatures near the melting point, but the existence of a disordered region on the surface of ice has not been confirmed at stratospheric temperatures.

Ellipsometry is a nondestructive surface-specific technique that allows direct monitoring of changes in the state of the ice surface with changes in temperature or HCl partial pressure. In ellipsometry, a light beam of known polarization is reflected from a smooth sample surface and the polarization of the reflected beam is measured. The change in polarization of the light beam upon reflection can be used to deduce the optical properties of the sample. In our system, by continuously monitoring the polarization state of the reflected beam while changing the ice sample temperature or HCl partial

pressure we are able to detect the development of an interfacial layer on the ice surface or changes in the thickness of that layer. See section 1.3 for a detailed description of the ellipsometer-CIMS experimental system.

The Beaglehole `bielli_multilayer` Igor Pro™ software tool can be used to simulate single-wavelength ellipsometry data for a system of multiple layers of different materials and varying thicknesses on a substrate[7]. The program takes as inputs the real and imaginary parts of the refractive index of each layer in the system, the wavelength of the He/Ne laser (632.8 nm), and the angle of incidence, and calculates the transmitted and reflected light intensities for the *s* and *p* polarizations through each interface in the system. The relevant refractive indices for this experimental system are listed in Table 2-1. The optical properties of the QLL are not known.

Substance	Refractive Index	
	Real Part, n	Imaginary Part, k
Ice	1.31 [8]	$1.1 \cdot 10^{-8}$ [8]
Liquid H_2O	1.33 [9,10]	$1.5 \cdot 10^{-8}$ [10]
HCl trihydrate	1.44 [11]	not available
Concentrated aqueous solution (HNO_3, H_2SO_4, NaCl, or sugars)	$\geq$ 1.33 [12,13]	not available
Helium	1.00 [14]	0

Table 2-1. Refractive index data relevant to the Ice-QLL-He system at 632.8 nm.

As shown in Table 2-1, at 632.8 nm, the values of the imaginary part of the refractive index, *k*, for ice, liquid water, and He are near zero. To the best of our knowledge, the optical properties of HCl hexahydrate are also unknown. For HCl

trihydrate, n was measured to be 1.44 by Foster et al.[11], and for the nitric acid hydrates, $n \geq 1.44$ [15].

Other parameters relevant to this system are the refractive indices of aqueous HCl solutions of various concentrations at 632.8 nm. To the best of our knowledge, these data are not available in the literature. However, refractive index data for concentrated aqueous solutions of HNO_3, H_2SO_4, NaCl, and various sugars[12,13] indicate that the addition of a solute to water increases the value of n, so that $n \geq 1.33$ at 632.8 nm.

Figures 2-1 and 2-2 show results of the `bielli_multilayer` simulation predicting ellipsometer signal vs. disordered layer thickness for an ice-QLL-He system for several assumed values of n_{QLL}, the real part of the refractive index for the QLL. The imaginary part of the refractive index, k_{QLL}, was assumed to be $1 \cdot 10^{-8}$.

For all of the tested values of n_{QLL}, the predicted ellipsometer signals change nonlinearly and nonmonotonically with layer thickness. In all cases, the dependence of the signals on layer thickness is periodic, but the period, amplitude, and overall functional form of the dependence on layer thickness changes dramatically with small changes in the assumed value of n_{QLL}. Because of this sensitivity to n_{QLL}, by analyzing any ellipsometer signal changes induced by changes in temperature or HCl partial pressure during the experiment, it should be possible to make an estimate of n_{QLL} as well as the thickness of any induced layer.

We studied the interaction of HCl with ice under stratospheric conditions using ellipsometry to monitor the ice surface and chemical ionization mass spectrometry (CIMS) detection of the gas phase. Here we show that trace amounts of HCl induce QLL formation near the solid-liquid equilibrium line on the HCl-ice phase diagram, including

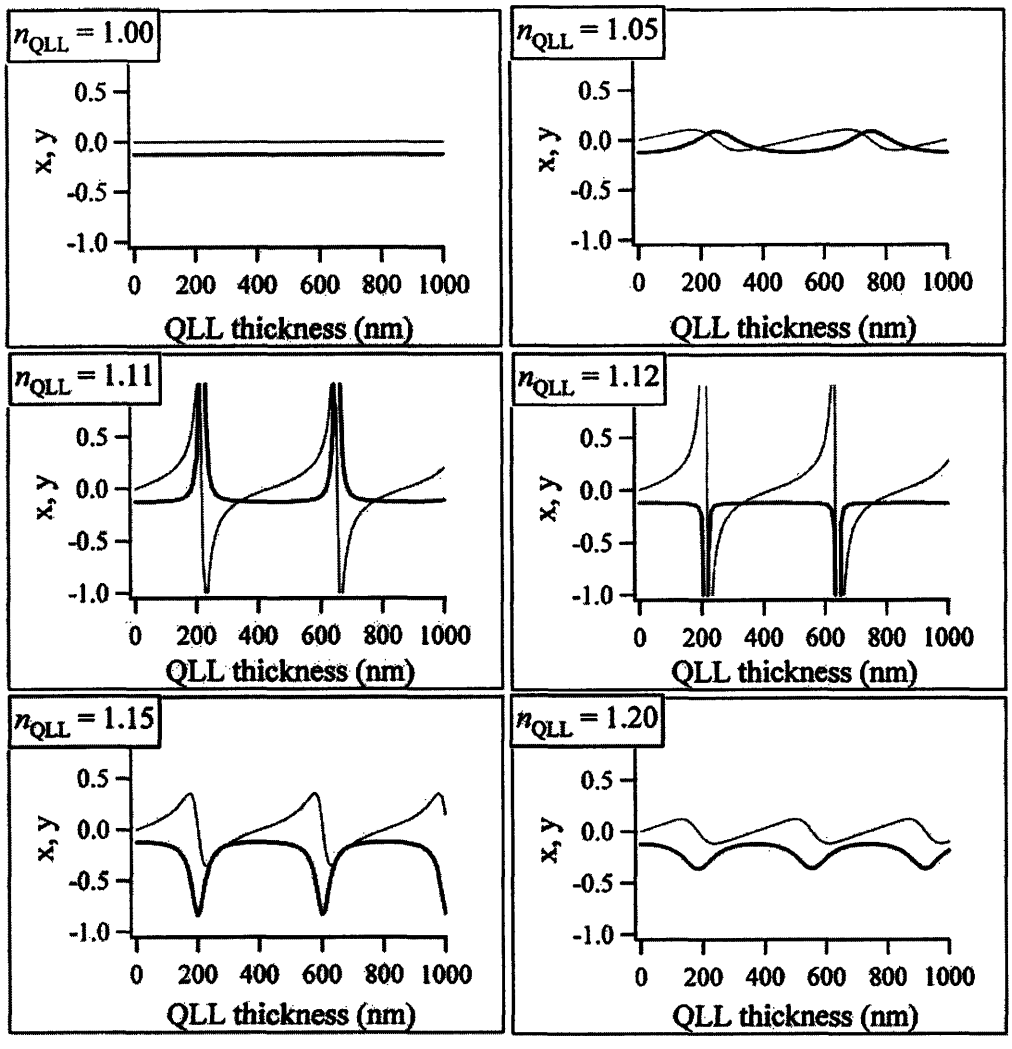

Figure 2-1. Results of Beaglehole multilayer simulation[7] for the ice-QLL-He system for $1.0 \leq n_{QLL} \leq 1.20$, where n_{QLL} is the real part of the refractive index of the QLL. The imaginary part of the refractive index, k_{QLL}, was assumed to be equal to $1 \cdot 10^{-8}$. The angle of incidence was 57°, and the wavelength was 632.8 nm. The grey curves represent the y ellipsometer signal, and the black curves represent the x-signal. The system for $n_{QLL} = n_{He} = 1.00$ is the equivalent of an ice-He interface with no interfacial layer.

at stratospherically relevant conditions, and that the optical properties of the QLL are closer to those of liquid water or what we would predict for a HCl solution ($n \geq 1.33$) than to those of ice.

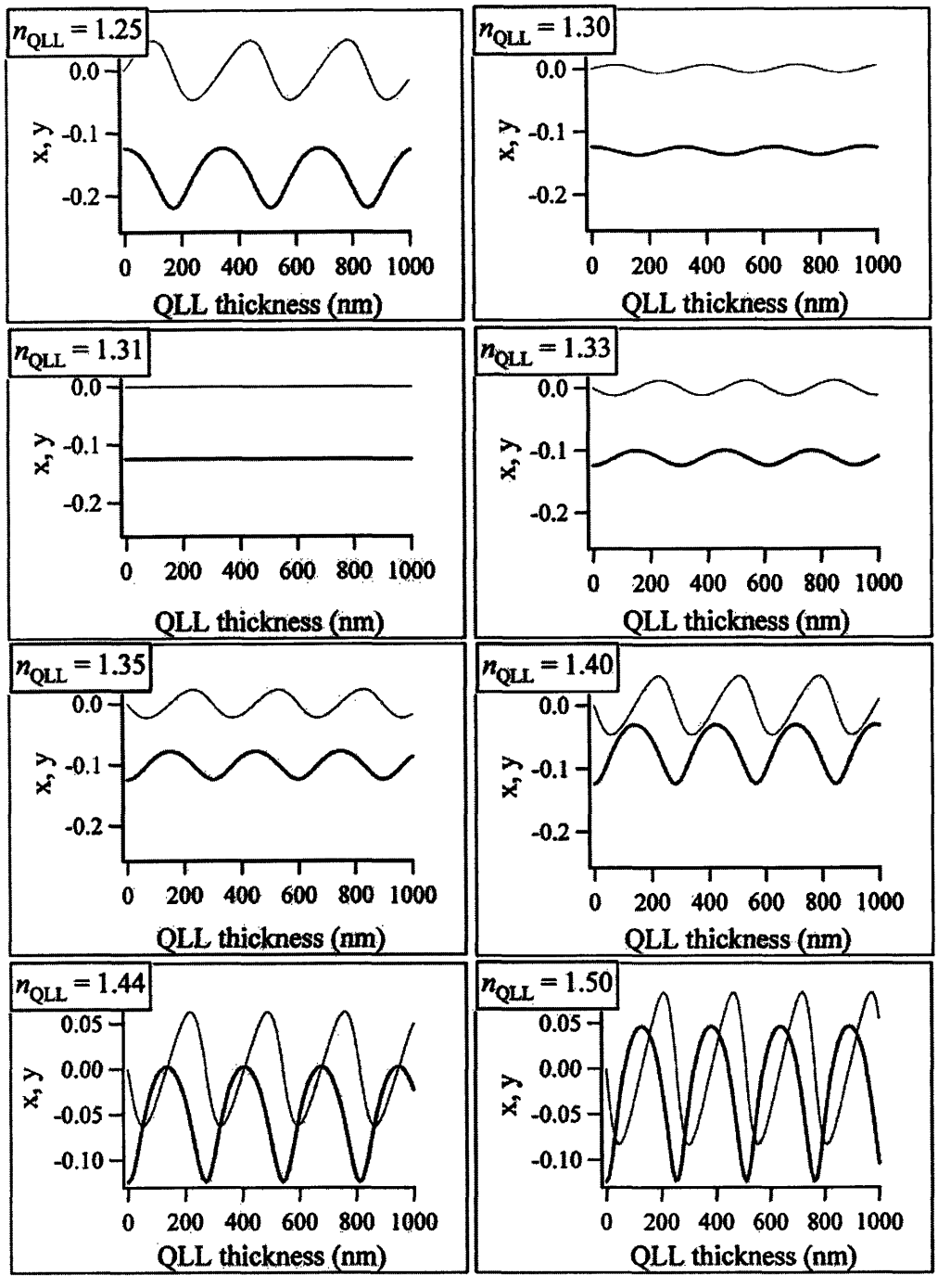

Figure 2-2. Results of Beaglehole multilayer simulation[7] for ice-QLL-He system for $1.25 \leq n_{QLL} \leq 1.50$, where n_{QLL} is the real part of the refractive index. The imaginary part of the refractive index, k_{QLL}, was assumed to be equal to $1 \cdot 10^{-8}$. The angle of incidence was 57°, and the wavelength was 632.8 nm. The grey curves represent the y ellipsometer signal, and the black curves represent the x-signal. The system for $n_{QLL} = n_{ice} = 1.31$ is the equivalent of an ice-He interface with no interfacial layer.

The ellipsometer measurements described in this chapter were performed with Dr. Thomas Loerting, currently at the University of Innsbruck, Austria.

2.2 Results

Surface disorder was observed via ellipsometry on pure single-crystalline hexagonal ice with no HCl present down to approximately -30 °C. This value is consistent with other experimentally determined values of QLL onset temperature for bare ice, which range from a few degrees below the melting point of water to less than -40 °C [16-19] (see Figure 1-2), and is also consistent with the theoretical predictions of Baker and Baker[20] and Ryzhkin and Petrenko[21].

Two types of HCl-ice experiment were performed using the ellipsometer-CIMS system: a) constant temperature experiments in which the ice sample is exposed to a step change in partial pressure of HCl and the ellipsometer signal is monitored over time, and b) constant HCl temperature-scanning experiments.

Ellipsometer signal time traces for a typical constant-temperature experiment are shown in Figure 2-3, which shows a time study of the phase-modulated ellipsometer signal for an ice sample at -55 °C. At time 0, the ice sample was exposed to $6 \cdot 10^{-6}$ Torr HCl. Both the *x*- and *y*-signals were observed to change after an induction time of a few hundred seconds. After approximately 4000 seconds, the HCl source was turned off and the signal was allowed to recover. Then, at approximately 6300 seconds, the sample was exposed to $2 \cdot 10^{-4}$ Torr HCl (conditions known to cause melting of the ice sample at this temperature). It can be seen that QLL formation can be distinguished from true melting in the ellipsometer signal. In the constant temperature experiments, after exposure to

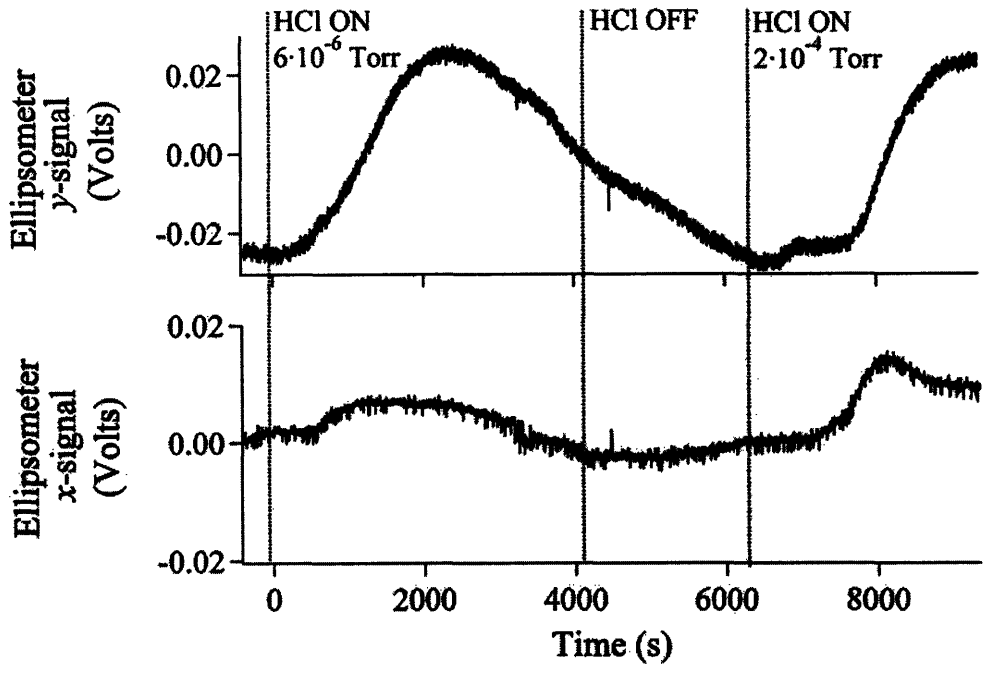

Figure 2-3. Time study of phase-modulated ellipsometry signals for an ice sample at -55 °C. The traces shown are the ellipsometer signals, in Volts, measured at 50 kHz (x-signal, bottom panel) and 100 kHz (y-signal, top panel). The x- and y- signals are related to the real and the imaginary parts of the reflectivity, respectively. At $t = 0$, the ice sample was exposed to $6{\cdot}10^{-6}$ Torr HCl. After approximately 4000 seconds, the HCl source was turned off. Then, at approximately 6300 seconds, the sample was exposed to $2{\cdot}10^{-4}$ Torr HCl.

HCl, surface change was observed only after an induction time of 1-10 min. An aging effect was observed in that induction times were seen to decrease after the first exposure of a surface to HCl. Both the surface disordering and this aging effect were seen to be reversible.

Ellipsometer signal time traces for a typical temperature-scanning experiment are shown in Figure 2-4, which shows the ellipsometer signals for an ice sample exposed to $5{\cdot}10^{-7}$ Torr HCl. The ice sample was initially equilibrated at -52.5 °C, was cooled to -77.2 °C, and then warmed again to -52.5 °C. As the temperature decreased, there was a

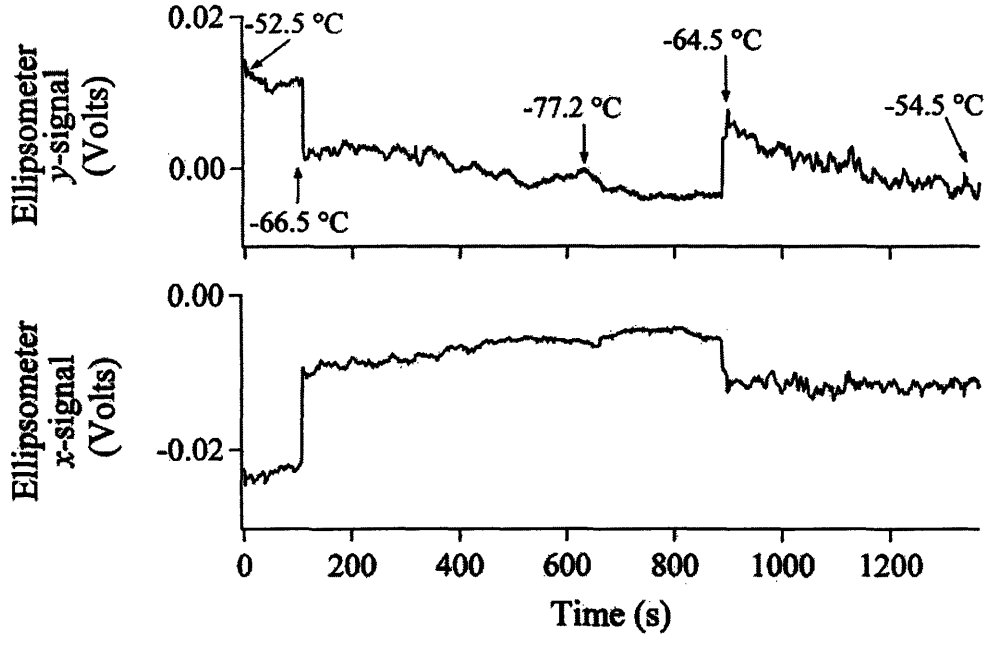

Figure 2-4. Time study of phase-modulated ellipsometry signals for an ice sample exposed to $5 \cdot 10^{-7}$ Torr HCl and temperatures ranging from -52.5 °C to -77.2 °C. The ice sample was held initially at -52.5 °C, cooled to -77.2 °C, and then warmed again to -52.5 °C. The traces shown are the ellipsometer signals, in Volts, measured at 50 kHz (*x*-signal, bottom panel) and 100 kHz (*y*-signal, top panel). The *x*- and *y*-signals are related to the real and the imaginary parts of the reflectivity, respectively.

discontinuity in the signals corresponding to a surface change at -66.5 °C. When the sample was then warmed to its original temperature, another discontinuity was observed, with the signals returning to their previous levels at -64.5 °C.

Figure 2-5 summarizes the results of our investigation of the HCl-ice phase diagram using the ellipsometer-CIMS approach. Temperature scanning experiments such as the one featured in Figure 2-4 are labeled using arrows. Constant-temperature experiments such as the one shown in Figure 2-3 are labeled using filled boxes in Figure 2-5. A change in ellipsometer signal consistent with the formation of a disordered

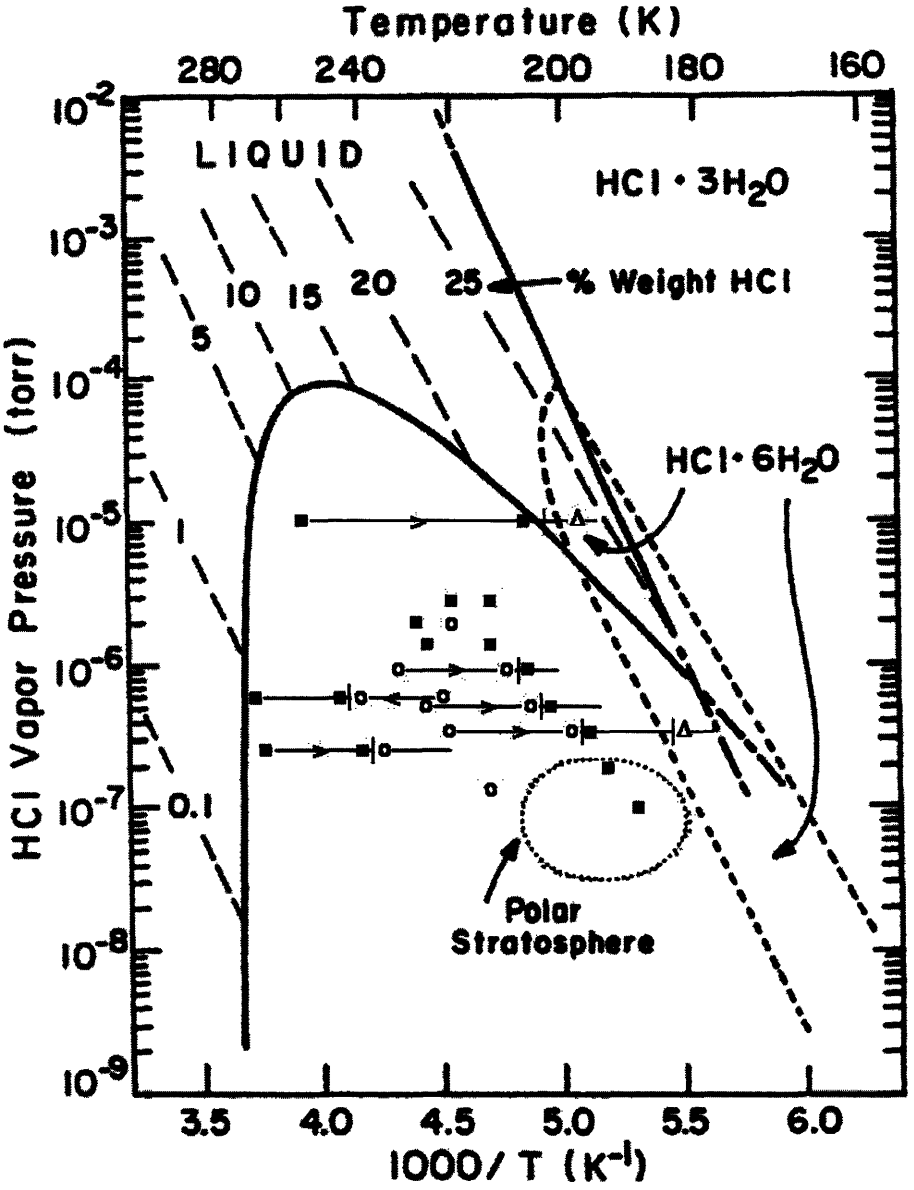

Figure 2-5. Summary of ellipsometer-CIMS study results: the HCl-ice phase diagram adapted from Molina.[6] Filled boxes (■) refer to conditions where a change in signal consistent with the formation of a disordered interfacial layer on the ice surface was observed upon exposure of the ice crystal to HCl, and open circles (o) refer to conditions where no change to the ice surface was observed. Arrows represent experiments involving a scan in temperature during exposure to a constant partial pressure of HCl. Bars represent temperatures at which we observe cease/onset of surface changes. Phase transition is indicated by delta symbols (Δ).

interfacial layer on the ice surface was observed in the range of HCl partial pressures and temperatures in the vicinity of the solid-liquid equilibrium line on the HCl-ice bulk phase diagram. This range of conditions includes those encountered in the polar stratosphere during PSC events. While surface disorder on ice at stratospheric conditions has been predicted theoretically[22], this is the first report of experimental evidence of HCl-induced QLL formation at stratospheric temperatures.

In the range of HCl partial pressures and temperatures in the interior of the ice stability envelope on the HCl-ice phase diagram, far from the solid-liquid equilibrium line, no surface change was observed. For example, exposing an ice surface to approximately 10^{-7} Torr HCl was observed to induce QLL formation for T > -35 °C and T < -65 °C, but in the region -35 °C > T > -65 °C we found no evidence of surface change. Figure 2-6 shows an example of a constant-temperature experiment at -55 °C and $2 \cdot 10^{-6}$ Torr HCl in which no surface change was observed upon exposure to HCl. The gas phase HCl CIMS signal is shown along with the ellipsometry signals. After the injector was withdrawn and the ice sample was exposed to HCl, the CIMS signal indicates HCl adsorption, but both the *x* and *y* ellipsometry signals stay roughly constant within the noise for 25 min. Experiments such as this one are labeled using open circles in Figure 2-5.

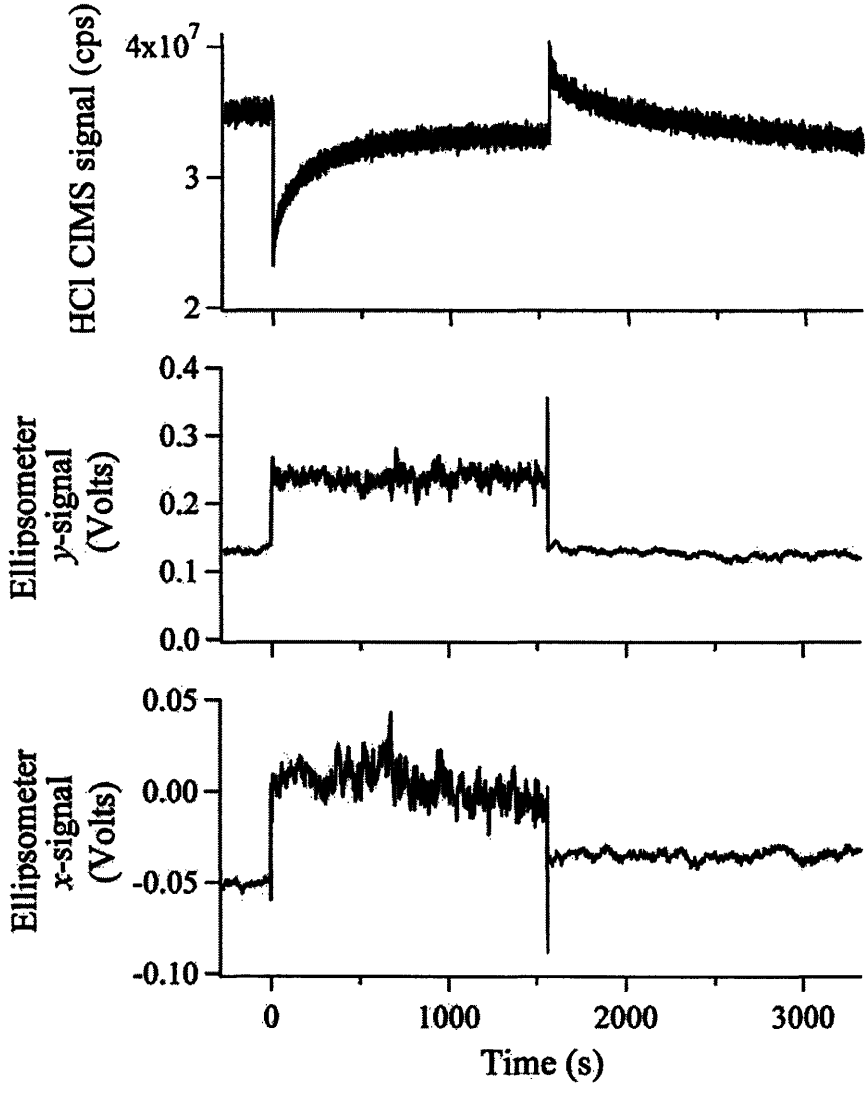

Figure 2-6. Time study of phase-modulated ellipsometry and CIMS signals for an ice sample at -55 °C exposed to $2 \cdot 10^{-6}$ Torr HCl. The traces shown are the SF_5Cl^- CIMS signal, corresponding to the gas phase HCl concentration (top panel), and the *x*- and *y*-ellipsometer signals in Volts (bottom and center panels, respectively). At $t = 0$, the injector was withdrawn, exposing the ice sample to $2 \cdot 10^{-6}$ Torr HCl. Before $t = 0$, the glass injector was pushed to the front of the flow tube, blocking the laser beam of the ellipsometer. This created the discontinuity in ellipsometer signals at $t = 0$.

2.3 Discussion

Surface disorder was observed via ellipsometry on pure single-crystalline hexagonal ice with no HCl present down to approximately -30 °C. This value is consistent with other experimentally determined values of QLL onset temperature for bare ice, which range from a few degrees below the melting point of water to less than -40 °C [16-19].

HCl-induced surface disordering has been predicted theoretically[23], but this is the first report of experimental evidence for HCl-induced QLL formation at stratospheric conditions.

Indirect support for our observation that HCl-induced surface change is confined to the region of the HCl-ice phase diagram near the solid-liquid equilibrium line is found in the work of Hynes et al.[24] In their coated wall flow tube experiments, at 10^{-6} Torr HCl, they observed that the uptake coefficient, γ, of HCl on ice decreased from $\gamma > 0.1$ at 200 K (conditions at which we observe surface change) to $\gamma < 0.01$ upon increasing the temperature to above 205 K (conditions at which no surface change was observed in our experiment). Surface disorder is expected to enhance HCl uptake efficiency. Our flow tube-CIMS studies, presented in Chapters 3, 4, and 5, lend further support for the observed trend.

In both Figure 2-3 and Figure 2-4, it can be seen that, upon QLL formation, the the x ellipsometer signal begins to increase. Comparing this observation to Figures 2-1 and 2-2, which show the predicted signal change for various assumed values of the refractive index, we see that an increase in x-signal with increasing thickness (starting at 0 nm) is consistent with the predicted signal change for $n_{QLL} > 1.31$.

From Figure 2-2 it can be seen that, in the range $1.31 \leq n_{QLL} \leq 1.5$, the amplitude of the dependence of the y-signal on QLL thickness increases with increasing n_{QLL}. Shown in Figure 2-7 is the amplitude as a function of n_{QLL} for $1.31 \leq n_{QLL} \leq 1.5$.

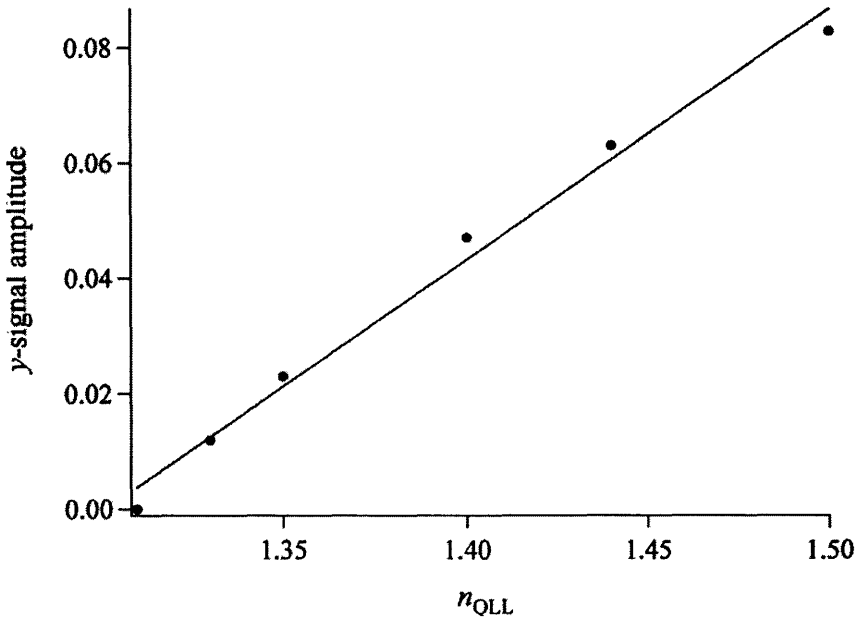

Figure 2-7. Predicted amplitude of the dependence of the y-signal on QLL thickness as a function of the real part of the refractive index of the QLL, n_{QLL}, obtained using Beaglehole multilayer software [7]. The imaginary part of the refractive index, k_{QLL}, was assumed to be equal to $1 \cdot 10^{-8}$. The angle of incidence was 57°, and the wavelength was 632.8 nm.

We can estimate the amplitude of the dependence of the y-signal on QLL thickness for this system to be 0.023 from Figure 2-3. Therefore, from Figure 2-7 we can estimate that $n_{QLL} \approx 1.35$. This suggests that the optical properties of the QLL are closer to those of liquid water, or what we would predict for an HCl solution ($n \geq 1.33$), than those of ice.

Shown in Figure 2-8 are results of the `bielli_multilayer` simulation predicting the expected signal change vs. disordered layer thickness for an ice-QLL-He system for n_{QLL} = 1.35 and k_{QLL} = $1.1 \cdot 10^{-8}$.

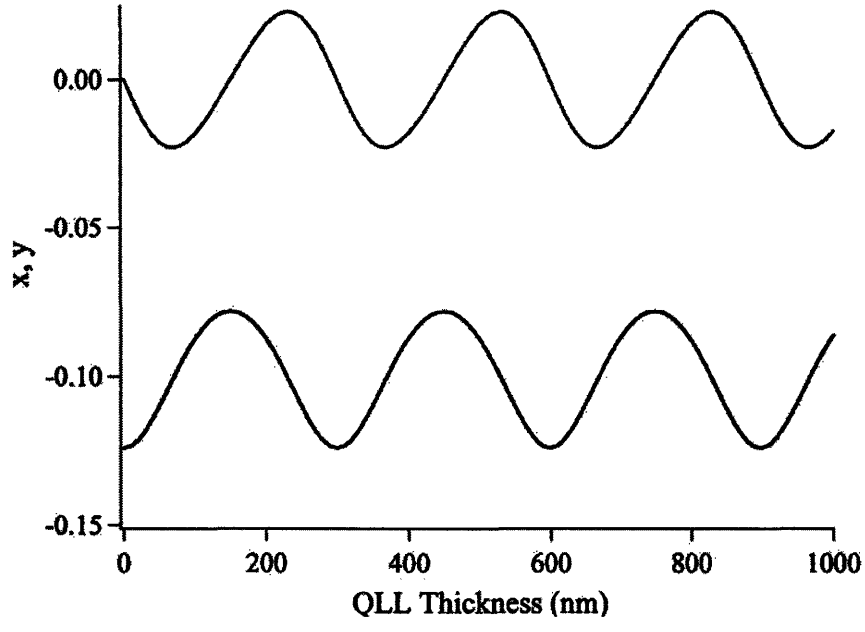

Figure 2-8. Simulated signal v. thickness for the ice-QLL-He system with n_{QLL} = 1.35 and k_{QLL} = $1.1 \cdot 10^{-8}$ obtained using Beaglehole multilayer software[7]. The angle of incidence was 57°, and the wavelength was 632.8 nm. The grey curve represents the *y* ellipsometer signal, and the black curve represents the *x*-signal.

In Figure 2-8, both the *x*- and *y*-signals undergo a full oscillation every ~ 300 nm. The *x*-signal increases monotonically until reaching its first peak at 150 nm. The *y*-signal decreases monotonically until reaching its first trough at 65 nm. Comparing Figure 2-4 to Figure 2-8, since both the *x*- and *y*-signals are still in the monotonic regime of the signal change, we estimate 0 nm < l_{QLL} < 65 nm. For Figure 2-3, since both traces have changed nonmonotonically but a full oscillation has not been completed, we can estimate 150 nm < l_{QLL} < 300 nm.

Generally, we observed signal changes corresponding to development of an interfacial layer of thickness on the order of 100 nm depending on the quality of measurements of QLL thickness on bare ice close to the melting point reported in the literature (see Figure 1-2), and with Fluckiger et al.[25,26], who estimated the thickness of an HCl-rich near-surface region to be 60 +/- 10 nm for single-crystalline ice and h = 130 +/- 20 nm for bulk (polycrystalline) ice using $ClONO_2$ titration[26].

2.4 Conclusions

Surface disorder was observed via ellipsometry on pure single-crystalline hexagonal ice with no HCl present down to approximately -30 °C.

We observed HCl-induced surface change in the region of the HCl-ice phase diagram near the solid-liquid equilibrium line, including conditions relevant to PSC events. This is the first report of experimental evidence for HCl-induced QLL formation at stratospheric conditions.

The experimental results suggest that $n_{QLL} \approx 1.35$. Therefore, the optical properties of the QLL are closer to those of liquid water, or what we would predict for an HCl solution ($n \geq 1.33$), than those of ice.

We estimate the thickness of the disordered layer to be up to a few hundred nanometers depending on the quality of the ice surface and the location in the phase diagram.

References for Chapter 2

1. Solomon, S., Garcia, R.R., Rowland, F.S. & Wuebbles, D.J. On the Depletion of Antarctic Ozone. *Nature* **321**, 755-758 (1986).

2. Molina, M.J., Tso, T.L., Molina, L.T. & Wang, F.C.Y. Antarctic Stratospheric Chemistry of Chlorine Nitrate, Hydrogen Chloride and Ice - Release of Active Chlorine. *Science* **238**, 1253-1257 (1987).

3. Leu, M.T. Laboratory Studies of Sticking Coefficients and Heterogeneous Reactions Important in the Antarctic Stratosphere. *Geophys. Res. Lett.* **15**, 17-20 (1988).

4. Hanson, D.R. & Ravishankara, A.R. Investigation of the Reactive and Nonreactive Processes Involving $ClONO_2$ and HCl on Water and Nitric-Acid Doped Ice. *J. Phys. Chem.* **96**, 2682-2691 (1992).

5. Chu, L.T., Leu, M.T. & Keyser, L.F. Heterogeneous Reactions of HOCl + HCl $\rightarrow$ $Cl_2 + H_2O$ and $ClONO_2 + HCl \rightarrow Cl_2 + HNO_3$ on Ice Surfaces at Polar Stratospheric Conditions. *J. Phys. Chem.* **97**, 12798-12804 (1993).

6. Molina, M.J. The Chemistry of the Atmosphere: The Impact of Global Change. Calvert, J.G. (ed.), pp. 27-38 (Blackwell Scientific Publications, Boston,1994).

7. Beaglehole Instruments. Picometer Ellipsometer Manual Version 2.0. (2001).

8. Warren, S.G. Optical Constants of Ice from the Ultraviolet to the Microwave. *Appl. Opt.* **23**, 1206-1225 (1984).

9. CRC handbook of chemistry and physics (1996).

10. Pope, R.M. & Fry, E.S. Absorption spectrum (380-700 nm) of pure water .2. Integrating cavity measurements. *Appl. Opt.* **36**, 8710-8723 (1997).

11. Foster, K.L., Tolbert, M.A. & George, S.M. Interaction of HCl with Ice: Investigation of the Predicted Trihydrate, Hexahydrate, and Monolayer Regimes. *J. Phys. Chem. A* **101**, 4979-4986 (1997).

12. Krieger, U.K., Mossinger, J.C., Luo, B.P., Weers, U. & Peter, T. Measurement of the refractive indices of H_2SO_4-HNO_3-H_2O solutions to stratospheric temperatures. *Appl. Opt.* **39**, 3691-3703 (2000).

13. Yunus, W.M.B. & Rahman, A.B. Refractive-Index of Solutions at High-Concentrations. *Appl. Opt.* **27**, 3341-3343 (1988).

14. Stone, J.A. & Stejskal, A. Using helium as a standard of refractive index: correcting errors in a gas refractometer. *Metrologia* **41**, 189-197 (2004).

15. Berland, B.S. *et al.* Refractive-Indexes of Amorphous and Crystalline HNO_3/H_2O Films Representative of Polar Stratospheric Clouds. *J. Phys. Chem.* **98**, 4358-4364 (1994).

16. Mizuno, Y. & Hanafusa, N. Studies of Surface-Properties of Ice Using Nuclear-Magnetic- Resonance. *J. Phys. (Paris)* **48**, 511-517 (1987).

17. Sadtchenko, V. & Ewing, G.E. Interfacial melting of thin ice films: An infrared study. *J. Chem. Phys.* **116**, 4686-4697 (2002).

18. Bluhm, H., Ogletree, D.F., Fadley, C.S., Hussain, Z. & Salmeron, M. The premelting of ice studied with photoelectron spectroscopy. *J. Phys.: Condens. Matter* **14**, L227-L233 (2002).

19. Doeppenschmidt, A. & Butt, H.-J. Measuring the Thickness of the Liquid-like Layer on Ice Surfaces with Atomic Force Microscopy. *Langmuir* **16**, 6709-6714 (2000).

20. Baker, M. & Baker, M.B. A model for the ice-vapor interface at equilibrium. *J. Cryst. Growth* **169**, 393-404 (1996).

21. Ryzhkin, I.A. & Petrenko, V.F. Violation of ice rules near the surface: A theory for the quasiliquid layer. *Phys. Rev. B* **65**, 012205 (2002).

22. Mantz, Y.A., Geiger, F.M., Molina, L.T., Molina, M.J. & Trout, B.L. First-Principles Theoretical Study of Molecular HCl Adsorption on a Hexagonal Ice (0001) Surface. *J. Phys. Chem. A* **105**, 7037-7046 (2001).

23. Mantz, Y.A., Geiger, F.M., Molina, L.T., Molina, M.J. & Trout, B.L. The interaction of HCl with the (0001) face of hexagonal ice studied theoretically via Car-Parrinello molecular dynamics. *Chem. Phys. Lett.* **348**, 285-292 (2001).

24. Hynes, R.G., Mossinger, J.C. & Cox, R.A. The Interaction of HCl With Water-ice at Tropospheric Temperatures. *Geophys. Res. Lett.* **28**, 2827-2830 (2001).

25. Fluckiger, B., Chaix, L. & Rossi, M.J. Properties of the HCl/ice, HBr/ice, and H_2O/ice interface at stratospheric temperatures (200 K) and its importance for atmospheric heterogeneous reactions. *J. Phys. Chem. A* **104**, 11739-11750 (2000).

26. Fluckiger, B., Chaix, L. & Rossi, M.J. Properties of the HCl/ice, HBr/ice, and H_2O/ice interface at stratospheric temperatures (200 K) and its importance for atmospheric heterogeneous reactions (vol 104, pg 11739, 2002). *J. Phys. Chem. A* **107**, 2768 (2003).

Chapter 3

$ClONO_2$ + HCl on ice

3.1 Introduction

The following reactions, which occur on the surfaces of PSC ice particles, act to convert chlorine in the stratosphere from the relatively inert reservoir species HCl and $ClONO_2$ to Cl_2:

$$ClONO_2 + HCl \rightarrow Cl_2 + HNO_3 \qquad (3.1)$$

$$ClONO_2 + H_2O \rightarrow HOCl + HNO_3 \qquad (3.2)$$

$$HOCl + HCl \rightarrow Cl_2 + H_2O \qquad (3.3)$$

The reaction probability, γ, of reaction (3.1) on ice has been found in several laboratory studies to be high ($\gamma > 0.1$)[1-7] and independent of HCl partial pressure, even at very high HCl partial pressures that are known to induce melting of the ice sample[8]. Several scenarios have been proposed for the mechanism of reaction (3.1).

It was suggested that reaction (3.1) may proceed through reaction (3.2) and then reaction (3.3)[3,4], with reaction (3.2) being the rate-limiting step. However, it was later found that, while this pathway is possible, the rate for the direct reaction (3.1) is greater than that for reaction (3.2), and therefore the direct reaction is likely to be more important than the two-step mechanism[5]. Lee et al.[6] observed that when exposing HCl-covered ice to $ClONO_2$ under

stratospherically relevant conditions, monitoring the evolution of the Cl_2 product signal or the $ClONO_2$ reactant signal gave the same result in kinetics analysis, indicating that reaction (3.1) is indeed the major channel for chlorine activation.

The fact that the reaction (3.1) proceeds as efficiently on ice at stratospheric conditions as it does at very high HCl partial pressures that are known to induce melting of the ice sample [8] suggests that reaction (3.1) proceeds via a direct ionic mechanism on ice under stratospheric conditions, as it would on a liquid $HCl{\cdot}H_2O$ solution. Oppliger et al. observed via Knudsen cell experiments that if HCl-covered ice is exposed to $ClONO_2$ under stratospheric conditions, Cl_2 is released immediately, without delay[7]. This was interpreted to mean that Cl_2 is most likely formed directly from reaction of $ClONO_2$ with the adsorbed HCl species to form Cl_2, rather than forming an intermediate precursor species. Furthermore, the same trend of immediate formation of Cl_2 was observed for HCl hexahydrate exposed to $ClONO_2$ [9]. Since HCl is in ionic form in the HCl hexahydrate crystal, the implication is that a direct ionic mechanism is at work under all conditions where immediate evolution of Cl_2 is observed upon exposure of HCl-ice systems to $ClONO_2$ (including stratospherically relevant conditions).

The presence of surface disorder on ice at stratospherically relevant conditions is one possible explanation for the observed efficiency of reaction (3.1) and its apparently ionic nature. Using reaction (3.1) to probe regions of the HCl-ice phase diagram where disorder was and was not observed using ellipsometry can provide a test of this hypothesis and support for our observation that HCl induces surface disordering only in the vicinity of the solid-liquid equilibrium line on the HCl-ice phase diagram.

We have studied the reaction of $ClONO_2$ with HCl adsorbed on zone-refined and smooth ice samples using the coated wall flow tube-CIMS technique. Here we show that the presence of

surface disorder enhances the efficiency of reaction (3.1).

3.2 General experimental procedure

For a general description of the flow tube-CIMS system and ice samples preparation, see section 1.3.

In the $ClONO_2$ + HCl experiments, the ice film was exposed to dilute samples of HCl and $ClONO_2$ via separate heated moveable injectors. The dilute $ClONO_2$ samples were prepared using vapor from a high-purity liquid sample maintained at -77 °C, diluted in He and stored in a darkened glass bulb to prevent UV decomposition. The purity of each dilute sample was checked using UV-vis spectroscopy. A fresh dilute sample was prepared for each day of experiments. The liquid $ClONO_2$ sample was prepared from ClF and $Pb(NO_3)_2$ using the method of Schmeisser[10] (see the Appendix to this chapter for details of the synthesis).

The reactive uptake experiments began with the injectors pushed to the front of the flow tube, past the ice, near the detector inlet. First, constant flows of HCl and $ClONO_2$ were established and the corresponding baseline signals were recorded. The HCl injector was withdrawn and the entire length of the ice sample was allowed to reach equilibrium with the gas phase HCl.

The $ClONO_2$ injector was then withdrawn to expose the desired length of HCl-covered ice to $ClONO_2$. The uptake $ClONO_2$ and the associated Cl_2 evolution were monitored. To obtain reaction probability data, reactive uptake measurements were performed for several exposed ice lengths (and thus reaction times). The slope of a plot of the natural logarithm of the observed change in partial pressure of the product species, Cl_2, versus reaction time yields the observed reaction rate constant. The observed reaction rate constant can then be converted into a

wall loss rate constant and reaction probability using the Brown algorithm, which accounts for diffusion to the wall in the laminar flow tube[11].

Values of reaction probability reported here were calculated using a $ClONO_2$ diffusion coefficient in He of 176 cm^2sec^{-1}Torr at -73 °C, assuming a $T^{1.76}$ dependence (with T in Kelvin)[12]. Reported uncertainties reflect an assumed 20% uncertainty in diffusion coefficient and the uncertainty in observed loss rates.

3.3 Results

3.3.1 Zone-refined ice samples

The reaction of $ClONO_2$ with adsorbed HCl on zone-refined ice cylinders was studied using the flow tube-CIMS technique. The results of this study are shown in Figure 3-1 and Figure 3-2. Experiments shown were conducted at approximately 10^{-6} Torr HCl and $5{\cdot}10^{-7}$ Torr $ClONO_2$ (pseudo-first-order conditions). The left and right panels show studies of the reaction at -77 °C and -56 °C, respectively, and the upper and lower panels show $ClONO_2$ and Cl_2 mass spectrometer signals, respectively. The production of Cl_2, and thus the efficiency of the reaction, decreased as we moved from conditions where surface change was observed with the ellipsometer (the 'QLL' region of the phase diagram) to those where no surface change was observed (the 'non-QLL' region of the phase diagram). At -77 °C, the reaction was observed to proceed efficiently ($\gamma > 0.1$), and HCl was readily available on the surface for reaction, as has been observed by previous investigators [1,2,4-7]. At -55 °C, with the same reactant concentrations, HCl was no longer readily available on the surface for reaction, despite the constant gas-phase

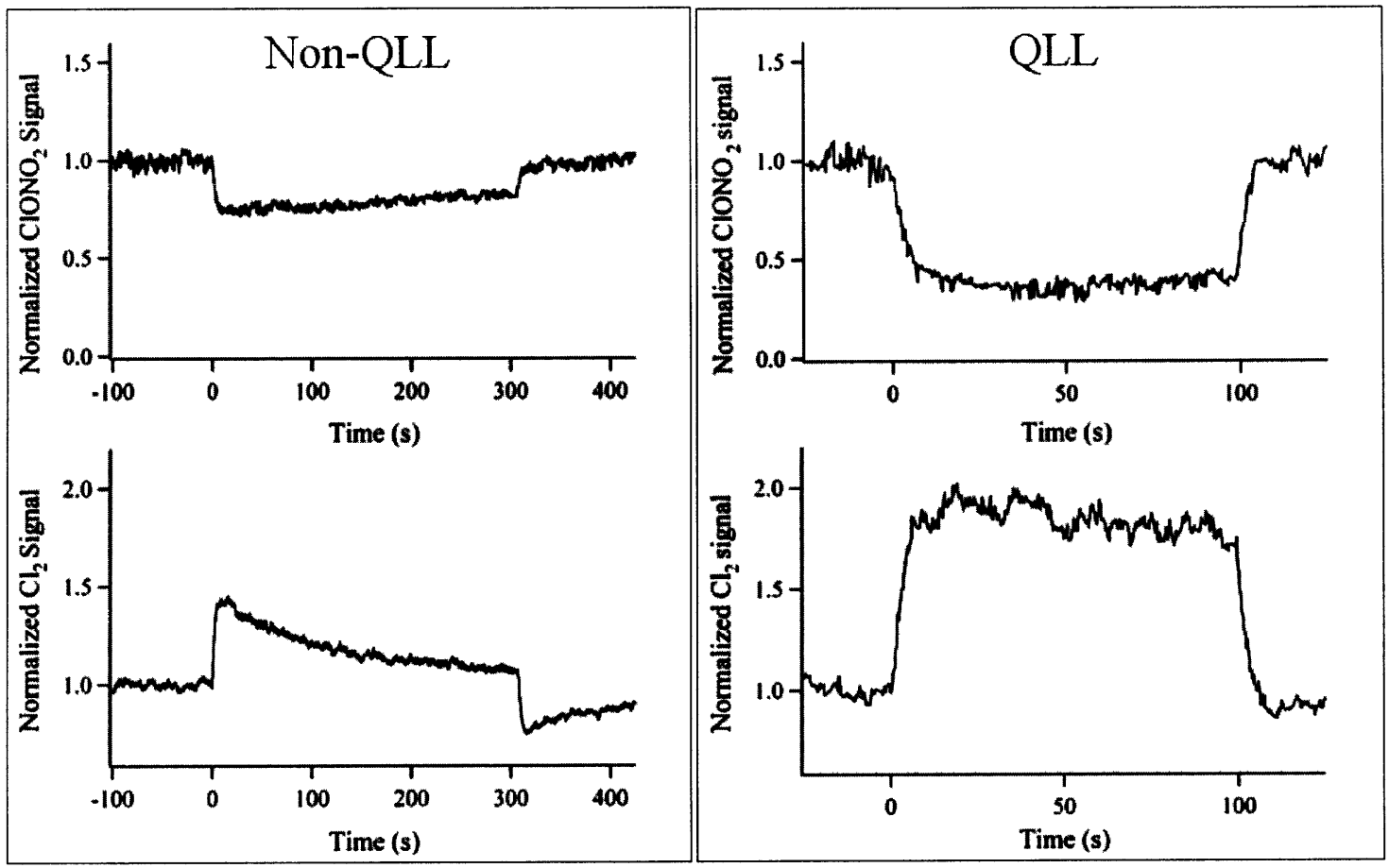

Figure 3-1. The reaction of $ClONO_2$ with adsorbed HCl on zone-refined ice cylinders. Experiments shown were conducted at approximately $1 \cdot 10^{-6}$ Torr HCl, $5 \cdot 10^{-7}$ Torr $ClONO_2$ (pseudo-first-order conditions). The left and right panels show studies of the reaction at -56 °C and -77 °C, respectively, and the upper and lower panels show $ClONO_2$ and Cl_2 mass spectrometer signals, respectively.

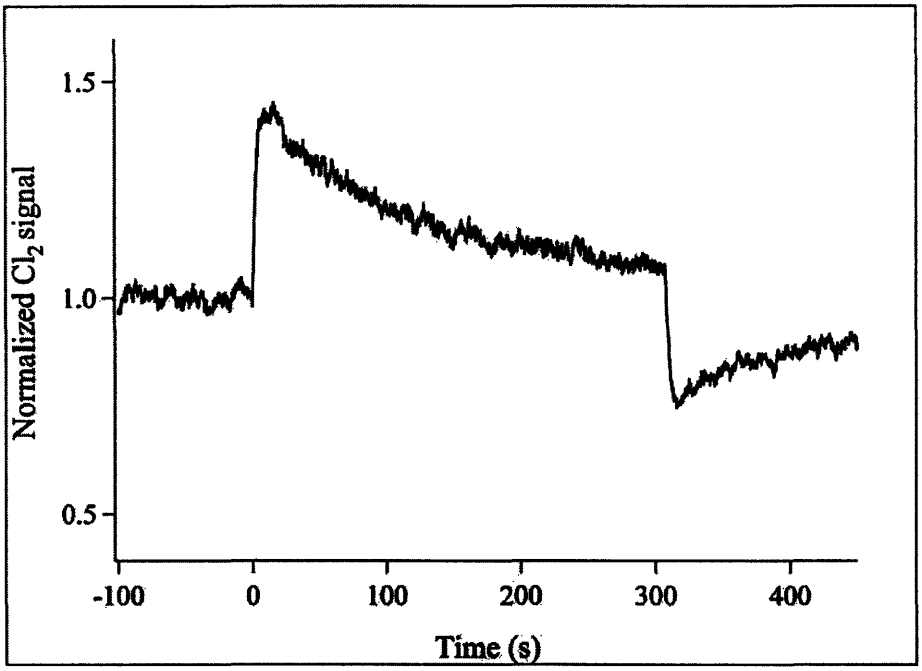

Figure 3-2. Cl_2 mass spectrometer signal for the reaction of $ClONO_2$ with adsorbed HCl on zone-refined ice at approximately $1 \cdot 10^{-6}$ Torr HCl, $5 \cdot 10^{-7}$ Torr $ClONO_2$ and -56 °C.

presence of HCl. Under these conditions, Cl_2 evolution consisted of an initial 'burst' followed by a tailing off of Cl_2 release. Kinetic analysis of the 'burst' portion of the Cl_2 signal yields a reactive uptake coefficient at least one order of magnitude smaller ($\gamma = 0.014$ +/- 0.005) than the same reaction at temperatures where surface change was observed using ellipsometry.

3.3.2 Smooth ice films

Reaction (3.1) was also studied on smooth ice films using the flow tube-CIMS technique at a variety of conditions (-77 °C, -73 °C, and -55 °C, and 10^{-7} Torr < P_{HCl} < $2 \cdot 10^{-6}$ Torr). P_{ClONO2} was again controlled to half or less of the value of P_{HCl} so as to maintain pseudo-first-order conditions. When only $ClONO_2$ loss was monitored, kinetic analysis of the data obtained

in this study yielded in all cases a corroboration of literature results ($\gamma > 0.1$), regardless of the location within the 'ice' stability region of the phase diagram.

The Cl_2 evolution traces for this study showed a difference in HCl surface availability in the 'QLL' and 'non-QLL' regions of the HCl-ice phase diagram similar to that observed in the zone-refined ice study, although the distinction was more pronounced for the zone-refined ice samples. The results of this study are shown in Figure 3-3 and Figure 3-4. Experiments shown were conducted at approximately 10^{-6} Torr HCl and $5 \cdot 10^{-7}$ Torr $ClONO_2$ (pseudo-first-order conditions). The left and right panels of Figure 3-2 show studies of the reaction at -55 °C and -75 °C, respectively, and the upper and lower panels show $ClONO_2$ and Cl_2 mass spectrometer signals, respectively. Figure 3-3 shows in further detail the Cl_2 evolution trace for the reaction at -55 °C.

For the reaction at -75 °C, 10^{-6} Torr HCl and $4.5 \cdot 10^{-7}$ Torr $ClONO_2$, HCl was observed to be readily available on the surface for reaction. At -55 °C with the same reactant concentrations, Cl_2 evolution was less in relative magnitude and consisted of an initial 'burst' followed by a decrease of Cl_2 release, however, the relative magnitudes of the 'burst' and the following plateau were closer than what was observed in the zone-refined ice study.

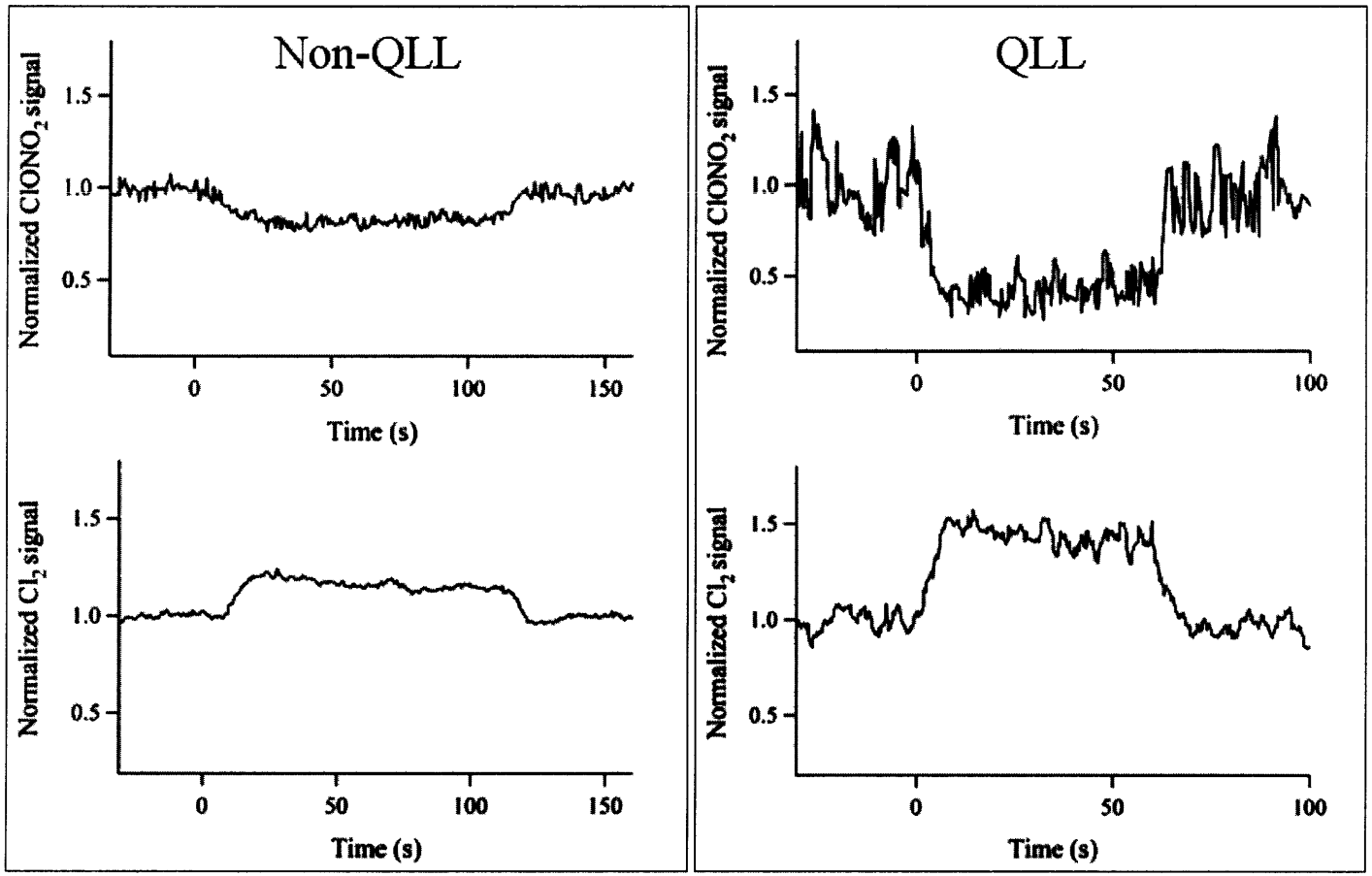

Figure 3-3. The reaction of $ClONO_2$ with adsorbed HCl on smooth ice films. Experiments shown were conducted at approximately $1 \cdot 10^{-6}$ Torr HCl, $5 \cdot 10^{-7}$ Torr $ClONO_2$ (pseudo-first-order conditions). The left and right panels show studies of the reaction at -55 °C and -75 °C, respectively, and the upper and lower panels show $ClONO_2$ and Cl_2 mass spectrometer signals, respectively.

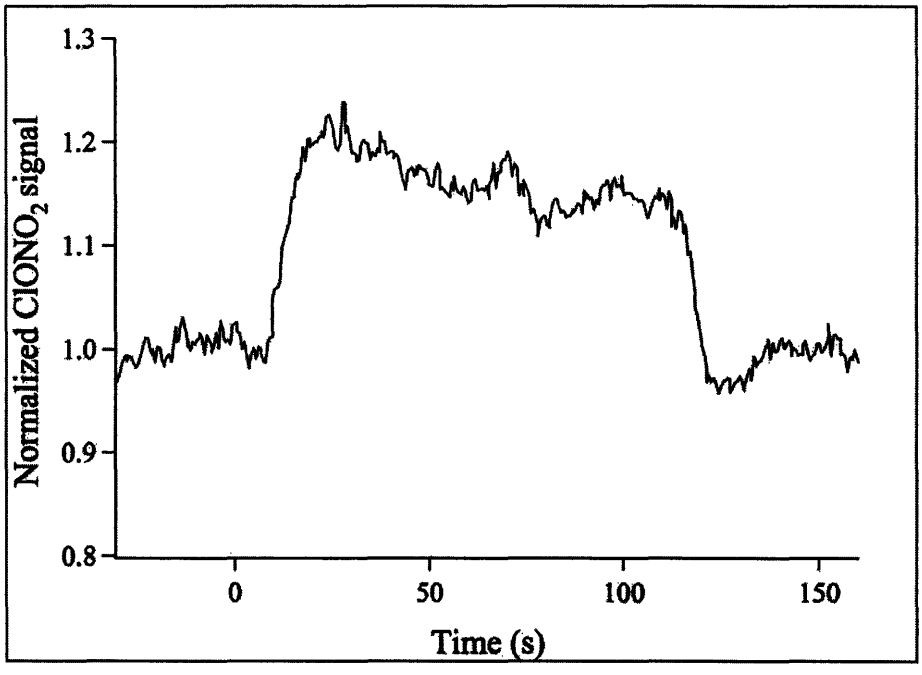

Figure 3-4. Cl_2 mass spectrometer signal for the reaction of $ClONO_2$ with adsorbed HCl on smooth ice film at approximately $1{\cdot}10^{-6}$ Torr HCl, $5{\cdot}10^{-7}$ Torr $ClONO_2$ and -55 °C.

3.4 Discussion

The efficiency of the $ClONO_2$ + HCl reaction on zone-refined ice was observed to be enhanced in the 'QLL' region of the HCl-ice phase diagram compared to the range of conditions where HCl was not observed to induce surface disorder with the ellipsometer. It is clear that the presence of the QLL serves to enhance the reaction. The reaction-enhancing role of the QLL may lie in its ability to supply HCl to the reaction, and/or in its ability to facilitate ionization of the reactants.

The reaction was observed to proceed less efficiently when no surface disorder was present than under QLL conditions. No detectable delay was observed in Cl_2 evolution upon exposure of the HCl-covered ice samples to $ClONO_2$; in fact, Cl_2 evolution under 'non-QLL'

conditions was observed to consist of an initial burst followed by a by a tailing off of Cl_2 release. While the flow tube-CIMS technique does not provide us with direct experimental evidence of the molecules on the surface during reaction, following the logic of Oppliger et al.[7] and Horn et al.[9], this suggests that reaction (3.1) proceeds via a direct mechanism in the absence of the QLL, but is limited by the availability of HCl on the surface.

For the reactive uptake measurements on smooth ice, when $ClONO_2$ loss was monitored rather than Cl_2 evolution, this study yielded high reaction probability ($\gamma > 0.1$), regardless of the location within the 'ice' stability region of the phase diagram. One possible explanation for this is the following: it is expected that $ClONO_2$ loss would be efficient both on bare ice ($ClONO_2$ hydrolysis, reaction (3.2)) and in the presence of HCl under these conditions, and therefore this probe is insensitive to the availability of HCl on the surface. This suggests that the degree of surface disorder does not affect the rate of $ClONO_2$ hydrolysis.

3.5 Conclusions

We have shown that the presence of surface disorder enhances the chlorine-activation reaction of HCl with chlorine nitrate ($ClONO_2$). The results of this study lend support for the trend observed via ellipsometry that surface disorder is induced by the presence of HCl in the vicinity of the solid-liquid equilibrium line on the HCl-ice phase diagram, but that no detectable disorder was observed on the interior of the 'ice' phase envelope.

Appendix: Synthesis of $ClONO_2$

In atmospheric chemistry laboratories, the synthesis of $ClONO_2$ is most commonly achieved via reactions of chlorine oxides with NO_2 or N_2O_5 [2,12-14]. Another approach to $ClONO_2$ synthesis, which was first suggested by Shack, is the reaction of ClF with HNO_3[15]. This approach is less environmentally friendly than the chlorine oxide/nitrogen oxide reactions, but avoids the preparation and handling of hazardous chlorine oxides and simplifies the synthesis to a single step. The main drawback of the Shack approach is that that gaseous HF is produced as a byproduct of the reaction. HF requires careful handling, and it also has a boiling point very close to that of $ClONO_2$ ($ClONO_2$: 22.3 °C, HF: 19.5 °C), making separation difficult[10].

The approach used in this study was originally presented by Schmeisser[10,16,17]. This approach produces high purity $ClONO_2$ in a single reaction step:

$$2\ ClF(g) + Pb(NO_3)_2\ (s) \rightarrow 2\ ClONO_2(g) \qquad (3.4)$$

1. Fill a glass bulb with 0.2 mol ClF(g) (i.e., for 4.8 L bulb fill to 760 Torr). Both the bulb and the vacuum line (including the cold trap) should be dry to avoid HF formation and glass etching. When shutting down vacuum line after handling ClF, the trap should be purged with dry N_2 or He (rather than room air). The vacuum line and the bulb should also be free of organics in order to avoid the oxidation reaction with ClF. Every precaution should be taken to avoid exposure to and/or release of ClF.

2. Dry $Pb(NO_3)_2$ overnight in oven at 110 °C [18]. Any lumps should be broken up or discarded. $Pb(NO_3)_2$ should be in excess by at least 20% in order to ensure complete

conversion of ClF to $ClONO_2$. Skin contact with $Pb(NO_3)_2$ should be avoided.

3. Transfer dry $Pb(NO_3)_2$ to a clean, dry 1200 mL stainless steel reactor vessel. Evacuate and seal the reactor, and place in liquid nitrogen bath.

4. Arrange the ClF-filled bulb and the reactor vessel on the vacuum line as shown in Figure 3-5. The valve to the vacuum line is closed during the procedure.

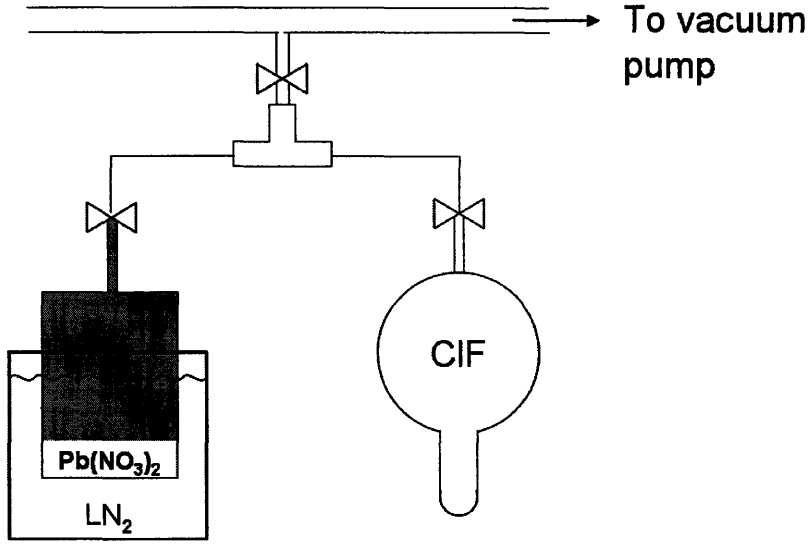

Figure 3-5. Experimental setup for $ClONO_2$ synthesis.

5. Open the reactor and ClF-filled bulb to the evacuated line and allow 1-2 hours for ClF to condense onto $Pb(NO_3)_2$.

6. Seal the reactor and transfer to a dry ice-isopropanol bath (-77 °C). Leave overnight.

7. The reaction is complete when the pressure inside the reactor has decreased to the $ClONO_2$ vapor pressure at -77 °C (approximately 1 Torr). See Table 3-1 for a list of ClF vapor pressures at relevant temperatures.

Temperature	ClF Vapor Pressure (Torr)
-196 °C (liquid nitrogen)	< 0.75
-95 °C (toluene-liquid nitrogen)	465
-77 °C (dry ice-isopropanol)	1425

Table 3-1. Vapor pressure of ClF at select temperatures[19].

8. Transfer the $ClONO_2$ product via the vacuum line to a sample finger held at liquid nitrogen temperature. The finger should be clean, dry, $ClONO_2$ conditioned, evacuated, and equipped with Viton® o-ring seal. Shroud finger to avoid exposing the product to light. Gradually warm the reactor to room temperature to collect all product.

9. Distill product repeatedly at -95 °C (toluene-liquid nitrogen) and -77 °C (dry ice-isopropanol) until high purity is reached. Check purity via UV-vis spectroscopy. Each distillation stage involves condensing product from one finger held at the distillation temperature to another finger held at liquid nitrogen temperature. For the -77 °C distillation, pure sample and high-vapor-pressure impurities will be collected in the liquid nitrogen finger and low-vapor-pressure impurities, such as HNO_3, will remain. For the -95 °C distillation, high-vapor-pressure impurities, such as chlorine oxides, will be

collected in the liquid nitrogen finger and the pure sample will remain.

Store the pure sample in a double-valved sample finger with Viton® o-ring seals in a dry ice-isopropanol bath in the dark.

References for Chapter 3

1. Molina, M.J., Tso, T.L., Molina, L.T. & Wang, F.C.Y. Antarctic Stratospheric Chemistry of Chlorine Nitrate, Hydrogen Chloride and Ice - Release of Active Chlorine. *Science* **238**, 1253-1257 (1987).

2. Leu, M.T. Laboratory Studies of Sticking Coefficients and Heterogeneous Reactions Important in the Antarctic Stratosphere. *Geophys. Res. Lett.* **15**, 17-20 (1988).

3. Abbatt, J.P.D. & Molina, M.J. Heterogeneous Interactions of $ClONO_2$ and HCl on Nitric-Acid Trihydrate at 202 K. *J. Phys. Chem.* **96**, 7674-7679 (1992).

4. Hanson, D.R. & Ravishankara, A.R. Investigation of the Reactive and Nonreactive Processes Involving $ClONO_2$ and HCl on Water and Nitric-Acid Doped Ice. *J. Phys. Chem.* **96**, 2682-2691 (1992).

5. Chu, L.T., Leu, M.T. & Keyser, L.F. Heterogeneous Reactions of HOCl+HCl $\rightarrow$ Cl_2+H_2O and $ClONO_2$+HCl $\rightarrow$ Cl_2+HNO_3 on Ice Surfaces at Polar Stratospheric Conditions. *J. Phys. Chem.* **97**, 12798-12804 (1993).

6. Lee, S.H., Leard, D.C., Zhang, R., Molina, L.T. & Molina, M.J. The HCl+$ClONO_2$ reaction rate on various water ice surfaces. *Chem. Phys. Lett.* **315**, 7-11 (1999).

7. Oppliger, R., Allanic, A. & Rossi, M.J. Real-time kinetics of the uptake of $ClONO_2$ on ice and in the presence of HCl in the temperature range $160K \leq T \leq 200K$. *J. Phys. Chem. A* **101**, 1903-1911 (1997).

8. Abbatt, J.P.D. *et al.* Interaction of HCl vapor with water-ice: Implications for the stratosphere. *J. Geophys. Res.* **97**, 15819-15826 (1992).

9. Horn, A.B., Sodeau, J.R., Roddis, T.B. & Williams, N.A. Mechanism of the heterogeneous reaction of hydrogen chloride with chlorine nitrate and hypochlorous acid on water ice. *J. Phys. Chem. A* **102**, 6107-6120 (1998).

10. Schmeisser, M., Eckermann, W., Gundlach, K.P. & Naumann, D. New Methods for the Preparation of Chlorine Nitrate $ClONO_2$. *Z. Naturforsch. B* **35**, 1143-1145 (1980).

11. Brown, R.L. Tubular Flow Reactors with 1st-Order Kinetics. *J. Res. Natl. Bur. Stand.* **83**, 1-8 (1978).

12. Hanson, D.R. & Ravishankara, A.R. The Reaction Probabilities of $ClONO_2$ and N_2O_5 on Polar Stratospheric Cloud Materials. *J. Geophys. Res.-Atmos.* **96**, 5081-5090 (1991).

13. Molina, L.T., Spencer, J.E. & Molina, M.J. Rate Constant for Reaction of O(P-3) Atoms with $ClONO_2$. *Chem. Phys. Lett.* **45**, 158-162 (1977).

14. Geiger, F.M., Tridico, A.C. & Hicks, J.M. Second Harmonic Generation Studies of Ozone Depletion Reactions on Ice Surfaces under Stratospheric Conditions. *J. Phys. Chem. B* **103**, 8205-8215 (1999).

15. Schack, C.J. A New Synthesis of Chlorine Nitrate. *Inorg. Chem.* **6**, 1938-1939 (1967).

16. Xu, S.L., Blake, T.A. & Sharpe, S.W. High-resolution infrared spectroscopy of the upsilon(4) fundamental band of chlorine nitrate. *J. Mol. Spec.* **175**, 303-314 (1996).

17. LAMOCS Final Report, p. 91 (1998).

18. The decomposition temperature of $Pb(NO_3)_2$ is 290 °C, and its melting point is 470 °C

19. CRC handbook of chemistry and physics (1996).

Chapter 4

HCl-Ice interaction: Flow tube-CIMS studies

4.1 Introduction

Characterization of the interaction of HCl with PSC ice particles is essential to understanding chlorine activation. As was discussed in detail in Chapter 1, the HCl-ice system has been investigated using a variety of experimental and theoretical approaches. While these studies have shown that HCl has a high affinity for PSC surfaces, with near-monolayer surface coverages at conditions relevant to PSC events, the roles HCl and the ice surface play in the reaction of $ClONO_2$ and HCl on ice remain to be clarified. At the heart of this uncertainty are the state of the ice surface under stratospheric conditions and the fate of HCl upon adsorption onto the ice surface.

Here we present a detailed flow tube-CIMS investigation of the interaction of HCl with zone-refined, smooth, and vapor-deposited ice films. The results of this study give new information about the fate of HCl upon adsorption to different types of ice under conditions where HCl-induced disordering on ice was and was not observed using ellipsometry, and under conditions where HCl hexahydrate is formed. They also provide additional support to our observation made via ellipsometry that HCl induces surface disordering only in the vicinity of the solid-liquid equilibrium line on the HCl-ice phase diagram.

The study of HCl hexahydrate formation on smooth ice described in this chapter was performed in conjunction with Prof. Franz Geiger, currently of Northwestern University.

4.2 General experimental procedure

For a general description of the flow tube-CIMS system and ice sample preparation, please see section 1.3.

In the HCl uptake experiments, the ice sample was exposed to a dilute mixture of HCl (0.09% HCl mixture in Nitrogen, Matheson, further diluted in helium) via a heated moveable injector positioned near the centerline of the flow tube. The experiments began with the injector pushed to the front of the flow tube, past the ice, near the detector inlet. After a baseline HCl signal was established, the injector was then withdrawn, exposing the desired length of ice film to HCl. In most cases, upon withdrawing the injector, the HCl signal was observed to drop and then slowly recover as the surface approached equilibrium. After the desired uptake time had passed, the injector was returned to the front of the flow tube, and the observed signal reflected the original baseline signal plus the signal from any desorbing HCl.

Surface coverage data was extracted from the uptake curves by numerically integrating to find the area between the curve and the baseline. To account for unknown irregularities at the front of the ice film, and any artifacts due to mixing at the tip of the injector, absolute surface coverages reported here are the difference in coverage between two uptake curves for two different exposed areas. Reported uncertainties in surface coverage reflect the noise in the signal, which was carried through the arithmetic operations according to Jeffries[1].

4.3 Results

4.3.1 Zone-refined ice samples

The results of our flow tube-CIMS studies of HCl adsorption on zone-refined ice cylinders, as shown in Figure 4-1, demonstrate that the nature of the interaction of HCl with the ice samples differs at the conditions under which surface change was observed with ellipsometry from the HCl-ice interaction at conditions under which no surface change was observed.

In flow tube-CIMS studies of HCl uptake at -59 °C and $6.5 \cdot 10^{-7}$ Torr HCl, conditions under which no surface change was observed with ellipsometry, we observed uptake that appeared to be largely irreversible. Uptake under these conditions is shown in the top panel of Figure 4-1. We observed the signal returning to the baseline within the experimental noise within 1000 seconds of initiation of desorption, with recovery of roughly 20% of the adsorbed HCl molecules. We observed an initial fast mode of HCl adsorption ($6.0(1) \cdot 10^{14}$ molecules$\cdot$cm^{-2} over 500 seconds), followed by a slower uptake mode, with the signal returning to at least 90% of the baseline within 3000 seconds. Total HCl uptake was $1.2(1) \cdot 10^{15}$ molecules$\cdot$cm^{-2}. A memory effect was observed in that uptake decreased in magnitude with subsequent exposures of the same ice cylinder, with the third exposure resulting in roughly 60% of the uptake measured upon the first exposure of the ice cylinder to HCl.

Uptake at -77 °C and $7.4 \cdot 10^{-7}$ Torr HCl (QLL-forming conditions) is shown in the bottom panel of Figure 4-1. An initial fast uptake mode was observed, resulting in uptake of approximately $2 \cdot 10^{14}$ molecules$\cdot$cm^{-2} over 180 seconds. A second adsorption mode was observed that consisted of a nearly constant flux of HCl ($5 \cdot 10^{11}$ molecules$\cdot$cm$^{-2}\cdot$s^{-1}) from the surface to the interior of the ice sample, which persisted throughout the time scale of the

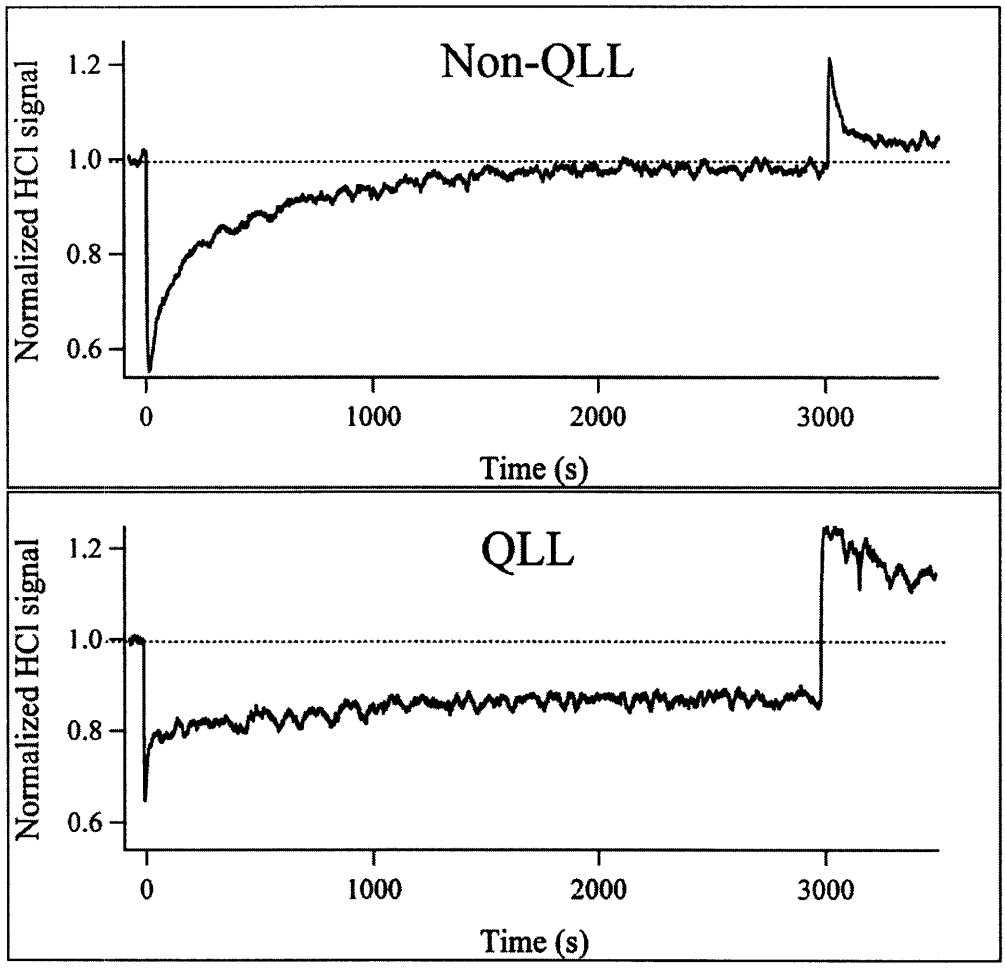

Figure 4-1. HCl adsorption on zone-refined ice under non-QLL and QLL-forming conditions. Each panel shows normalized HCl mass spectrometer signal on the left axis and time on the bottom axis. The top and bottom panels are for adsorption at approximately $7 \cdot 10^{-7}$ Torr HCl, and at -77 °C and -59 °C, respectively.

experiment (1 hour). A memory effect was observed in that this flux appeared to increase in magnitude with subsequent exposures of the same ice crystal. Complete desorption data is not available for adsorption under these conditions, but we observed that, upon initiation of desorption, roughly 80% of the adsorbed HCl molecules were desorbed within the amount of time that had elapsed during adsorption, and desorption continued beyond this point, indicating

that adsorption on zone-refined ice under QLL-forming conditions is largely reversible.

Figure 4-2 shows HCl-induced melting at -70.5 °C and $1.1 \cdot 10^{-5}$ Torr HCl along with uptake at -77 °C and $7.4 \cdot 10^{-7}$ Torr HCl (QLL-forming conditions). It can be seen that the signal vs. time curve for adsorption in QLL-forming conditions is distinct from that of HCl-induced melting.

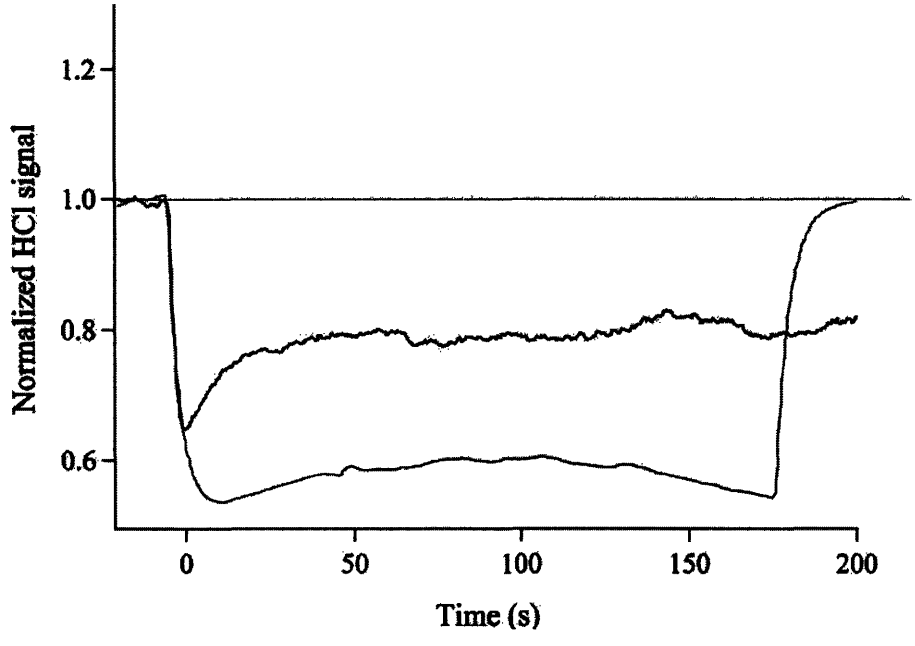

Figure 4-2. HCl adsorption on zone-refined ice under QLL-forming and melt conditions. The black trace shows adsorption at $7 \cdot 10^{-7}$ Torr HCl and -77 °C ('QLL' conditions). The grey trace is for HCl–induced melting at -70.5 °C and $1.1 \cdot 10^{5}$ Torr HCl.

4.3.2 Smooth and vapor-deposited ice films

The uptake of HCl on smooth and vapor-deposited ice films was studied at -77 °C, -70 °C, and -60 °C, and $5 \cdot 10^{-8}$ Torr < P_{HCl} < $3 \cdot 10^{-6}$ Torr. Uptake curves that illustrate the results of this study are shown in Figures 4-3 and 4-4. Generally, we again observed an initial fast mode

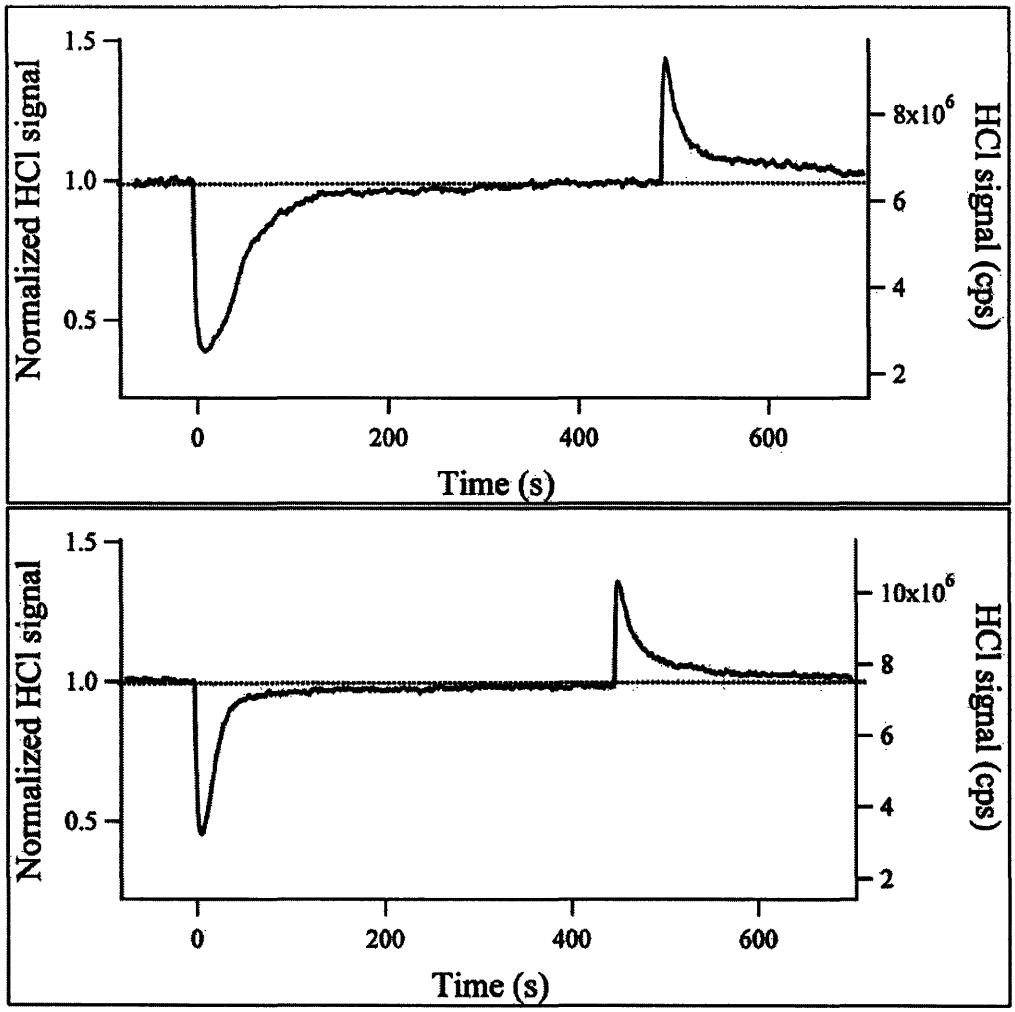

Figure 4-3. HCl uptake on smooth ice samples at -60 °C and $7.4 \cdot 10^{-7}$ Torr HCl. Each panel shows HCl mass spectrometer signal for an uptake experiment, with the normalized signal on the left axis and the raw signal on the right axis. The upper panel shows adsorption onto a 'fresh' ice sample. The lower panel shows adsorption for subsequent exposures.

of HCl adsorption, accounting for at least 75% of the total uptake within 180 seconds, followed by a slower uptake mode, with the signal returning to at least 95% of the baseline within 1000 seconds.

Upon the first exposure of a fresh ice surface to HCl, only a fraction of the adsorbed HCl

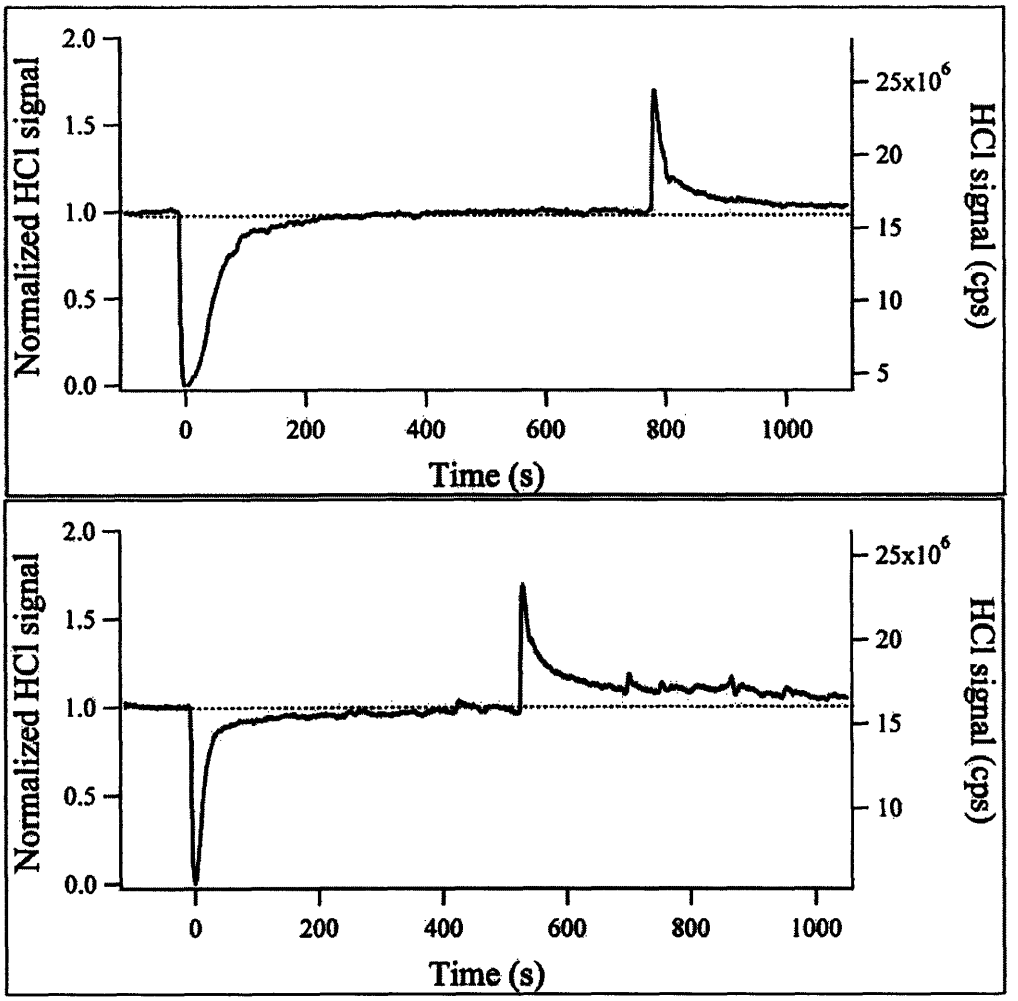

Figure 4-4. HCl uptake on smooth ice samples at -77 °C and 10^{-6} Torr HCl. Each panel shows HCl mass spectrometer signal for an uptake experiment, with the normalized signal on the left axis and the raw signal on the right axis. The upper panel shows adsorption onto a 'fresh' ice sample. The lower panel shows adsorption for subsequent exposures.

was recovered when the injector was returned to the front of the flow tube and desorption was initiated. This is an indication of both reversible and irreversible adsorption processes on the surface. Adsorption curves of this type are depicted in the upper panels of Figure 4-3 and 4-4. All subsequent exposures resulted in adsorption that is fully reversible on the time scale of the

experiment (minutes). Adsorption curves of this type are depicted in the lower panels of Figure 4-3 and 4-4. Surface coverage was observed to be essentially constant for the second, third and fourth exposures of an ice film to HCl. This effect was not observed to be reversible: after removing the HCl source for up to 1.5 hours, additional HCl desorption was not detected, and in the next uptake experiment no additional irreversible uptake was observed. The uptake curve was typical of an ice surface that has been previously exposed to HCl rather than a refreshed ice surface.

Saturation surface coverage was measured to be $2\text{-}3.10^{14}$ molecules·cm^{-2} on smooth ice after the first HCl exposure, depending on temperature. Surface coverages for the first exposure of a fresh ice surface to HCl were observed to be 1.5-2 times greater than aged ice surface coverages on smooth ice, depending on temperature. At -77 °C, the ratio of irreversibly adsorbed HCl molecules to reversibly adsorbed HCl molecules was 0.99(9):1. At -60 °C, the ratio of irreversibly adsorbed HCl molecules to reversibly adsorbed HCl molecules was 0.76(8):1. Each of these ratios is an average of ratios calculated from uptake data from five aging experiments, with each experiment consisting of a sequence of four exposures (HCl adsorption and desorption) on one ice film. No dependence of the ratio on P_{HCl} was observed at any temperature.

The ratio of irreversibly adsorbed HCl molecules to reversibly adsorbed HCl molecules was not observed to be appreciably different for smooth ice films and vapor-deposited ice films. The only difference in uptake on smooth and vapor-deposited ice films was in the magnitude of observed uptake, due to the higher surface area of the vapor-deposited ice. HCl surface coverage for a ~200 μm thick ice film deposited from the vapor phase at a rate of 4 mg·min^{-1} was approximately 7 times greater than coverage on smooth ice at the same conditions.

4.3.3 HCl hexahydrate formation

On smooth ice films, at -87 °C and HCl partial pressures above $4.5 \cdot 10^{-7}$ Torr, we observed HCl losses beyond the expected profile for an adsorption/saturation process consistent with the formation of the HCl hexahydrate. Figure 4-5 shows uptake curves for HCl adsorption on smooth ice at -87 °C for HCl partial pressures of $3.9 \cdot 10^{-7}$ Torr and $5.8 \cdot 10^{-7}$ Torr. For the lower HCl partial pressure, the uptake curve exhibits an initial fast adsorption mode followed by slower adsorption leading to saturation. At the higher HCl partial pressure, which lies in the region of the HCl-ice phase diagram where HCl hexahydrate is the stable phase (see Figure 1-2), the same fast adsorption mode is observed initially, but then approximately 150 seconds after exposure a pronounced dip appears in the signal which is indicative of a secondary adsorption process. Uptake curves of this form were only found within the HCl hexahydrate stability region of the HCl-ice phase diagram.

We tested this secondary adsorption process to confirm that it was hexahydrate formation by measuring the water vapor pressure of several smooth ice films held between -85 °C and -78 °C as a function of HCl partial pressure in the flow tube. At each ice film temperature, the water vapor pressure remained at the equilibrium ice vapor pressure for small P_{HCl}, and decreased for HCl partial pressures above the HCl hexahydrate stability line on the phase diagram, with slopes corresponding to the molar ratio of water to HCl (6:1) of the HCl hexahydrate.

HCl uptake beyond saturation corresponding to HCl hexahydrate formation was also observed on zone-refined ice and on single-crystalline ice samples. HCl hexahydrate formation was not observed on vapor-deposited ice samples under any conditions. Shown in Figure 4-6

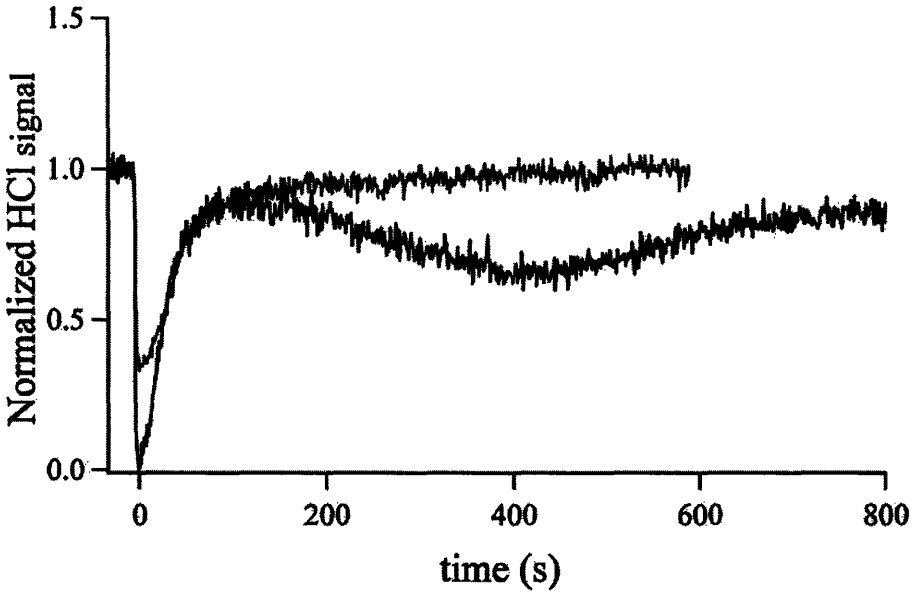

Figure 4-5. HCl adsorption on smooth ice at -87 °C. The gray trace was obtained for an HCl partial pressure of $3.9 \cdot 10^{-7}$ Torr; the black trace was obtained for an HCl partial pressure of $5.8 \cdot 10^{-7}$ Torr.

is a summary of the results of several HCl uptake experiments on smooth, vapor-deposited, zone-refined, and single-crystal ice samples under the range of conditions known to produce HCl hexahydrate, superimposed on a detail of the HCl-ice phase diagram from Molina[2]. Experiments were performed on single-crystal ice samples as part of the ellipsometer-CIMS study, as described in Chapter 2.

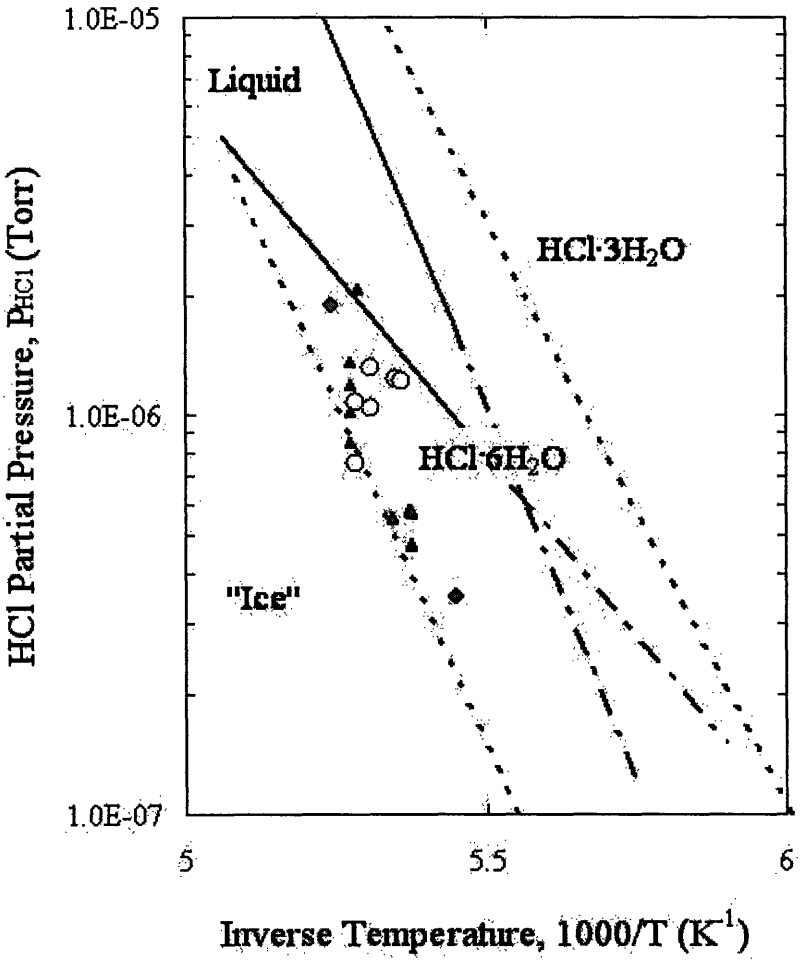

Figure 4-6. HCl hexahydrate formation for different types of ice surface. The background is a detail of the HCl-ice phase diagram from Molina[2]. Triangles represent experiments on smooth ice, circles represent experiments on vapor-deposited ice films, and diamonds represent experiments on zone-refined or single-crystalline ice samples. Filled symbols indicate observed HCl uptake beyond saturation corresponding to HCl hexaydrate formation, and open circles indicate no observed HCl hexahydrate formation.

4.4 Discussion

4.4.1 QLL formation

The results of this study lend support for the trend observed via ellipsometry that surface disorder is induced by the presence of HCl in the vicinity of the solid-liquid equilibrium line on the HCl-ice phase diagram, but that no detectable disorder was observed on the interior of the 'ice' phase envelope. The results of the HCl uptake experiments on zone-refined ice, as shown in Figure 4-1, provide further evidence that the nature of HCl adsorption on ice differs at the conditions under which surface change was observed with ellipsometry from the HCl-ice interaction at conditions under which no surface change was observed.

On zone-refined ice in the 'QLL' region of the HCl-ice phase diagram, a nearly constant flux of HCl from the surface to the interior of the ice sample was observed, which persisted throughout the time scale of the experiment (1 hour). To further investigate this effect, we employed our flow tube model as described in section 1.4 with a model of (a) absorption of HCl to a true liquid water layer, (b) absorption to a bulk ice layer, and (c) absorption to a surface layer with an HCl solubility, and thus desorption rate constant, intermediate between that of water and ice. In all cases the model accounted for diffusion from the surface layer into the bulk (as in eq. 1-22), assuming a diffusion constant for HCl in ice of 10^{-12} cm^2s^{-1} [3]. The adsorption rate was calculated based on gas kinetic theory (eq.1-1) and the rates of desorption for ice and water were calculated based on solubility data (as in eq. 1-4). Note that, when calculating the rates of desorption from equilibrium data, rates are scaled with the ratio of the volume element of film to the volume element of gas, and are therefore dependent on the thickness of the surface layer. For bulk ice, the desorption parameter $k_{des} \cdot V_{film}/V_{gas} = 5.2 \cdot 10^{-4}$ s^{-1}, based on a solubility of

$3.5 \cdot 10^{-7}$ moles HCl·cm^{-3} ice at -73 °C and 10^{-6} Torr HCl, from Thibert and Domine[3]. For liquid water, $k_{des} \cdot V_{film}/V_{gas} = 6.7 \cdot 10^{-31}$ s^{-1}, based on a solubility of 25 % by weight at -77 °C and $1.5 \cdot 10^{-5}$ Torr HCl, from the phase diagram of Molina[2].

The results of the simulations are shown along with the experimental data for comparison in Figure 4-7. HCl uptake on zone-refined ice under QLL-forming conditions can be best be described at long times by absorption to a surface layer with a desorption rate of $k_{des} \cdot V_{film}/V_{gas} = 1.5.10^{-6}$ s^{-1}, intermediate between that of a true liquid layer and bulk ice. For $k_{des} \cdot V_{film}/V_{gas} = 1.5.10^{-6}$ s^{-1} and a surface layer 100 nm thick, assuming $\gamma = 0.1$, and $D_i = 10^{-12}$ cm^{2}s^{-1}, we find that, after 3000 seconds of exposure to gas phase HCl, the near-surface concentration throughout the exposed area of the film reaches a value of approximately $9 \cdot 10^{-5}$ moles HCl·cm^{-3}, and the diffusive flux from the near-surface region into the interior of the film is $5.3 \cdot 10^{11}$ molecules·cm^{-2}·s^{-1}.

Recalling Figure 1-9, the results of this analysis suggest that the surface-to-bulk loss we observe at long times can be explained in part by diffusion from a relatively concentrated surface layer into the bulk. This interpretation is consistent with those put forth by Huthwelker et al.[4] and the Rossi group[5-9].

At long times, our model is insensitive to surface layer thickness. This can be seen by comparing the curves labeled (c) and (d) in Figure 4-7, which show adsorption for surface layers 100 nm and 1 nm thick, respectively, both with $k_{des} \cdot V_{film}/V_{gas} = 1.5.10^{-6}$ s^{-1}. The reason for this is that, regardless of the thickness of the layer, the same equilibrium near-surface concentration is achieved within a relatively short time. At long times the surface-to-bulk diffusive flux, in eq. 1-22, is determined only by the near-surface concentration and the diffusivity. Therefore, we find that adsorption to a true liquid layer, even a very thin one, overestimates the observed surface-to-

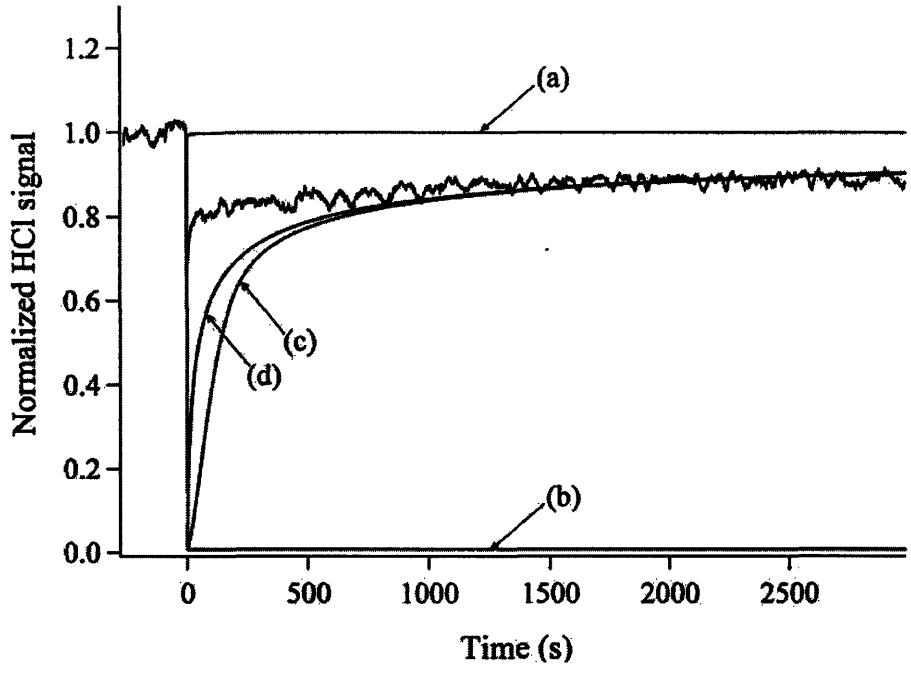

Figure 4-7. Experimental data and simulation results for HCl adsorption on zone-refined ice under QLL-forming conditions (-77 °C, $7 \cdot 10^{-7}$ Torr). Simulations were performed using the flow tube model framework and a model of absorption of HCl to a) a bulk ice layer, b) a true liquid layer, and a surface layer with $k_{des} \cdot V_{film}/V_{gas} = 1.5.10^{-6}$ s^{-1}, which was c) 100 nm thick and d) 1 nm thick. All models account for diffusion from the surface layer to the bulk. The adsorption rate was calculated based on gas kinetic theory and the rates of desorption for ice and water were calculated using solubility data.

bulk flux of HCl at long times, and adsorption to a solid ice layer, even a very thick one, underestimates the observed surface-to-bulk flux of HCl.

In our ellipsometry experiments, QLL formation was observed to begin after a delay of 600 seconds. The model presented here only describes adsorption to and diffusion from a surface layer, and we have not made an attempt here to model QLL induction, or HCl adsorption to the surface prior to QLL formation. Therefore, comparison of model to experiment is only relevant after the 600 second induction period. Additionally, from Figure 2-3, it is clear that

after QLL formation was initiated, QLL thickness continued to increase for as long as the crystal was exposed to gas-phase HCl, reaching a thickness of 150 nm < l_{QLL} < 300 nm after 4000 seconds. Our model assumes a surface layer of constant thickness.

A value of $k_{des} \cdot V_{film}/V_{gas} = 1.5 \cdot 10^{-6}$ s^{-1}, regardless of assumed value for γ or layer thickness between 1 nm and 300 nm, corresponds to a solubility of $C_s = 9.3 \cdot 10^{-5}$ moles HCl·cm^{-3} ice for the QLL at -77 °C and $7 \cdot 10^{-7}$ Torr HCl.

4.4.2 HCl adsorption on ice

Generally, our observations of an initial fast uptake mode followed by a diffusive-type loss for HCl adsorption on all ice films used in this study are consistent with the findings of other investigators[4,6]. The memory, or 'aging' effect that was observed for all types of ice film used in this study has been reported previously [4,6,10,11], although a detailed study of the effect is not available in the literature. Hanson and Ravishankara's report that HCl uptake decreased by approximately 50% after the first exposure of each ice sample to HCl is in good agreement with our findings[10]. Hynes et al. reported that up to 70% of incident HCl molecules were irreversibly adsorbed in their experiments on smooth ice at -68 °C [11].

4.4.2.1 Smooth and vapor-deposited ice films

The Langmuir model for surface adsorption is described in detail in section 1.4.1. To determine the effective saturation surface coverage, S, and the surface adsorption equilibrium constant, b, at each temperature, the adsorption isotherm data obtained in the uptake experiments on smooth ice under non-QLL conditions were analyzed using a weighted linear least squares fit according to the following equation:

$$\frac{1}{c_s} = \frac{1}{S} + \frac{1}{S} \cdot \frac{1}{bP_{HCl}} \quad . \qquad 4\text{-}1.$$

The uptake data was tested to determine whether $1/c_s$ exhibited a linear dependence on P_{HCl}, or on $1/P_{HCl}^{1/2}$. Within the Langmuir framework, a $1/P_{HCl}^{1/2}$ dependence would imply that each adsorbed molecule would occupy two adjacent, identical adsorption sites (i.e., dissociative adsorption). While such a simple model seems unlikely to sufficiently describe dissociative adsorption on a real ice surface, a $P_{HCl}^{1/2}$ dependence has been reported previously by other investigators[4,11,12]. The results of this test for the -60 °C adsorption isotherm are shown in Figure 4-8. Throughout the analysis, errors were propagated according to Jeffrey[1]. The linear $1/P_{HCl}^{1/2}$ model equation is a poor fit to the $1/c_s$ data, and the parameters from the fit are nonphysical: $S = -4(2)\cdot10^{14}$ molecules·cm^{-2}, and $b = -8(5)\cdot10^{4}$ Torr^{-1}. The linear $1/P_{HCl}$ model, eq. 4.1, fits the$1/c_s$ data well and the fit yields parameters that make reasonable physical sense: $S = 2.7(2)\cdot10^{14}$ molecules·cm^{-2}, and $b = 1.5(3)\cdot10^{6}$ Torr^{-1}. Therefore, we conclude that the dissociative Langmuir model is not suitable, and that the data is better described by the classical, nondissociative Langmuir model.

The saturation surface coverage, S, and the equilibrium adsorption constant, b, obtained via Langmuir analysis of the HCl adsorption isotherms on previously exposed smooth ice films for the range of conditions where surface disorder was not observed using ellipsometry are listed in Table 4-1. The HCl adsorption isotherms for -77 °C, -70 °C, and -60 °C are shown in Figures 4-9, 4-10, and 4-11.

Comparing Figure 4-3, which shows uptake curves for adsorption on smooth ice under non- QLL conditions, and Figure 4-4, which shows uptake curves for adsorption under QLL-forming conditions, demonstrates that, unlike what was observed in the zone-refined ice study, there was no strong qualitative contrast found between the HCl uptake curves under QLL-forming versus non-QLL conditions for adsorption on smooth and vapor-deposited ices.

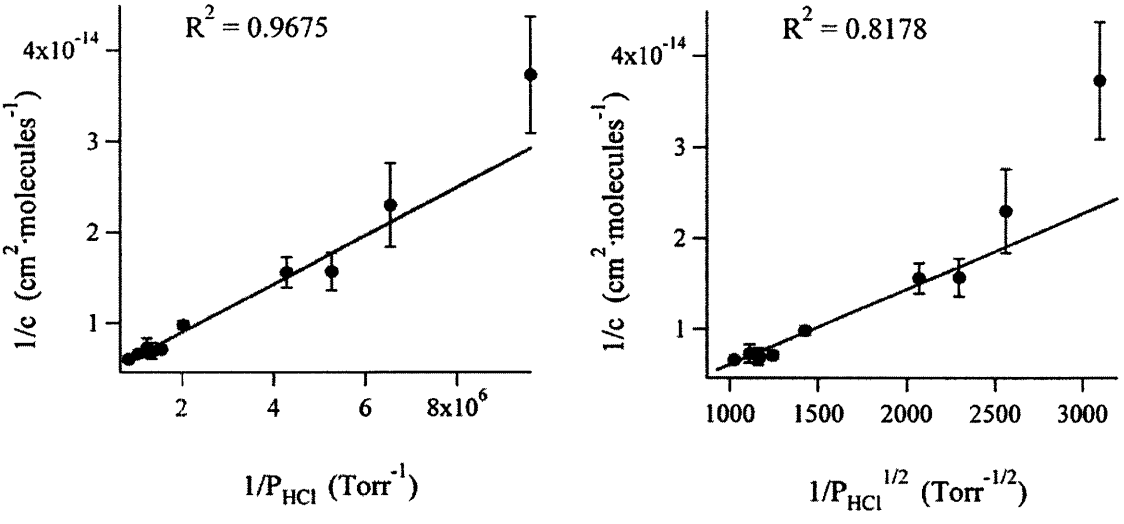

Figure 4-8. Langmuir fits of adsorption data for -60 °C. The inverse of the surface coverage is plotted against the inverse of the HCl partial pressure (left panel), and the same data plotted against the square root of the inverse of the HCl partial pressure (right panel). The lines indicate the results of a weighted linear least squares fit. The parameters for the $1/P_{HCl}^{1/2}$ fit are $S = -4(2)\cdot10^{14}$ molecules·cm^{-2}, and $b = -8(5)\cdot10^{4}$ Torr^{-1}. The parameters for the $1/P_{HCl}$ fit are $S = 2.7(2)\cdot10^{14}$ molecules·cm^{-2}, and $b = 1.5(3)\cdot10^{6}$ Torr^{-1}.

T (°C)	S (molecules·cm^{-2})	b (Torr^{-1})
-60	$2.7(2)\cdot10^{14}$	$1.5(3)\cdot10^{6}$
-70	$2.6(4)\cdot10^{14}$	$4(1)\cdot10^{6}$
-77	$3.1(9)\cdot10^{14}$	$1.8(8)\cdot10^{6}$

Table 4-1. Langmuir parameters S (saturation surface coverage) and b (adsorption equilibrium constant) calculated via isotherm analysis for HCl adsorption on smooth ice films for the range of conditions where surface disorder was not observed using ellipsometry.

However, as shown in Figures 4-9, 4-10, and 4-11, for the range of HCl partial pressure where surface disorder was observed with ellipsometry, scatter in the uptake increased for each isotherm, and in the case of the -77 °C and -60 °C isotherms (Figures 4-9 and 4-11), a unique dependence of uptake on HCl partial pressure for each ice sample became apparent. For each of

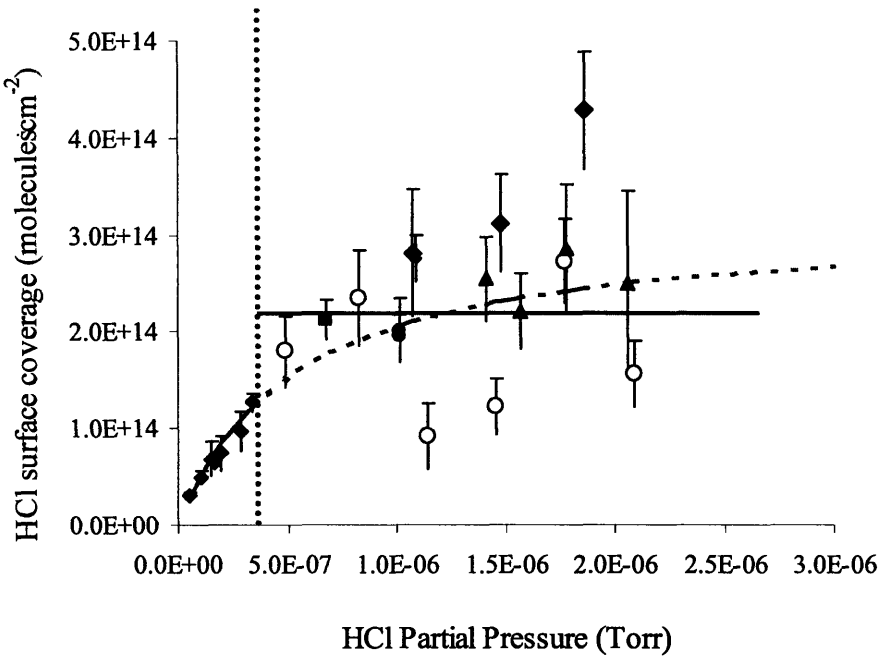

Figure 4-9. Adsorption isotherm for HCl on smooth ice at -77 °C. The dotted line demarcates the 'non-QLL'/'QLL' transition at -77 °C (P_{HCl} ~$3 \cdot 10^{-7}$ Torr HCl). The Langmuir adsorption isotherm fit using 'non-QLL' data only is indicated. The parameters for the fit are listed in Table 4-2. The horizontal line indicates the average surface coverage in the 'QLL' region, $2.11(8) \cdot 10^{14}$ molecules·cm^{-2}. In the QLL region, uptake data from the same ice sample have been represented using like symbols.

the three temperatures studied, the adsorption isotherm showed a Langmuir-like dependence on HCl partial pressure for the range of conditions where no surface disorder was observed with ellipsometry. However, as demonstrated in Table 4-1, the equilibrium adsorption constant, *b*, does not exhibit the linear temperature dependence expected for a true Langmuir system, as described in section 1.4.1. One possible contribution to this disagreement with the Langmuir paradigm is that it is possible that, due to the finite resolution of our ellipsometer, HCl-induced disordering exists below the non-QLL/QLL boundary P_{HCl} values we have set based on our ellipsometer data, introducing error into Langmuir fits including data at those borderline values.

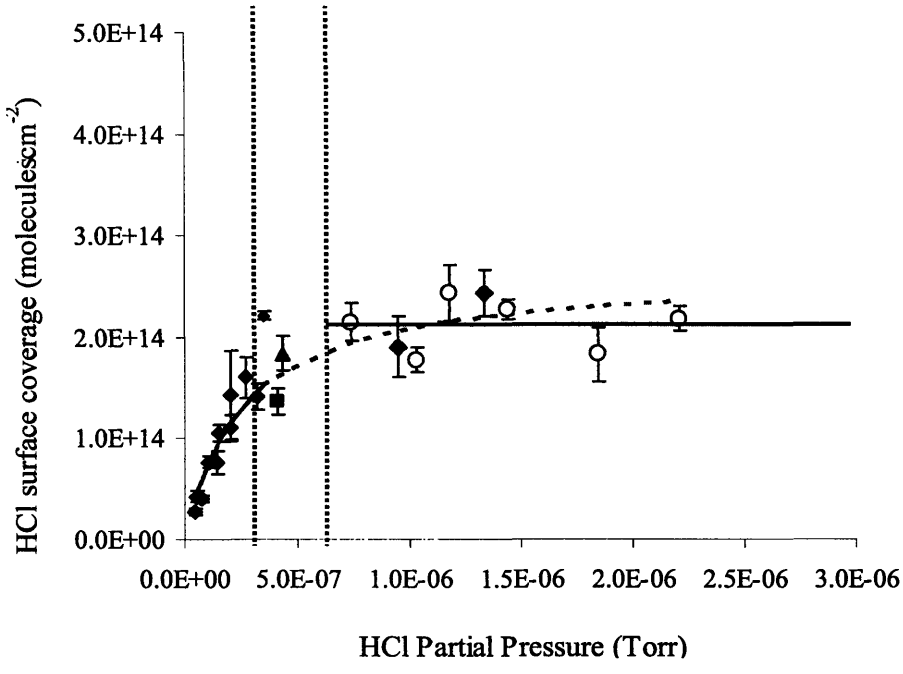

Figure 4-10. Adsorption isotherm for HCl on smooth ice at -70 °C. The dotted line demarcates the 'non-QLL'/'QLL' transition at -70 °C (P_{HCl} ~$3.5 \cdot 10^{-7}$-$7 \cdot 10^{-7}$ Torr HCl). The Langmuir adsorption isotherm fit using 'non-QLL' data only is indicated. The parameters for the fit are listed in Table 4-2. The horizontal line indicates the average surface coverage in the 'QLL' region, $2.12(9) \cdot 10^{14}$ molecules·cm^{-2}. In the QLL region, uptake data from the same ice sample have been represented using like symbols.

The limited ability of a model as simple as the Langmuir model to describe adsorption on the ice surface, given what we know about its changeable nature, is not surprising. However, recognizing its limitations, the Langmuir model can be a useful tool in our analysis.

Using our flow tube modeling framework with a Langmuir model to describe the HCl-ice interaction we can simulate both the shape of the uptake curves and the measured surface coverage for HCl uptake on smooth ice samples which had been previously exposed to HCl ('aged' samples). Based on the best fit to a sample of three measured uptake curves, we find that HCl adsorption on smooth ice at -60 °C and non-QLL levels of HCl is well described by our

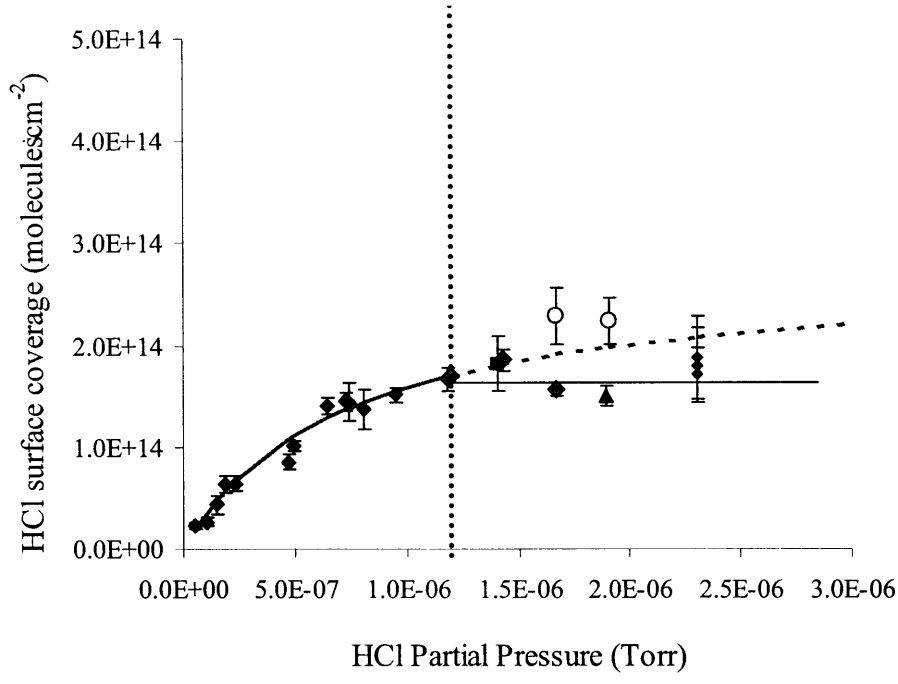

Figure 4-11. Adsorption isotherm for HCl on smooth ice at -60 °C. The dotted line demarcates the 'non-QLL'/'QLL' transition at -60 °C (P_{HCl} ~$1.2 \cdot 10^{-6}$ Torr HCl). The Langmuir adsorption isotherm fit using 'non-QLL' data only is indicated. The parameters for the fit are listed in Table 4-2. The horizontal line indicates the average surface coverage in the 'QLL' region, $1.67(4) \cdot 10^{14}$ molecules·cm^{-2}. In the QLL region, uptake data from the same ice sample have been represented using like symbols.

model with $\gamma = 0.04$ and $b = 9.8 \cdot 10^5$ Torr^{-1}. This value of b is consistent with the value obtained via isotherm analysis (see Table 4-1) and this value of γ is consistent with the findings of Hynes et al[11]. The total number of sites, S, was assumed to be the measured saturation surface coverage (see Table 4-1). The results of the simulation are shown in the plotted along the experimental data for comparison in Figure 4-12. The simulation predicts a surface coverage of $1.2 \cdot 10^{14}$ molecules·cm^{-2}. The measured surface coverage was $1.5(2) \cdot 10^{14}$ molecules.cm^{-2}. The surface coverages and shapes of the adsorption and desorption curves for fresh ice not previously exposed to HCl, as shown in the top panels of Figures 4-3 and 4-4, can be reproduced to a

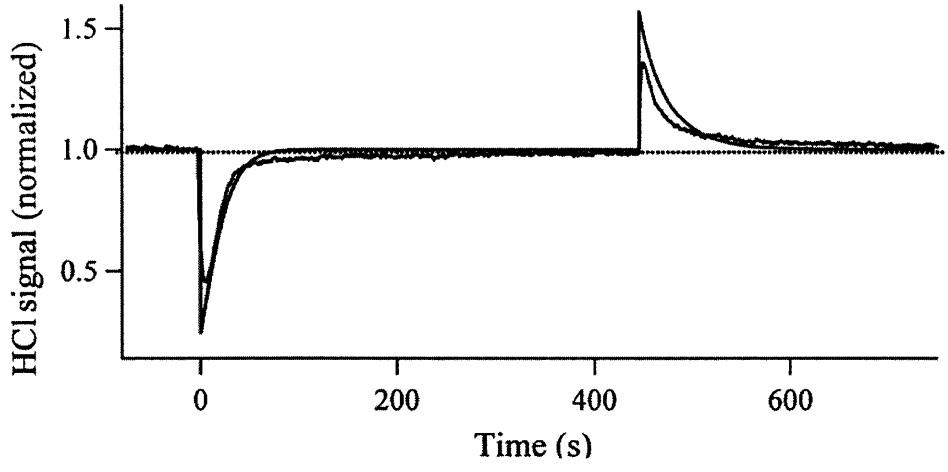

Figure 4-12. Flow tube model simulation results for adsorption of HCl onto an aged smooth ice surface at -60 °C and $P_{HCl} = 7.4 \cdot 10^{-7}$ Torr.

reasonable approximation using a model that includes Langmuir adsorption of HCl to two types of adsorption sites: one set of sites identical to the model used to describe the adsorption curves on aged ice, as shown in Figure 4-12, and another set of adsorption sites with stronger binding energy and a slightly lower sticking coefficient. The results of the simulation for -60 °C and $7.4 \cdot 10^{-7}$ Torr HCl are shown in Figure 4-13 along with the experimental data for comparison. The best agreement with the observed amounts of adsorbed and desorbed HCl was obtained with $\gamma = 0.02$ and $b = 2.0 \cdot 10^{7}$ Torr^{-1} for the second set of adsorption sites. The total number of sites, S, was assumed to be equal to the measured saturation surface coverage in the case of the weaker-binding sites (see Table 4-1), and that value divided by the experimentally determined ratio of irreversibly adsorbed HCl molecules to reversibly adsorbed HCl molecules in the case of the stronger-binding sites. The simulation predicted a surface coverage of $2.9 \cdot 10^{14}$ molecules·cm^{-2}. The measured surface coverage was $3.1(3) \cdot 10^{14}$ molecules.cm^{-2}. The predicted ratio of desorbed HCl to adsorbed HCl was 0.62. The measured ratio was 0.76(8).

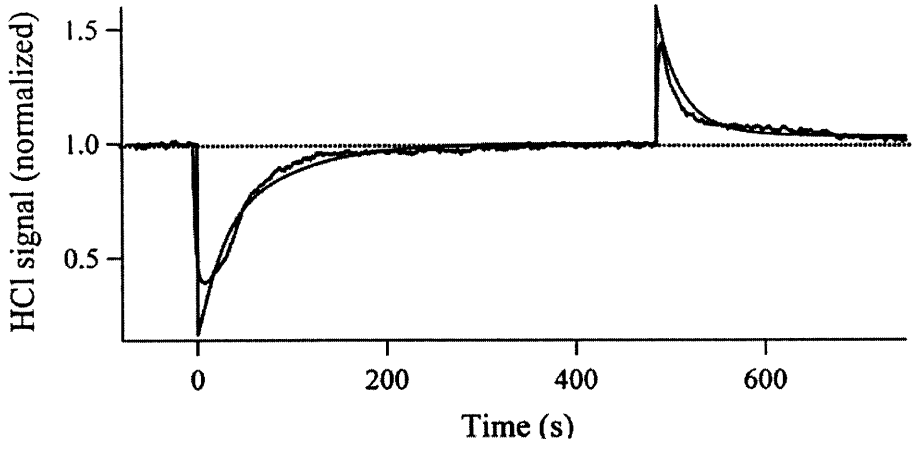

Figure 4-13. Flow tube model simulation results for adsorption of HCl onto a fresh smooth ice surface at -60 °C and $P_{HCl} = 7.4 \cdot 10^{-7}$ Torr. Simulation was performed using a model of the HCL-ice interaction that includes Langmuir adsorption of HCl to two types of adsorption sites: one set of sites identical to the model used to describe the adsorption curves on aged ice, as shown in Figure 4-11, and another set of adsorption sites with stronger binding energy and a slightly lower sticking coefficient.

4.4.2.2 Zone-refined ice samples

In the range of conditions where QLL induction was not observed with ellipsometry, we observed largely irreversible uptake. The $ClONO_2$ + HCl reactive uptake experiments on zone-refined ice indicate that only a small fraction of the HCl adsorbed under these conditions is readily available on the surface for reaction with $ClONO_2$.

Full isotherm data is not available for HCl adsorption on to zone-refined ice samples so we are not able to rule out a $P_{HCl}^{1/2}$-dependence Langmuir model as we did for the smooth ice adsorption isotherms. Both (a) a model of Langmuir adsorption, and (b) a $P_{HCl}^{1/2}$-dependence Langmuir model were tested against the experimental data. Both models were tested with and without incorporation of HCl from the surface into the bulk and diffusion to the interior of the

film, as in eqs. 1-13 and 1-14.

The results of simulations (a) and (b) are shown along with the experimental data in Figure 4-14. Based on analysis of a sample of four measured uptake curves, we find that both models reproduce the uptake characteristics of HCl adsorption under non-QLL conditions on zone-refined ice reasonably well. For simulation (a), the best agreement with the observed amounts of adsorbed and desorbed HCl was obtained with $\gamma = 0.012$, $b = 8.1 \cdot 10^{6}$ Torr^{-1}, $S = 6 \cdot 10^{14}$ molecules·cm^{-2} and $k_{inc} = 0.00035$ s^{-1}. The near-surface region was assumed to have a depth of 100 nm. Note that, in this model, this depth does not have a physical significance as in the QLL model, but a near-surface region must be defined in order to determine the near-surface concentration that drives diffusion into the bulk (see eq. 1-22). In simulation (a), the concentration of HCl in the near-surface region was $6 \cdot 10^{-16}$ moles HCl·cm^{-3} ice after 3000 s of adsorption, many orders of magnitude less than the solubility of HCl in bulk ice ($3.5 \cdot 10^{-7}$ moles HCl·cm^{-3} [3]). For simulation (b), the best agreement with the observed amounts of adsorbed and desorbed HCl was obtained with $\gamma = 0.012$, $b = 4.9 \cdot 10^{6}$ Torr^{-1}, $S = 1 \cdot 10^{15}$ molecules·cm^{-2}, and $k_{inc} = 0.00035$ s^{-1}. The near-surface region was again assumed to have a depth of 100 nm, and the concentration of HCl in the near-surface region was $4.5 \cdot 10^{-16}$ moles HCl·cm^{-3} ice after 3000 s of adsorption. Simulation (a) predicts an uptake of $9.5 \cdot 10^{14}$ molecules·cm^{-2} adsorbed and $1.7 \cdot 10^{14}$ molecules·cm^{-2} recovered within 570 seconds of when the injector was returned to the front of the flow tube and desorption initiated. Simulation (b) predicts a surface coverage of $9.5 \cdot 10^{14}$ molecules·cm^{-2} and $1.5 \cdot 10^{14}$ molecules·cm^{-2} desorbed after 570 seconds. The measured surface coverage was $1.2(1) \cdot 10^{15}$ molecules.cm^{-2} and $1.7(1) \cdot 10^{14}$ molecules·cm^{-2} were recovered after 570 seconds of desorption.

The best agreement between simulation and experiment for uptake curve shape and

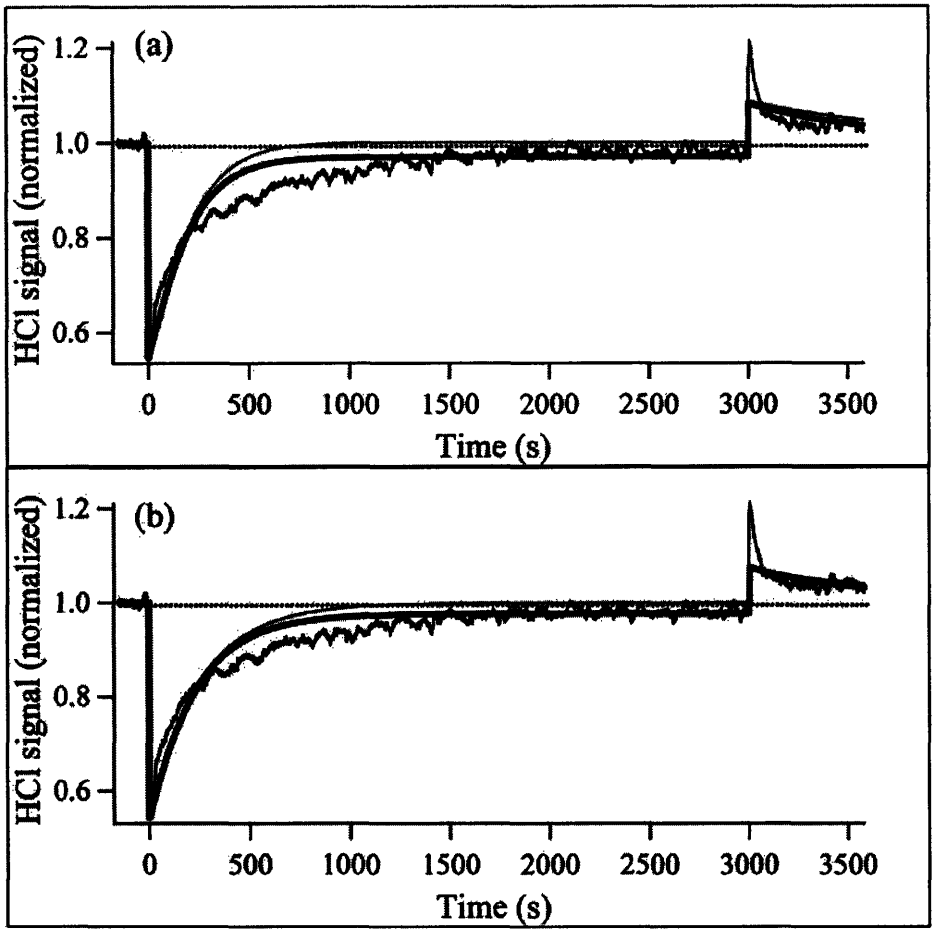

Figure 4-14. Experimental data and simulation results for HCl adsorption on zone-refined ice under non-QLL conditions (-60 °C, $7 \cdot 10^{-7}$ Torr). Simulations were performed using the flow tube model framework and (a) a model of conventional Langmuir adsorption with (thick curve) and without (thin curve) incorporation of HCl from the surface into the bulk and diffusion to the interior of the film, and (b) a Langmuir model with $P_{HCl}^{1/2}$-dependence, with (thick curve) and without (thin curve) incorporation of HCl from the surface into the bulk and diffusion to the interior of the film to describe the HCl-ice interaction.

quantity of adsorbed molecules was achieved with the models that include incorporation and diffusion into the bulk. The incorporation rate constant of 0.00035 s^{-1} corresponds to a maximum surface-to-bulk loss rate of $1.7 \cdot 10^{11}$ molecules $HCl \cdot cm^{-2} s^{-1}$.

4.4.2.3 The fate of HCl upon adsorption to ice

The ratio of irreversibly adsorbed HCl molecules to reversibly adsorbed HCl molecules on fresh ice samples was not observed to be appreciably different for smooth ice films and rough ice films formed by deposition from the vapor phase. The only observed difference in uptake on smooth and vapor-deposited ice films was in the magnitude of HCl uptake due to the higher surface area of the vapor-deposited ice. However, a qualitative and quantitative difference was observed between HCl uptake on these two types of ice film versus on the zone-refined ice samples. The zone-refined ice samples were thicker than the other two types of ice film, although from Figure 1-8 it can be seen that only the topmost few microns of the ice film are penetrated within the timescale of the experiment, and so the three types of ice film effectively would have the same thickness. The key difference between the zone-refined ice cylinders and the other two film types is that the zone-refined ice cylinders have larger grain sizes, or fewer grain boundaries per unit surface area.

The fact that the most significant difference between the zone-refined ice samples and the other two types of ice film studied is the degree of polycrystallinity, along with the results of our simulation as shown in Figure 4-13, indicates that the two modes of adsorption that we have observed can be attributed to adsorption on two different types of available adsorption sites on the polycrystalline ice surface: sites located on grain boundaries and those located on crystal faces. We do not have experimental evidence that conclusively identifies whether the irreversible loss associated with adsorption on fresh smooth and vapor-deposited ice samples can be attributed to adsorption into the grain boundaries, and the reversible adsorption associated with adsorption on both fresh and aged smooth and vapor-deposited ice samples can be attributed to adsorption on the crystal faces, or vice-versa.

Table 4-2 lists the adsorption parameters obtained using our simulations that describe the three types of HCl adsorption under non-QLL conditions that we have observed in our experiments. The data summarized in Table 4-2 suggest that two of the three types of HCl adsorption under non-QLL conditions that we have observed in our experiments can be described as exhibiting strong binding: non-QLL adsorption to zone-refined ice cylinders, and the irreversible adsorption on fresh smooth ice cylinders. This suggests that the irreversible loss observed upon HCl adsorption to fresh smooth and vapor-deposited ice samples can be attributed to adsorption onto the crystal face, and that the reversible adsorption observed upon HCl adsorption to both fresh and aged smooth and vapor-deposited ice samples can be attributed to adsorption into the grain boundaries.

Model	γ	k_{des} (s^{-1})	b ($Torr^{-1}$)
Non-QLL adsorption, Aged smooth ice	0.035	0.053	$9.8 \cdot 10^5$
Strong-binding non-QLL adsorption, fresh smooth ice	0.02	0.001	$2.0 \cdot 10^7$
non-QLL adsorption, zone-refined ice *from Simulation (a)*	0.012	0.001	$8.1 \cdot 10^6$

Table 4-2. Adsorption parameters for HCl adsorption to smooth and zone-refined ice films at -60 °C and non-QLL levels of HCl obtained via simulations.

It has been suggested previously[13,14] that HCl loading at the grain boundaries could lead to local disorder in the ice lattice. The HCl-loaded, disordered grain boundaries could have properties similar to the zone-refined ice samples which have been exposed to HCl under QLL-forming conditions; they would exhibit largely reversible adsorption and act as a source of HCl that is readily available for reaction.

Unlike what was observed in the zone-refined ice study, there was no strong qualitative contrast found between the HCl uptake curves under QLL-forming versus non-QLL conditions for adsorption on smooth and vapor-deposited ices, as can be seen by comparing Figures 4-3 and 4-4. However, there are other indications of HCl-induced surface disorder on the smooth ice films at the conditions at which it was observed on single-crystalline ice using the ellipsometer: The Cl_2 evolution traces for the $ClONO_2$ + HCl reaction on smooth ice did reveal a difference in HCl surface availability under QLL-forming versus non-QLL conditions similar to that observed in the zone-refined ice study, although the distinction was more pronounced for the zone-refined ice samples. One explanation for this is that in the reaction on smooth ice, the grain boundary regions served as an additional reservoir for readily available HCl. Additionally, for each adsorption isotherm, scatter in the uptake increased under QLL-forming conditions, and in some cases a unique dependence of uptake on HCl partial pressure for each ice sample became apparent. This indicates that the qualitative character of the HCl uptake curves for ice films, whether fresh or aged, is mainly determined by adsorption at the grain boundaries. This also is consistent with the picture of the irreversible loss associated with adsorption on fresh ice samples being due to adsorption onto the crystal face, and the reversible adsorption associated with adsorption on fresh and aged smooth and vapor-deposited ice samples can being associated with adsorption into the grain boundaries.

However, no direct evidence exists, either in our work or in the literature, to support the picture of preferential adsorption leading to disordering at grain boundaries. In the absence of disordering at the grain boundaries, HCl molecules adsorbed there would be presumably less available for reaction than molecules adsorbed to the surface. Therefore, the argument could also be made in favor of the irreversible loss associated with adsorption on fresh smooth and

vapor-deposited ice samples resulting from adsorption into the grain boundaries, and the reversible adsorption associated with adsorption on both fresh and aged smooth and vapor-deposited ice samples being due to adsorption on the crystal faces.

4.4.3 HCl hexahydrate formation

Generally, our observations of an initial fast adsorption mode followed by a pronounced dip in the signal after approximately 150 seconds for HCl adsorption on smooth and zone-refined ice films in the region of the HCl-ice phase diagram where HCl hexahydrate is the stable phase are consistent with the findings of other investigators that there is a nucleation barrier to HCl hexahydrate formation[15-19].

As shown in Figure 4-5, HCl hexaydrate formation was observed on smooth and zone-refined ice samples. However, HCl uptake beyond saturation corresponding to hexahydrate formation was not observed on vapor-deposited ice samples at the same conditions. Surface roughness is the characteristic that distinguishes vapor-deposited ice from the other two sample types. While the flow tube-CIMS technique does not offers only indirect information about the chemical state of HCl on the ice surface, this observation indicates that HCl hexahydrate formation at these conditions is a process involving hydrate nucleation and propagation on the crystal surface, rather than one originating in grain boundaries, as has been suggested for ice formed at lower temperatures[20].

4.5. Conclusions

The results of this study lend support for the trend observed via ellipsometry that surface disorder is induced by the presence of HCl in the vicinity of the solid-liquid equilibrium line on the HCl-ice phase diagram, but that no detectable disorder was observed on the interior of the

'ice' phase envelope. The results of the HCl uptake experiments on zone-refined ice, as shown in Figure 4-1, provide further evidence that the nature of HCl adsorption on ice differs at the conditions under which surface change was observed with ellipsometry from the HCl-ice interaction at conditions under which no surface change was observed.

Analysis of our HCl uptake experiments on zone-refined ice samples indicates that the QLL is not truly liquid-like in its ability to absorb HCl, but rather has a solubility intermediate between that of liquid water and that of bulk ice I_h.

We have indirect evidence that HCl adsorption on polycrystalline ice films consists of two modes of adsorption on two different types of available adsorption sites: sites located at grain boundaries and those located on crystal faces. We also have evidence that the qualitative character of the uptake curves is dominated by adsorption at the grain boundaries. However, further investigation is necessary before each adsorption mode can be assigned conclusively to one type of adsorption site.

Finally, we have indirect evidence that HCl hexahydrate formation on crystalline ice at conditions relevant to the polar stratosphere is a process involving hydrate nucleation and propagation on the crystal surface, rather than one originating in grain boundaries, as has been suggested for lower temperature ices[20].

References for Chapter 4

1. Jeffrey, A. Mathematics for engineers and scientists. Barnes & Noble, New York (1969).

2. Molina, M.J. The Chemistry of the Atmosphere: The Impact of Global Change. Calvert, J.G. (ed.), pp. 27-38 (Blackwell Scientific Publications, Boston,1994).

3. Thibert, E. & Domine, F. Thermodynamics and Kinetics of the Solid Solution of HCl in Ice. *J. Phys. Chem. B* **101**, 3554-3565 (1997).

4. Huthwelker, T., Malmstrom, M.E., Helleis, F., Moortgat, G.K. & Peter, T. Kinetics of HCl uptake on ice at 190 and 203 K: implications for the microphysics of the uptake process. *J. Phys. Chem. A* **108**, 6302-6318 (2004).

5. Fluckiger, B., Thielmann, A., Gutzwiller, L. & Rossi, M.J. Real time kinetics and thermochemistry of the uptake of HCl, HBr and HI on water ice in the temperature range 190 to 210 K. *Ber. Bunsen. Phys. Chem.* **102**, 915-928 (1998).

6. Fluckiger, B., Chaix, L. & Rossi, M.J. Properties of the HCl/ice, HBr/ice, and H_2O/ice interface at stratospheric temperatures (200 K) and its importance for atmospheric heterogeneous reactions. *J. Phys. Chem. A* **104**, 11739-11750 (2000).

7. Fluckiger, B., Chaix, L. & Rossi, M.J. Properties of the HCl/ice, HBr/ice, and H_2O/ice interface at stratospheric temperatures (200 K) and its importance for atmospheric heterogeneous reactions (vol 104, pg 11739, 2002). *J. Phys. Chem. A* **107**, 2768 (2003).

8. Fluckiger, B. & Rossi, M.J. Common Precursor Mechanism for the Heterogeneous Reaction of D_2O, HCl, HBr, and HOBr with Water Ice in the Range 170-230 K: Mass Accommodation Coefficients on Ice. *J. Phys. Chem. A* **107**, 4103-4115 (2003).

9. Aguzzi, A., Fluckiger, B. & Rossi, M.J. The nature of the interface and the diffusion coefficient of HCl/ice and HBr/ice in the temperature range 190-205 K. *Phys. Chem. Chem. Phys.* **5**, 4157-4169 (2003).

10. Hanson, D.R. & Ravishankara, A.R. Investigation of the Reactive and Nonreactive Processes Involving $ClONO_2$ and HCl on Water and Nitric-Acid Doped Ice. *J. Phys. Chem.* **96**, 2682-2691 (1992).

11. Hynes, R.G., Mossinger, J.C. & Cox, R.A. The Interaction of HCl With Water-ice at Tropospheric Temperatures. *Geophys. Res. Lett.* **28**, 2827-2830 (2001).

12. Chu, L.T., Leu, M.T. & Keyser, L.F. Uptake of HCl in Water Ice and Nitric-Acid Ice Films. *J. Phys. Chem.* **97**, 7779-7785 (1993).

13. Wolff, E.W., Mulvaney, R. & Oates, K. Diffusion and Location of Hydrochloric-Acid in Ice - Implications for Polar Stratospheric Clouds and Ozone Depletion. *Geophys. Res. Lett.* **16**, 487-490 (1989).

14. Krieger, U.K. *et al.* Rutherford backscattering to study the near-surface region of volatile liquids and solids. *Science* **295**, 1048-1050 (2002).

15. Abbatt, J.P.D. *et al.* Interaction of HCl vapor with water-ice: Implications for the stratosphere. *J. Geophys. Res.* **97**, 15819-15826 (1992).

16. Hanson, D.R. & Mauersberger, K. HCl/H_2O Solid-Phase Vapor Pressures and HCl Solubility in Ice. *J. Phys. Chem.* **94**, 4700-5 (1990).

17. Henson, B.F. *et al.* Experimental isotherms of HCl on H_2O ice under stratospheric conditions: Connections between bulk and interfacial thermodynamics. *J. Chem. Phys.* **121**, 8486-8499 (2004).

18. Wooldridge, P.J., Zhang, R. & Molina, M.J. Phase Equilibria of H_2SO_4, HNO_3, and HCl Hydrates and the Composition of Polar Stratospheric Clouds. *J. Geophys. Res.* **100**, 1389-96 (1995).

19. Foster, K.L., Tolbert, M.A. & George, S.M. Interaction of HCl with Ice: Investigation of the Predicted Trihydrate, Hexahydrate, and Monolayer Regimes. *J. Phys. Chem. A* **101**, 4979-4986 (1997).

20. Sadtchenko, V., Giese, C.F. & Gentry, W.R. Interaction of Hydrogen Chloride with Thin Ice Films: The Effect of Ice Morphology and Evidence for Unique Surface Species on Crystalline Vapor-Deposited Ice. *J. Phys. Chem. B* **104**, 9421-9429 (2000).

Chapter 5

Other Probe Molecules: Acetic Acid and CFC-12

5.1 Introduction

5.1.1 Acetic acid

The interaction of acetic acid, CH_3COOH, with ice surfaces is relevant to the chemistry of the upper troposphere. Cirrus clouds form in the upper troposphere and consist almost exclusively of ice particles[1]. Cirrus cloud ice particles can potentially act as scavengers for semivolatile gas-phase species[2]. Surface disorder on the particles is expected to influence their scavenging ability[3], but this effect has not been well characterized. Understanding the scavenging potential of cirrus cloud ice particles and the state of the particle surface is important for accurate atmospheric chemistry and climate modeling.

Sokolov and Abbatt studied CH_3COOH uptake on smooth ice films at temperatures between -51 °C and -28 °C, and CH_3COOH partial pressures between 10^{-6} and 10^{-3} Torr. They found that the CH_3COOH-ice interaction is well described by a nondissociative Langmuir model in this range of conditions[3]. Their measurements of saturation surface coverage at each temperature studied are summarized in Figure 5-1. For temperatures between -51 °C and -35 °C,

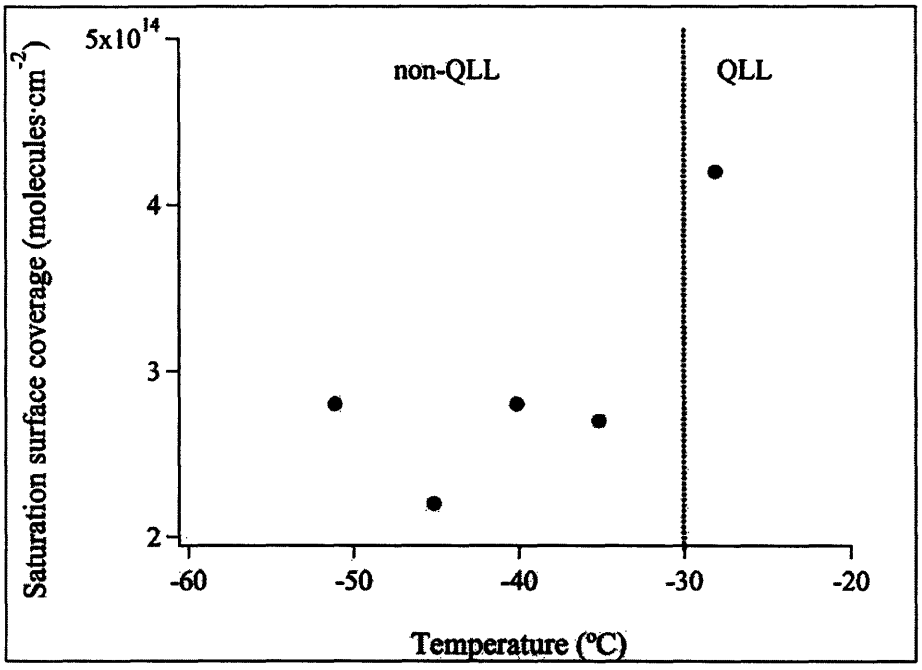

Figure 5-1. Saturation surface coverage data for CH_3COOH adsorption on ice from Sokolov and Abbatt.[3] The saturation surface coverage is shown as a function of temperature. The dotted grey line indicates the temperature below which we did not observe surface disorder on bare ice using ellipsometry (see Chapter 2).

Sokolov and Abbatt found the CH_3COOH saturation surface coverage to be roughly constant, with an average coverage of $2.6(3)\cdot10^{14}$ molecules·cm^{-2}. At -28 °C, they observed an increase in uptake to $4.2\cdot10^{14}$ molecules·cm^{-2}. As discussed in Chapter 2, we observed surface disordering on bare ice with ellipsometry at temperatures above -30 °C. This observation together with the results of Sokolov and Abbatt suggests that the presence of the QLL enhances the affinity of CH_3COOH for the ice surface.

Orem and Adamson found that the adsorption of *n*-alkanes to the surface of powdery ice samples resembled adsorption to the surface of liquid water, rather than ice, above -35 °C [4]. This

finding is another indication that the adsorption of gas-phase hydrocarbons to an ice surface is affected by the presence of surface disorder.

CH_3COOH does not react with HCl, and we do not have reason to suspect that the adsorption of CH_3COOH on ice would induce surface disordering at temperatures as low as -60 °C. For these reasons, in addition to the availability of information in the literature on CH_3COOH adsorption to bare ice[3,5], CH_3COOH was employed as a passive probe molecule to provide information about the state of the ice surface in the presence of HCl.

We performed CH_3COOH/HCl co-adsorption experiments on zone-refined ice samples to probe the nature of the ice surface across the HCl-ice phase diagram. This study was designed to further test our finding that HCl induces surface change detectable with ellipsometry only near the solid-liquid equilibrium line of the HCl-ice phase diagram.

5.1.2 CFC-12

CFC-12, CCl_2F_2, was also used as a nonreactive probe molecule to study the HCl-ice system. CCl_2F_2 is one of the synthetic chemicals directly implicated in the seasonal stratospheric ozone depletion that has been observed at polar latitudes. Studies exist on radiation-induced reactions of CCl_2F_2 embedded in ice films under UHV conditions[6-9]. It was found that Cl^- and F^- yields in electron-stimulated desorption of CFCs and hydrochlorofluorocarbons (HCFCs) are strongly enhanced by the presence of H_2O ice[7]. It was suggested by Lu and Sanche that the destruction in this manner of CFCs adsorbed on PSCs could play a role in ozone depletion[9], although the relative importance of this mechanism has been a subject of debate in the literature[10-13]. To the best of our knowledge, no studies exist in the literature on the uptake of gas-phase CCl_2F_2 on ice surfaces[10]. A hydrophobic molecule prized as an industrial and

commercial chemical for its chemical inertness, CCl_2F_2 is not expected to react with the ice surface in the absence of radiation.

We performed CCl_2F_2 uptake studies on smooth and vapor-deposited ices, before and after exposure to HCl. We found evidence of physical surface change of the ice films after exposure to HCl under QLL conditions. However, we also found that CCl_2F_2 exhibits unusual adsorption behavior on ice and therefore is not suitable as a passive probe molecule for investigating the HCl-ice system.

5.2 General experimental procedure

For a general description of the flow tube-CIMS system and ice sample preparation, please see section 1.3.

In the acetic acid/HCl co-adsorption experiments, first a constant flow of HCl was established. Once the surface reached equilibrium with the gas phase HCl, the uptake of a constant flow of CH_3COOH and the associated HCl desorption was monitored. Dimerization of gas-phase acetic acid was accounted for when determining the acetic acid sample concentration and thus the partial pressure of acetic acid in the flow tube. The equilibrium constant for dimerization at 25 °C and 1 atm is 0.972.[14]

In the CFC-12 experiments, CCl_2F_2 uptake was measured as in the HCl uptake experiments. Since both CCl_2F_2 and HCl yield the same daughter ions in chemical ionization reactions with SF_6^-, and no suitable substitute reagent ion was found, CCl_2F_2/HCl co-adsorption experiments were not possible. CCl_2F_2 uptake experiments were performed on smooth and vapor-deposited ice films before and after a full HCl experiment (adsorption + desorption) with the intent of demonstrating surface change.

5.3 Results

5.3.1 Acetic acid

CH_3COOH surface coverage was measured to be $2.7(8)\cdot10^{14}$ molecules$\cdot$cm^{-2} on zone-refined ice at -60 °C and $4.2\cdot10^{-6}$ Torr CH_3COOH, with no HCl present. This is consistent with measured CH_3COOH surface coverages reported by Sokolov and Abbatt for smooth ice films.

We also studied the co-adsorption of HCl and CH_3COOH on zone refined ice cylinders. The results of these experiments are shown in Figure 5-2. At a constant temperature of -61 °C and a partial pressure of HCl where no surface change was observed with ellipsometry (P_{HCl} = $7\cdot10^{-7}$ Torr), a CH_3COOH uptake of $1.4(2)\cdot10^{14}$ molecules$\cdot$cm^{-2} was observed. At the same temperature but at a higher HCl partial pressure ($P_{HCl} = 2\cdot10^{-6}$ Torr, QLL-forming conditions), twofold enhancement in CH_3COOH adsorption ($2.9(6)\cdot10^{14}$ molecules$\cdot$cm^{-2}) was observed.

5.3.2 CFC-12

A measured uptake curve for CCl_2F_2 adsorption on vapor-deposited ice at -70 °C and $6.5\cdot10^{-7}$ Torr CCl_2F_2 with no HCl present is shown in Figure 5-3. CCl_2F_2 adsorption on smooth ice at -70 °C and $5.8\cdot10^{-7}$ Torr CCl_2F_2 with no HCl present is shown in Figure 5-4.

CCl_2F_2 adsorption on both smooth and vapor deposited ice films was observed to be reversible. A full adsorption isotherm was not measured for CCl_2F_2 on ice, but an estimate based on adsorption data measured at -70 °C for three partial pressures of CCl_2F_2 on smooth ice yields $b = 9(4)\cdot10^6$ Torr^{-1}.

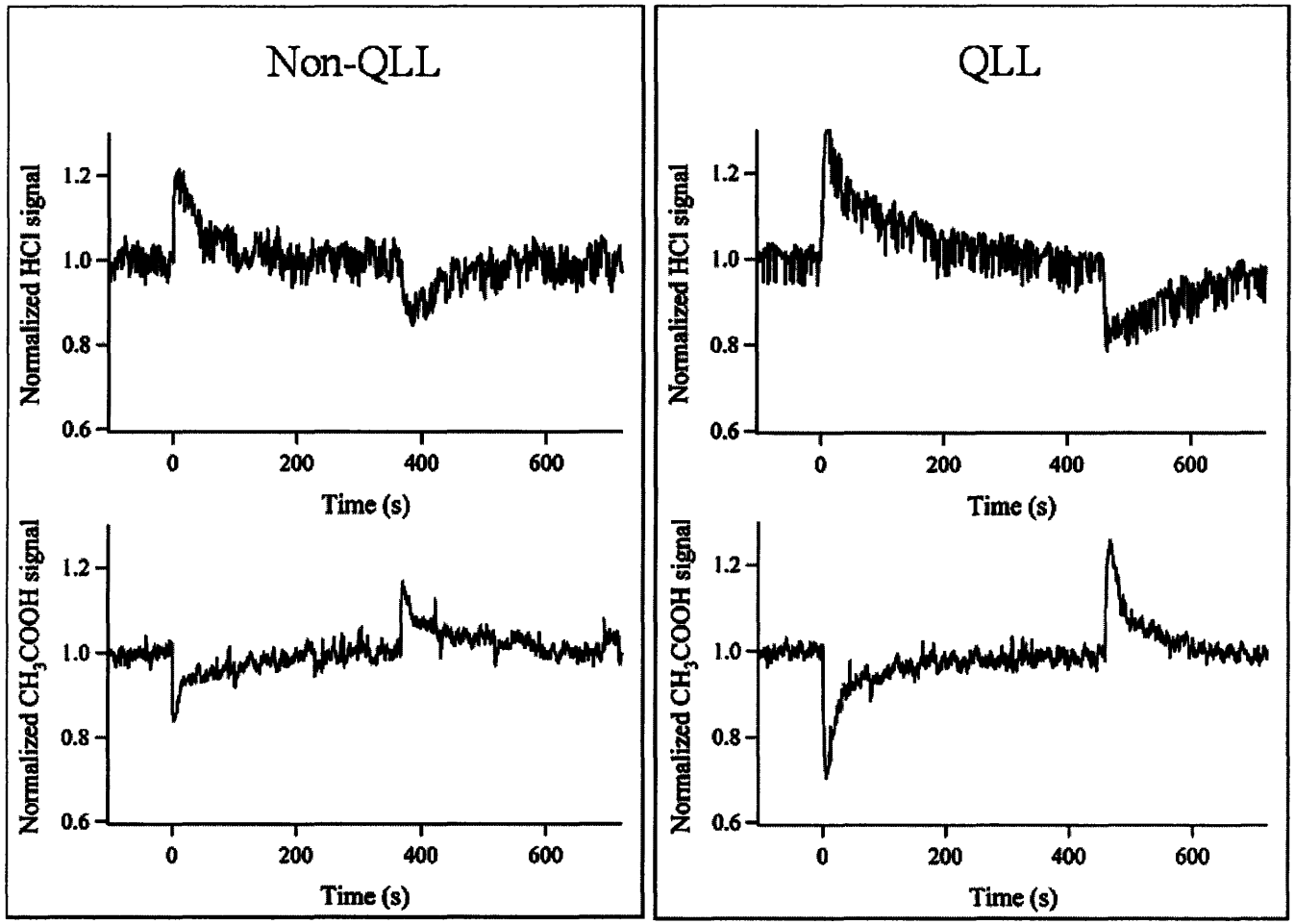

Figure 5-2. Acetic Acid-HCl co-adsorption experiments on zone-refined ice. Experiments shown were conducted at -60.6 °C and $4.2 \cdot 10^{-6}$ Torr CH_3COOH. The left and right panels show studies at $6.7 \cdot 10^{-7}$ Torr HCl and $2 \cdot 10^{-6}$ Torr HCl, respectively, and the upper and lower panels show HCl and CH_3COOH mass spectrometer signals, respectively.

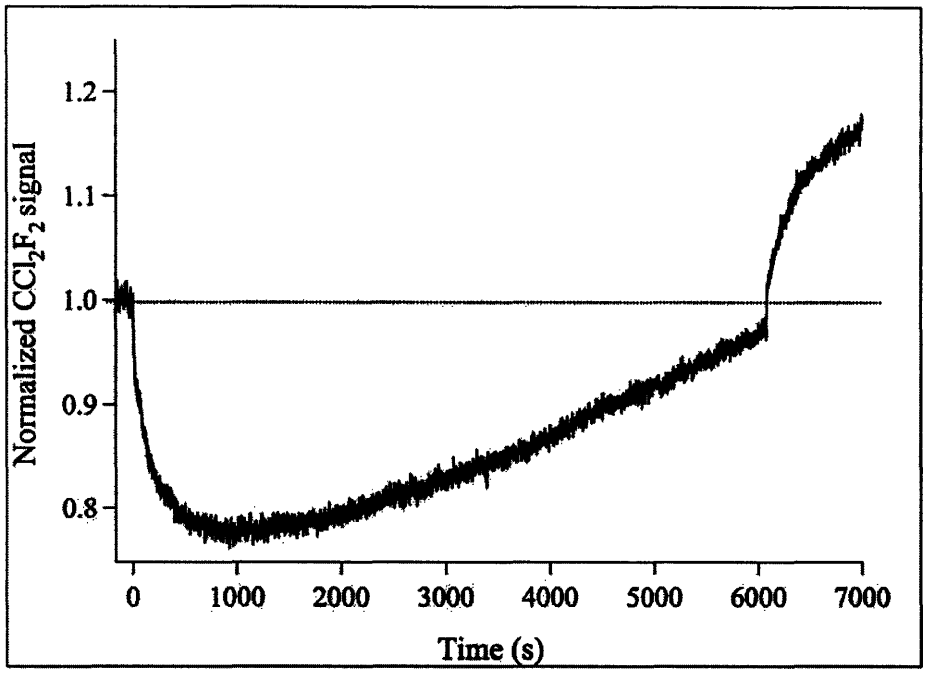

Figure 5-3. CFC-12 adsorption on vapor-deposited ice at -70 °C and $6.5 \cdot 10^{-7}$ Torr CCl_2F_2. The uptake curve corresponds to a surface coverage of $7.0(3) \cdot 10^{15}$ molecules·cm^{-2}.

The results of CCl_2F_2 uptake experiments performed on smooth and vapor-deposited ice films before and after HCl exposure are summarized in Figure 5-5. On smooth ice, equal amounts of CCl_2F_2 are adsorbed to the surface before and after an HCl uptake experiment under non-QLL conditions. On both smooth and vapor-deposited ice films, approximately 25% less CCl_2F_2 is adsorbed to the surface after the surface has been exposed to HCl under QLL-forming conditions.

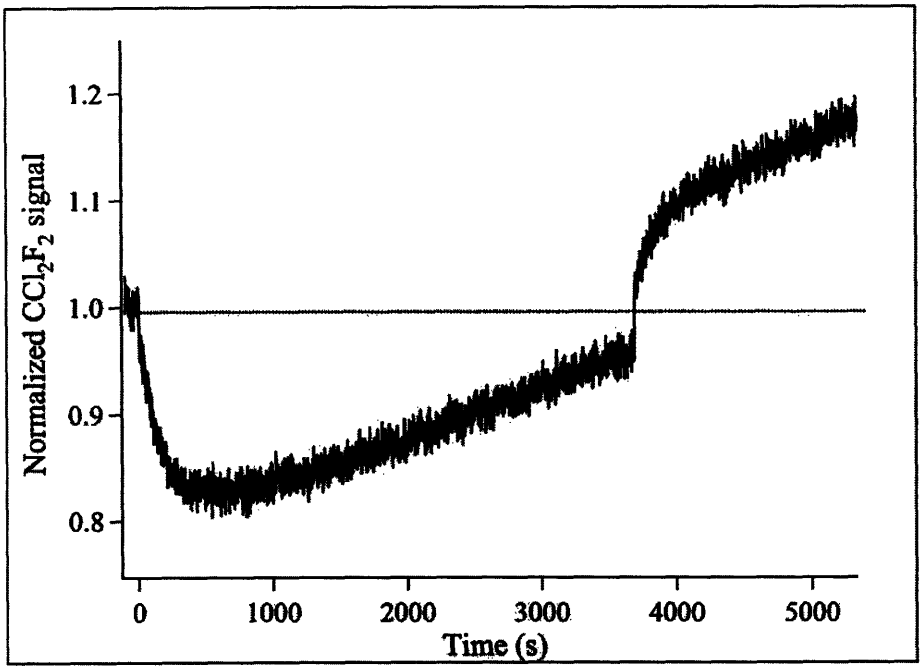

Figure 5-4. CFC-12 adsorption on smooth ice at -70 °C and $5.8 \cdot 10^{-7}$ Torr CCl_2F_2. The uptake curve corresponds to a surface coverage of $1.5(1) \cdot 10^{15}$ molecules·cm^{-2}.

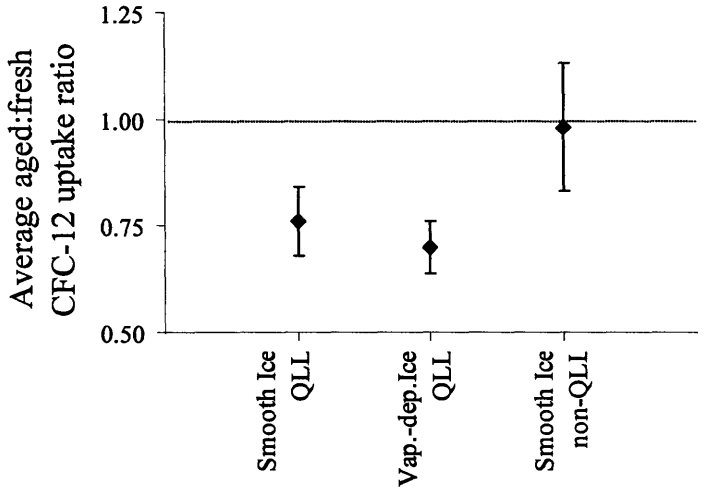

Figure 5-5. Summary of CFC-12 adsorption experiments on smooth and vapor-deposited ice films at -70 °C and $6.5 \cdot 10^{-7}$ Torr CCl_2F_2, before and after the ice has been exposed to HCl under QLL-forming and non-QLL conditions. The ratio of CCl_2F_2 uptake on the previously exposed ('aged') ice surface to the CCl_2F_2 uptake on the fresh ice surface is shown. Each point represents the average of data from at least two experiments. Error bars reflect noise in the uptake curves, propagated through the ratio and average calculations.

5.4 Discussion

5.4.1 Acetic acid

By an extrapolation of the data of Sokolov and Abbatt[3], we can estimate the Langmuir constant for CH_3COOH adsorption on bare ice at -60 °C to be $3 \cdot 10^5$ Torr $^{-1}$. Using our flow tube model with a conventional Langmuir model for the CH_3COOH-ice interaction, with this estimate for b and an assumed value of 0.0045 for the sticking coefficient, γ, we were able to reproduce both the shape of the measured uptake curve and the measured surface coverage to a reasonable approximation. Based on our based on our analysis of HCl uptake on zone-refined ice cylinders at -60 °C in section 4.4, we assumed that the total number of sites available for adsorption, S, is $6 \cdot 10^{14}$ molecules·cm^{-2}.

The results of the simulation are shown along with the measured uptake curve in Figure 5-6. The measured uptake curve corresponds to a surface coverage of $2.7(8) \cdot 10^{14}$ molecules·cm^{-2}. Simulated surface coverage is $2.4 \cdot 10^{14}$ molecules·cm^{-2}.

Consider the competitive adsorption of two chemical species, A, and B, that are assumed to occupy the same type of adsorption site on a surface[15]. The fraction of total surface sites occupied by species N, θ_N, is related to the surface coverage, $c_{s,N}$, as follows:

$$\theta_N = \frac{c_{s,N}}{S} \qquad 5\text{-}1.$$

where S is the surface site density. The equilibrium surface coverage for each species for the mixed system is

$$\theta_N = \frac{b_N P_N}{1 + b_A P_A + b_B P_B} \qquad 5\text{-}2.$$

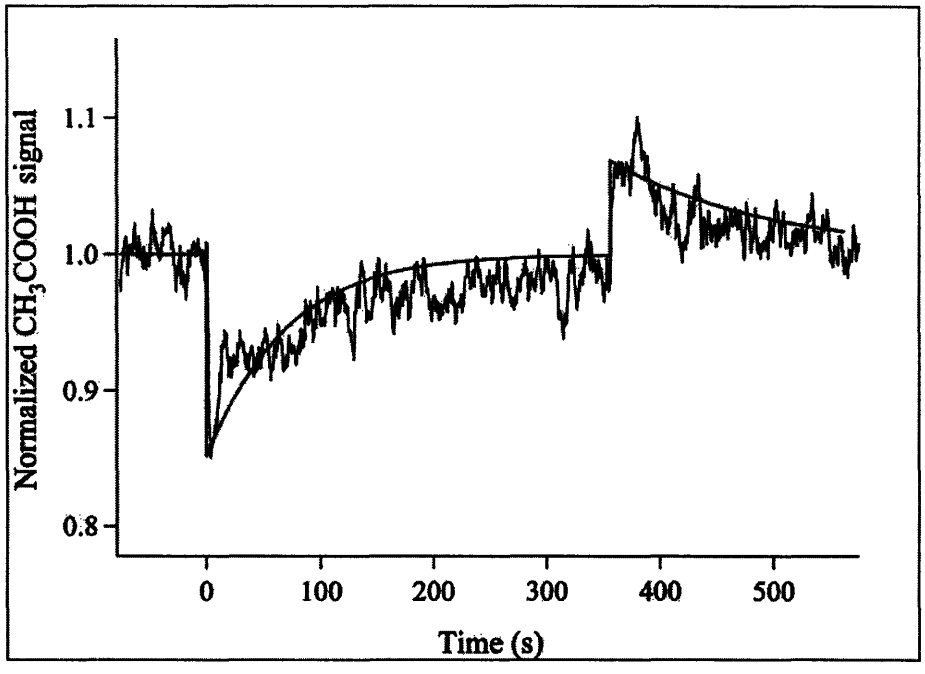

Figure 5-6. Simulated and measured CH_3COOH uptake curves for adsorption on zone-refined ice at -60.6 °C and $4.2 \cdot 10^{-6}$ Torr CH_3COOH. The solid line depicts the results of a flow tube simulation using a conventional Langmuir model for the CH_3COOH-ice interaction, with $b = 3 \cdot 10^5$ Torr^{-1} and $\gamma = 0.0045$.

Applying this model, we can predict the total CH_3COOH uptake for CH_3COOH/HCl co-adsorption at our experimental conditions.

Assuming that the presence of HCl does not affect the thermodynamics of adsorption of CH_3COOH, we use our value of $b_{CH3COOH} = 3 \cdot 10^5$ Torr^{-1} from our simulation of CH_3COOH adsorption on bare ice at -60 °C, as shown in Figure 5-6. Similarly, based on our analysis of HCl uptake on zone-refined ice cylinders at -60 °C from section 4.4, we use $b_{HCl} = 8.1 \cdot 10^6$ Torr^{-1} and assume that the total number of sites available for adsorption is $6 \cdot 10^{14}$ molecules·cm^{-2}.

The predicted CH_3COOH coverage for a) CH_3COOH adsorption with no HCl present, b) CH_3COOH/HCl co-adsorption at an HCl partial pressure where no surface change was observed

using ellipsometry, and c) CH_3COOH/HCl co-adsorption at QLL-inducing levels of HCl are shown, along with the actual measured CH_3COOH coverages, in Figure 5-7.

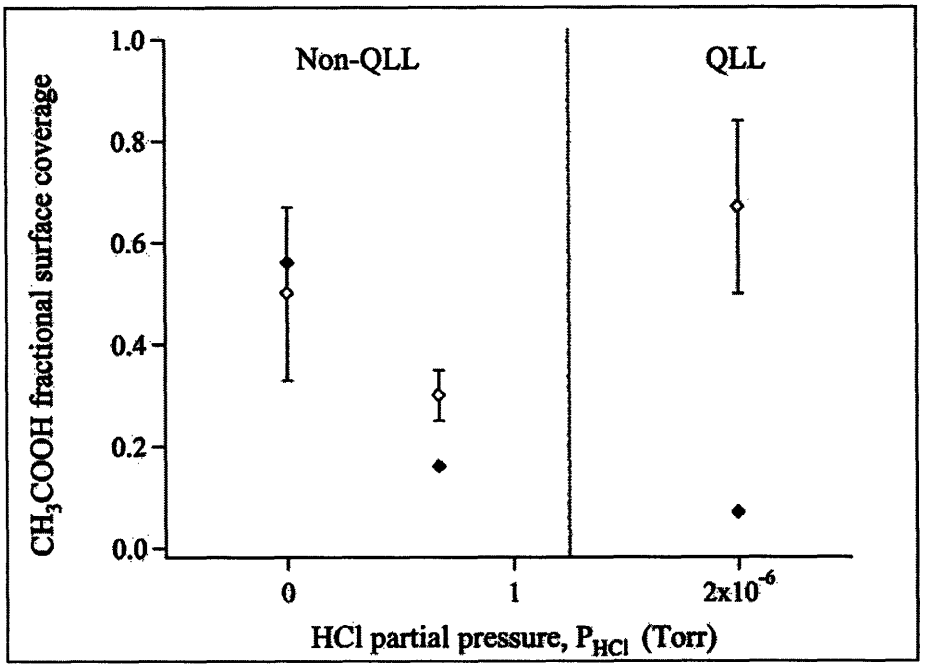

Figure 5-7. Measured acetic acid fractional surface coverages and coverages predicted using the CH_3COOH/HCl Langmuir co-adsorption model for T = -60.6 °C, $P_{CH3COOH} = 4.2 \cdot 10^{-6}$ Torr, and the three gas phase HCl concentrations studied. It is assumed that $S = 6 \cdot 10^{14}$ molecules·cm^{-2}. The filled markers represent predicted uptake, and the open markers represent measured uptake. Error bars reflect the noise in the data.

From Figure 5-7 it can be seen that, unsurprisingly, the model presented here of Langmuir CH_3COOH/HCl co-adsorption to an unchanging, refractory surface does not describe our experimental system under conditions where we observed surface disordering with the ellipsometer. The model underestimates the actual acetic acid fractional surface coverage under QLL-forming conditions by nearly a factor of ten. The affinity of CH_3COOH for the ice surface appears to increase in the presence of surface disorder.

From Figure 5-7 it is apparent that, even at levels of HCl where no induced surface disordering was observed with the ellipsometer, acetic acid adsorption appears to be enhanced slightly over the predicted value. This indicates that the presence of HCl enhances the affinity of acetic acid for the ice surface even when no surface change is observed via ellipsometry. The implication could be that some surface disordering below the limit of detection of our ellipsometer occurs in the presence of HCl under what we have termed 'non-QLL' conditions. Alternatively, the presence of adsorbed HCl molecules on the ice surface could in themselves enhance the affinity of CH_3COOH for the surface without surface disorder.

Acetic acid is infinitely soluble in liquid water.[16] Therefore, the fact that we did not observe infinite uptake of CH_3COOH under QLL-forming conditions is another indication that the QLL does not have truly liquid-like adsorption properties.

5.4.2 CFC-12

The uptake curves obtained in our HCl or CH_3COOH adsorption experiments reach a minimum immediately after the injector is withdrawn and the ice is exposed to the probe molecule. The CCl_2F_2 uptake curves shown in Figure 5-3 and Figure 5-4 slope down after the injector is withdrawn, reaching a minimum after approximately 1000 seconds in the case of adsorption on vapor-deposited ice. For adsorption on smooth ice, the minimum is reached between 500 and 600 seconds after the injector is withdrawn.

Uptake curves of this type are indicative of a sticking coefficient (and thus rate of adsorption) that is increasing with time. We simulated CCl_2F_2 adsorption onto smooth ice using our flow tube model with a conventional Langmuir model with a constant sticking coefficient to describe the CCl_2F_2-ice interaction, and also with a time-dependent sticking coefficient. The functional form of the sticking coefficient was arbitrarily chosen to be

$$\gamma = 0.01\left(1 + e^{-0.005t}\right) \qquad 5\text{-}3.$$

where t is in seconds. The adsorption rate constant, k_{ads}, was then calculated according to eq 1-7, with an assumed value of $S = 1 \cdot 10^{15}$ molecules·cm^{-2}. Figure 5-8 shows the measured and simulated uptake curves for CCl_2F_2 adsorption on smooth ice not previously exposed to HCl.

Possible reasons for a sticking coefficient that increases during an adsorption experiment include the existence of an attractive force between the adsorbate molecules, or a substrate surface that is changing with time in a way that increases the affinity of the adsorbate for the surface.

As shown in Figure 5-5, on both smooth and vapor-deposited ice films, approximately 25% less CCl_2F_2 is adsorbed to the surface after the surface has been exposed to HCl under QLL-forming conditions. This suggests that HCl-induced QLL formation causes a physical change to the ice surface that results in decreased surface area and persists after the source of HCl is removed. This surface change could be envisioned as a smoothing of the surface. However, the fact that the same percent decrease in surface area was observed for both the smooth and vapor-deposited ice films indicates that any smoothing occurring is on a smaller length scale than that of the overall porosity or roughness of the vapor-deposited ice film.

If a substrate change induced by CCl_2F_2 adsorption on our ice surfaces is the reason behind a CCl_2F_2-ice sticking coefficient that changes with time during adsorption, this change does not result in a permanent surface change that persists in the absence of CCl_2F_2, as indicated by the results shown in Figure 5-5 for CCl_2F_2 adsorption before and after exposure of the smooth ice film to non-QLL levels of HCl.

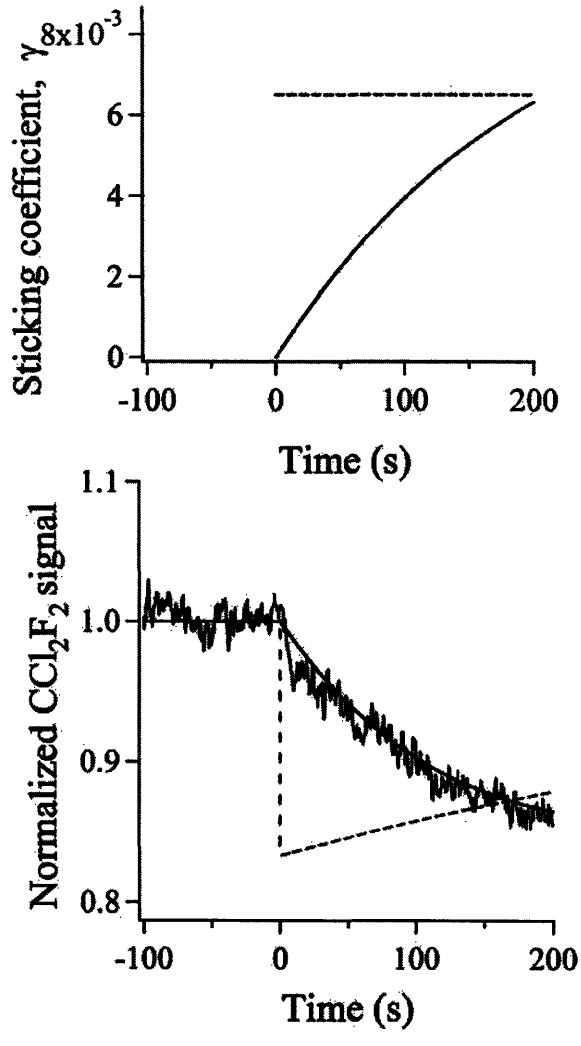

Figure 5-8. Measured and simulated uptake curves for CFC-12 adsorption on smooth ice not previously exposed to HCl. The grey dashed trace is a simulated uptake curve generated using our flow tube model with a conventional Langmuir model for the CCl_2F_2-ice interaction. The thick black trace represents simulation results obtained using a Langmuir model with a time-dependent sticking coefficient. The top panel shows the sticking coefficient used in each model as a function of time.

5.5 Conclusions

Based on the results of this study and the work of Sokolov et al.[3], it is clear that the presence of surface disorder enhances CH_3COOH uptake on ice. These findings suggest that the presence of surface disorder on cirrus cloud ice particles enhance their scavenging ability[3]. This effect should be important at temperatures above -30 °C. HCl concentrations in the free troposphere range from 50 to 100 pptv between 3 and 7 km[17], which is below the levels of HCl we have observed to be necessary to induce surface disordering for tropospherically relevant temperatures below -30 °C. However, we also observed that the presence of HCl appears to enhance acetic acid uptake slightly even under conditions where no surface change is observed using ellipsometry. Therefore in general the scavenging ability of cirrus clouds may be greater than previously estimated.

The results of this study lend further support for the trend observed via ellipsometry that surface disorder is induced by the presence of HCl in the vicinity of the solid-liquid equilibrium line on the HCl-ice phase diagram, but that no detectable disorder was observed on the interior of the 'ice' phase envelope. Additionally, since enhanced, but not unlimited, uptake of CH_3COOH was observed on ice under QLL conditions, and acetic acid is infinitely soluble in water[16], this work provides further support for our observation that the QLL is not truly liquid-like in its adsorption properties.

CCl_2F_2 adsorbs to ice with a time-dependent sticking coefficient. Further investigation is necessary to determine the cause of the time-dependence. The concentrations of CCl_2F_2 used in this study are significantly greater than those encountered in the stratosphere[18].

For both smooth and vapor-deposited ice films we have observed lower accessible area for CFC-12 adsorption after exposure of the films to HCl under QLL-forming conditions. This

implies that exposing polycrystalline ice films to levels of HCl which were observed to induce surface disorder on single-crystalline ice with ellipsometry induces a physical change in the surface that persists after the HCl source has been removed. However, the results are not conclusive since CCl_2F_2 adsorption to ice is not fully understood.

References for Chapter 5

1. Seinfeld, J.H. & Pandis, S.N. Atmospheric chemistry and physics: From air pollution to climate change. Wiley, New York (1998).

2. Abbatt, J.P.D. Interactions of atmospheric trace gases with ice surfaces: Adsorption and reaction. *Chem. Rev.* **103**, 4783-4800 (2003).

3. Sokolov, O. & Abbatt, J.P.D. Adsorption to ice of *n*-alcohols (ethanol to 1-hexanol), acetic acid, and hexanal. *J. Phys. Chem. A* **106**, 775-782 (2002).

4. Orem, M.W. & Adamson, A.W. Physical adsorption of vapor on ice. II. *n*-Alkanes. *J. Colloid Sci.* **31**, 278-286 (1969).

5. Sokolov, O. & Abbatt, J.P.D. Competitive adsorption of atmospheric trace gases onto ice at 228 K: HNO_3/HCl, 1-butanol/acetic acid and 1-butanol/HCl. *Geophys. Res. Lett.* **29**, (2002).

6. Perry, C.C. *et al.* Chemical Reactions in CF_2Cl_2/Water (Ice) Films Induced by X-ray Radiation. *J. Phys. Chem. B* **107**, 12740-12751 (2003).

7. Lu, Q.-B. & Sanche, L. Enhancements in dissociative electron attachement to CF_4, chlorofluorocarbons, and hydrochlorofluorocarbons adsorbed on H_2O ice. *J. Chem. Phys.* **120**, 2434-2438 (2004).

8. Faradzhev, N.S., Perry, C.C., Kusmierek, D.O., Fairbrother, D.H. & Madey, T.E. Kinetics of electron-induced decomposition of CF_2Cl_2 coadsorbed with water (ice): A comparison with CCl_4. *J. Chem. Phys.* **121**, 8547-8561 (2004).

9. Lu, Q.B. & Sanche, L. Effects of cosmic rays on atmospheric chlorofluorocarbon dissociation and ozone depletion. *Phys. Rev. Lett.* **8707**, 078501 (2001).

10. Harris, N.R.P., Farman, J.C. & Fahey, D.W. Comment on "Effects of cosmic rays on atmospheric chlorofluorocarbon dissociation and ozone depletion". *Phys. Rev. Lett.* **89**, 219801 (2002).

11. Lu, Q.B. & Sanche, L. Comment on "Effects of cosmic rays on atmospheric chlorofluorocarbon dissociation and ozone depletion" - Reply. *Phys. Rev. Lett.* **89**, 219802 (2002).

12. Patra, P.K. & Santhanam, M.S. Comment on "Effects of cosmic rays on atmospheric chlorofluorocarbon dissociation and ozone depletion". *Phys. Rev. Lett.* **89**, 219803 (2002).

13. Lu, Q.B. & Sanche, L. Comment on "Effects of cosmic rays on atmospheric chlorofluorocarbon dissociation and ozone depletion" - Reply. *Phys. Rev. Lett.* **89**, 219804 (2002).

14. Chao, J. & Zwolinski, B.J. Ideal-Gas Thermodynamic Properties of Methanoic and Ethanoic Acids. *J. Phys. Chem. Ref. Data* **7**, 363-377 (1978).

15. Adamson, A.W. Physical chemistry of surfaces. Wiley, New York (1990).

16. CRC handbook of chemistry and physics (1996).

17. Vierkorn-Rudolf, B., Bachmann, K., Schwartz, B. & Meixner, F.X. Vertical profile of hydrogen chloride in the troposphere. *J. Atmos. Chem* **2**, 47-63 (1984).

18. Stratospheric Ozone: An Electronic Textbook. NASA GSFC Atmospheric Chemistry and Dynamics Branch (2000).

Chapter 6

Conclusions and Recommendations for Future Work

6.1 QLL formation under stratospherically relevant conditions

The primary goal of this research has been to test the hypothesis that HCl induces the formation of a disordered region on the ice surface, or 'quasi-liquid layer' (QLL), at stratospheric conditions[1]. We have shown here via several approaches that HCl does induce surface disorder on ice under conditions in the vicinity of the solid-liquid equilibrium line on the HCl-ice phase diagram, including stratospherically relevant conditions. A summary of the results from the various approaches are summarized in Figure 6-1.

It appears that the value of the refractive index of the QLL formed via exposure to gas-phase HCl is closer to the refractive index of liquid water or what we would predict for an aqueous HCl solution than to the refractive index of ice. We estimate the thickness of the QLL in our experiments to be on the order of 100 nm.

A second goal of this research was to show whether the existence of the QLL explains the catalytic role PSC particle surfaces play during chlorine activation. In Chapter 3 we showed that the presence of surface disorder enhances the chlorine activation reaction of $ClONO_2$+HCl on

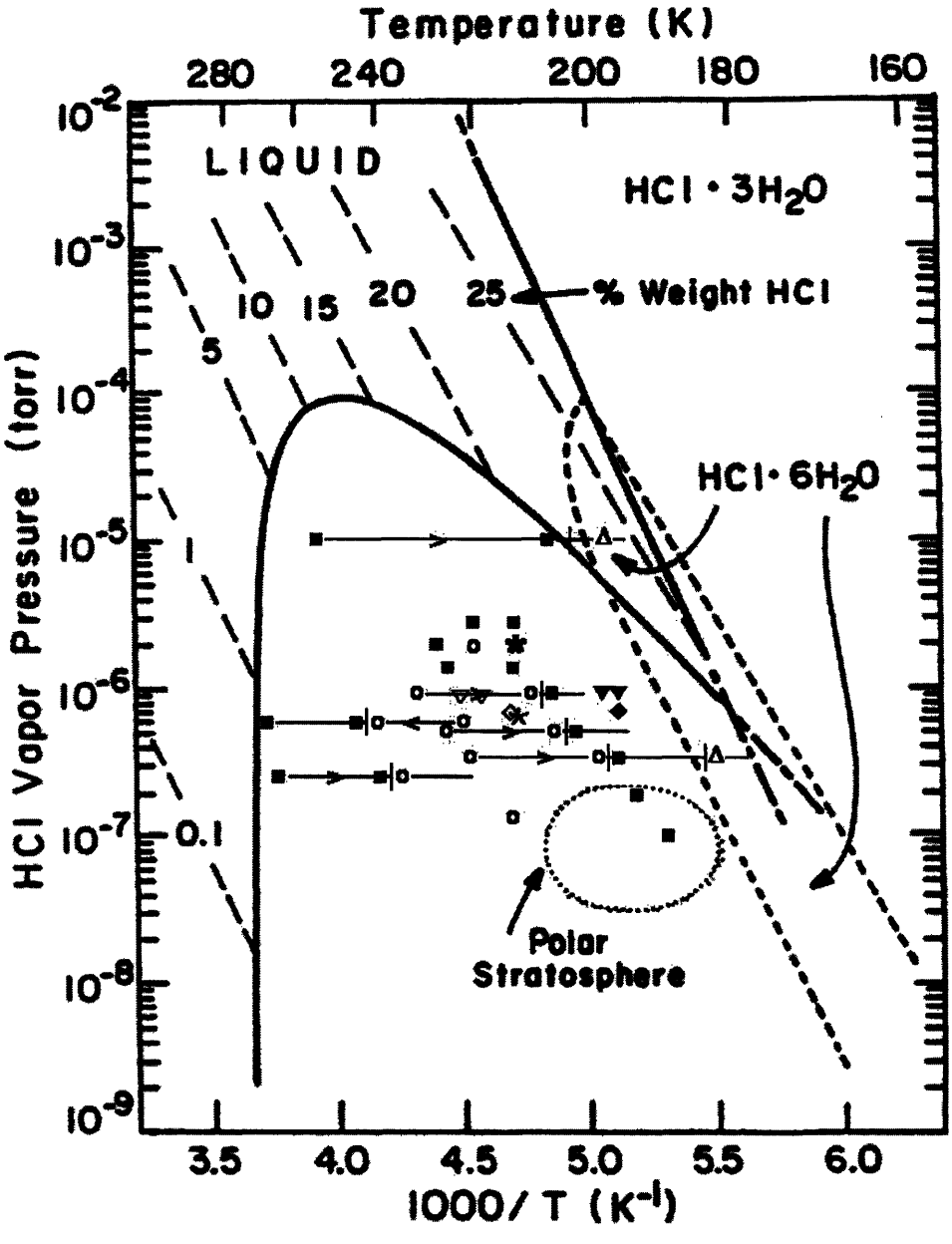

Figure 6-1. Summary of results of this work regarding surface disordering: the HCl-ice phase diagram adapted from Molina[1]. Ellipsometry data is labeled as in Figure 2-5. Filled boxes (■) and open circles (o) refer to conditions where QLL formation was, or was not observed via ellipsometry upon exposure of the ice crystal to HCl, respectively. Phase transition is indicated by delta symbols (Δ). Inverted triangles refer to the results of flow tube-CIMS studies of the $ClONO_2$+HCl reaction on smooth and zone-refined ice under non-QLL (▽) and QLL forming (▼) conditions. Diamonds refer to flow tube-CIMS HCl uptake experiments on zone-refined ice under non-QLL (◇) and QLL forming (◆) conditions. Stars refer to CH_3COOH/HCl co-adsorption experiments on zone-refined ice under non-QLL (⋆) and QLL forming (✱) conditions.

ice.

It is clear that the presence of this disordered region is an important feature of ice I_h in determining its surface chemistry. We have found that the QLL enhances the ability of the ice surface to take up HCl and CH_3COOH molecules. We find that the solubilities of HCl and CH_3COOH in the QLL are intermediate between the solubilities of each species in liquid H_2O and those in ice.

In the future, additional ellipsometry-CIMS experiments should be performed to map out the 'non-QLL' and 'QLL' regions of the phase diagram in more detail, particularly at stratospherically relevant conditions.

Another question that should be addressed in future work is whether HCl induces QLL formation on the surface of nitric acid trihydrate (NAT), the principal component of Type I PSC particles. The chlorine activation reaction of $ClONO_2$ + HCl is known to proceed as efficiently on NAT as on ice surfaces, and HCl has been seen in the laboratory to have a high affinity for the NAT surface[2-5]. Abbatt and Molina found that the water vapor pressure over the NAT surface had a strong influence on the rates of the $ClONO_2$ + HCl and $ClONO_2$ hydrolysis reactions, and on the tendency for NAT to take up HCl [3]. They found that NAT with water vapor pressures approaching that of ice exhibited higher reaction probabilities than HNO_3-rich NAT. The *ab initio* simulations of Mantz et al. indicated that HCl has a lower affinity for NAT than it does for water-ice surfaces, and that adsorbed HCl will not dissociate on NAT surfaces.[6] Mantz et al. did not observe disordering in their model NAT crystal upon HCl adsorption to the surface.

The insight into the microphysics of the HCl-ice surface interaction that is provided by this work can inform our understanding of ice chemistry involving other compounds. One

example of this is hydrogen bromide, HBr, another compound that is significant to ozone depletion chemistry. HBr adsorption on ice under laboratory conditions results in large surface coverages[7-10] and in co-adsorption experiments HBr shows a higher affinity for ice than HCl does[10]. These studies were performed at HBr partial pressures above 10^{-8} Torr, which is significantly higher than the HBr partial pressures typically encountered in the stratosphere, where $P_{HBr} \sim 10^{-11}$ Torr. Measured surface coverages were then extrapolated down to stratospherically relevant conditions. The possibility of HBr-induced ice surface disordering should be investigated, and the question of whether the presence of surface disorder could explain the large uptakes that have been observed should be addressed. If this is the case, it should be determined whether extrapolation of measured amounts of HBr uptake from high to low partial pressures of HBr is valid. Such extrapolation would not be valid with the HCl-ice system.

6.2 HCl adsorption on ice

Another goal of this research was to gain insight into the fate of HCl upon adsorption to various types of ice. In Chapter 4 we showed that HCl adsorption onto polycrystalline ice samples consists of two modes of adsorption: one relatively strong mode leading to irreversible adsorption, and one relatively weak binding mode leading to reversible adsorption. We believe that these two modes of adsorption correspond to adsorption to sites at crystal faces and those at grain boundaries, but there is not enough experimental evidence to conclusively assign each adsorption mode to a type of site. Such an assignment would probably not be possible without further studies using a technique that is sensitive to the chemical state of adsorbed molecules on the ice surface, unlike our flow tube-CIMS technique, which can only provide information about

molecules in the gas phase. TPD-MS is a technique that requires ultrahigh vacuum conditions, and therefore TPD-MS studies of ice generally must be conducted at temperatures lower than those relevant to the stratosphere. However, a high-temperature TPD-MS technique is being developed by Prof. Vladislav Sadtchenko at George Washington University[11] that allows TPD-MS studies of ice at temperatures near 0 °C. A technique such as this could provide molecular-level information about the fate of HCl adsorption to ice surfaces, and also could provide confirmation of our conclusion that HCl hexahydrate forms on the surface of crystalline ice I_h, as in the low-temperature studies performed by Sadtchenko et al.[12]

Valuable information could also be gained from *ab initio* modeling or surface-sensitive studies of polycrystalline ice using a technique capable of detecting whether HCl induces local disordering at grain boundaries before it occurs on crystal faces. Ellipsometry cannot be used on polycrystalline ice due to its low reflectivity.

A detailed study of HCl adsorption on zone-refined ice such as the one presented in Chapter 4 on smooth ice films would likely yield energetic information about HCl adsorption on crystal faces. Such information was not obtained from our study on smooth ice due to the complexity of adsorption to the polycrystalline ice surface.

As a final note, information about the fate of HCl upon adsorption to polycrystalline ice samples is useful to consider when designing experiments and when interpreting HCl adsorption studies in the literature, which have generally been conducted on smooth or vapor-deposited polycrystalline ice. However, PSC particles are believed to be single-crystalline, and therefore should have the characteristics of the ice samples used in the ellipsometer-CIMS study and the zone-refined ice samples.

6.3 QLL in the troposphere

In Chapter 5, we showed that the presence of the QLL enhances acetic acid (CH_3COOH) adsorption. Further investigation is necessary to determine whether other tropospheric trace species besides HCl may induce significant disordering at temperatures below -30 °C. In addition to enhancing scavenging of semivolatile gas-phase species, the presence of the QLL on cirrus cloud ice particles may also play a role in the heterogeneous chemistry of the upper troposphere, particularly in mid-latitude ozone depletion. Additionally, the presence of the QLL on ice particles can influence calculations of contributions of cirrus clouds to the earth's albedo.

6.4 CFC-ice interaction

We also showed in Chapter 5 that the sticking coefficient of CCl_2F_2 changes with time during adsorption to smooth and vapor-deposited polycrystalline ice surfaces. The concentrations of CCl_2F_2 used in this study were significantly greater than those encountered in the stratosphere[13]. *Ab initio* modeling or an experimental study using a surface-sensitive technique could provide information about whether or not this effect is due to a reversible change in the ice surface induced by adsorption.

References for Chapter 6

1. Molina, M.J. The Chemistry of the Atmosphere: The Impact of Global Change. Calvert, J.G. (ed.), pp. 27-38 (Blackwell Scientific Publications, Boston,1994).

2. Hanson, D.R. & Ravishankara, A.R. The Reaction Probabilities of $ClONO_2$ and N_2O_5 on Polar Stratospheric Cloud Materials. *J. Geophys. Res.-Atmos.* **96**, 5081-5090 (1991).

3. Abbatt, J.P.D. & Molina, M.J. Heterogeneous Interactions of $ClONO_2$ and HCl on Nitric-Acid Trihydrate at 202 K. *J. Phys. Chem.* **96**, 7674-7679 (1992).

4. Leu, M.T., Moore, S.B. & Keyser, L.F. Heterogeneous Reactions of Chlorine Nitrate and Hydrogen- Chloride on Type-I Polar Stratospheric Clouds. *J. Phys. Chem.* **95**, 7763-7771 (1991).

5. Moore, S.B., Keyser, L.F., Leu, M.T., Turco, R.P. & Smith, R.H. Heterogeneous Reactions on Nitric-Acid Trihydrate. *Nature* **345**, 333-335 (1990).

6. Mantz, Y.A., Geiger, F.M., Molina, L.T., Molina, M.J. & Trout, B.L. A theoretical study of the interaction of HCl with crystalline NAT. *J. Phys. Chem. A* **106**, 6972-6981 (2002).

7. Hanson, D.R. & Ravishankara, A.R. Heterogeneous chemistry of hydrogen bromide and hydrogen fluoride. *J. Phys. Chem.* **96**, 9441-6 (1992).

8. Abbatt, J.P.D. Heterogeneous reaction of HOBr with HBr and HCl on ice surfaces at 228 K. *Geophys. Res. Lett.* **21**, 665-8 (1994).

9. Chu, L.T. & Heron, J.W. Uptake of HBr on ice at polar atmospheric conditions. *Geophys. Res. Lett.* **22**, 3211-3214 (1995).

10. Chu, L.T. & Chu, L. Studies of HBr Uptake on Ice Films at 188 K. *J. Phys. Chem. A* **103**, 384-395 (1999).

11. Sadtchenko,V. Personal Communication (2004).

12. Sadtchenko, V., Giese, C.F. & Gentry, W.R. Interaction of Hydrogen Chloride with Thin Ice Films: The Effect of Ice Morphology and Evidence for Unique Surface Species on Crystalline Vapor-Deposited Ice. *J. Phys. Chem. B* **104**, 9421-9429 (2000).

13. Stratospheric Ozone: An Electronic Textbook. NASA GSFC Atmospheric Chemistry and Dynamics Branch (2000).